ISTANBUL TECHNICAL UNIVERSITY ★ GRADUATE SCHOOL OF SCIENCE ENGINEERING AND TECHNOLOGY

BIAS CORRECTION OF PRECIPITATION SIMULATED BY REGIONAL CLIMATE MODEL WITH DIFFERENT CONFIGURATIONS OVER TURKEY

M.Sc. THESIS

Ceren BALLI

Department of Meteorological Engineering

Atmospheric Science Programme

APRIL 2014

ISTANBUL TECHNICAL UNIVERSITY ★ GRADUATE SCHOOL OF SCIENCE ENGINEERING AND TECHNOLOGY

BIAS CORRECTION OF PRECIPITATION SIMULATED BY REGIONAL CLIMATE MODEL WITH DIFFERENT CONFIGURATIONS OVER TURKEY

M.Sc. THESIS

Ceren BALLI
(511111003)

Department of Meteorological Engineering

Atmospheric Science Programme

Thesis Advisor: Prof. Dr. Yurdanur ÜNAL

APRIL 2014

İSTANBUL TEKNİK ÜNİVERSİTESİ ★ FEN BİLİMLERİ ENSTİTÜSÜ

BÖLGESEL İKLİM MODELİNİN FARKLI KONFİGÜRASYONLARIYLA SİMÜLE EDİLMİŞ YAĞIŞ VERİSİNİN TÜRKİYE ÜZERİNDEKİ YANLILIK DÜZELTMESİ

YÜKSEK LİSANS TEZİ

Ceren BALLI
(511111003)

Meteoroloji Mühendisliği Anabilim Dalı

Atmosfer Bilimleri Programı

Tez Danışmanı: Prof. Dr. Yurdanur ÜNAL

NİSAN 2014

Ceren BALLI, a M.Sc. student of ITU Graduate School of Science Engineering and Technology 511111003 successfully defended the thesis entitled **"BIAS CORRECTION OF PRECIPITATION SIMULATED BY REGIONAL CLIMATE MODEL WITH DIFFERENT CONFIGURATIONS OVER TURKEY"**, which he/she prepared after fulfilling the requirements specified in the associated legislations, before the jury whose signatures are below.

Thesis Advisor :	**Prof. Dr. Yurdanur ÜNAL** Istanbul Technical University	.....
Jury Members :	**Prof. Dr. Harald KUNSTMANN** Karlsruhe Institute of Technology	.....
	Prof. Dr. Mikdat KADIOĞLU Istanbul Technical University	.....
		.....

Date of Submission : **February 3, 2014**
Date of Defense : **April 24, 2014**

FOREWORD

First and foremost, I would like to express my deepest appreciation to my advisor Prof. Dr. Yurdanur ÜNAL for her invaluable guidance, caring and encouragement to me and this research. Without her motivation and collaboration, the completion of this work would never have been possible.

I am grateful to Prof. Dr. Harald KUNSTMANN for suggesting this investigation and helpful commendations from different perspectives. I am also owing a great thank to him for supporting me during my stay in IMK-IFU Garmisch-Partenkirchen.

I would like to thank Dr. Stefanie Vogl, for her assistance to get familiar the techniques and her supports to develop my knowledge.

This thesis owes to thanks to my dear colleagues: Dr. Patrick Laux, Ganquan Mao and Ferat Çağlar. I would also like to thank to my all friends for their continuous supports and hospitality at very hard days and nights.

Specially, nothing would have been possible without the everlasting love and outstanding support of my family. What I have achieved until today is through my dear mother Şengül Yağmur and my precious sister Özge Can Şahin.

April 2014

Ceren BALLI
(Meteorological Engineer)

TABLE OF CONTENTS

Page

ABBREVIATIONS

AGCM : Atmospheric general circulation model
AM : Analogue Method
AVHRR : Advanced Very High Resolution Radiometer
BATS : Biosphere-Atmosphere Transfer Scheme
CRCM : Canadian Regional Climate Model
CDF : Cumulative Distribution Function
CLM : Community Land Model
CNRM-CM3 : The Centre National de Recherches Météorologiques Coupled global climate Model version 3
COSMO-CLM : Consortium for Small scale Modeling model in Climate Model
CCSM : Community Climate System Model
CRU : Climate Research Unit
DBC : Daily Bias Correction
DDM : Dynamical Downscaling Method
DECM : Downscaling and Error Correction Methods
DT : Daily Translation
DWD : German Weather Service
ECMWF : European Center of Medium Weather Forecast
EM : Eastern Mediterranean
ERA-40 : Global Re-analysis Data
EU WATCH : European Union Water and Global Change Project
GAMMA : Gamma Quantile Distribution Mapping
GCM : General Circulation Model
GCN : Global Climate Normals
GISST : Global Sea-Ice and Sea Surface Temperature
HadRM3-PPE-UK : Hadley Centre Regional Model Perturbated Physics Ensemble over Great Britain
HRM3 : Hadley Regional Model 3
GLCC : Global Land Cover Characterization
GOF : Goodness-Of-Fit
IAP : The Institute of Atmospheric Physics
ICTP : Abdus Salam International Centre for Theoretical Physics
IPCC : Intergovernmental Panel on Climate Change
IPSL-CM4 : Institute Pierre Simon Laplace Coupled Model version 4
LOCI : Local Intensity Scaling
LSM : Land Surface Model
MLE : Maximum Likelihood Estimation
MLR : Multiple Linear Regression
MLRR : Multiple Linear Regression with Randomization
MPI-HM : Max Planck Institute – Hydrology Model
MV : Mean Value Bias Correction Method

NCAR : National Center of Atmospheric Research
NCEP : National Center for Environmental Prediction
NNAM : Nearest Neighbour Analogue Method
NSE : Nash-Sutcliffe Efficiency
PBL : Planetary Boundary Layer
PDF : Probability Density Function
PET : Potential Evapo-Transpiration
QM : Quantile Mapping Method
RCM : Regional Climate Model
REGNIE : REGionalisierung der NIEderschlagshönen
RMSE : Root Mean Square Error
QM : Quantile Mapping Bias Correction Method
SDM : Statistical Downscaling Method
SST : Sea Surface Temperature
SUBEX : Subgrid Explicit Moisture Scheme
TSMS : Turkish State Meteorological Service
USGS : United States Geological Survey
WRF : Weather Research and Forecasting Model

LIST OF TABLES

Page

LIST OF FIGURES

Page

BIAS CORRECTION OF PRECIPITATION SIMULATED BY REGIONAL CLIMATE MODEL WITH DIFFERENT CONFIGURATIONS OVER TURKEY

SUMMARY

In this study, 2.5 degree grid size ECMWF ERA40 reanalysis data are downscaled to first 50 km coarse resolution and then 10 km high resolution over Turkey by regional climate model, RegCM4.3. The precipitation field has been simulated for the period 1971 to 2000, while the first 20 years are calibrated and the last 10 years are validated. RegCM is coupled with two different land surface models (LSMs); BATS and CLM. Coarse resolution simulations are carried out for BATS and CLM while high-resolution simulations only for BATS.

The simulated precipitation climatology of two different land surface models is compared to the CRU TS3.10 data set. Also, 245 station-observations of Turkish Meteorological Service are used to estimate model biases in the precipitation field. Two common bias correction methods, Mean Value (MV) and Quantile Mapping (QM), have been carried out to reduce the bias of the precipitation simulations for monthly, seasonal and yearly bases. The QM method is also applied with two fitted distributions, Gamma (Gamma QM) and the best-fitted cumulative distribution functions (best-fitted QM) and the results are compared with each other. The results of these methods are tested by three quantitative validation measures such as Spearman rank correlation, Root Mean Square Error (RMSE) and Nash-Sutcliffe Efficiency (NSE).

Generally, RegCM is good at modeling the general precipitation patterns. Mostly, the positive biases have been obtained over Turkey and the mountainous regions when compared with CRU observations during winter and spring seasons. The dryness of the summer season is very well captured by two configurations of RegCM. Meanwhile, the highest positive bias is estimated in the spring with the amount of 300 mm. However, the autumn season has been simulated drier than the CRU climatology.

The precipitation is underestimated for two LSMs (BATS50, CLM50 and BATS10) along the Black Sea and the Mediterranean Sea regions where the mountains run parallel to the coastlines. Throughout the Aegean Sea and inland parts of Turkey, the overestimations have been observed. The winter correction factor distribution of BATS50 is similar with BATS10. Although, the systematic errors are becoming smaller with the increasing resolution over the shorelines. While BATS50 produces more precipitation over high topography, CLM50 generates more precipitation throughout inland.

According to the correlation results between the corrected simulations and station observations, the highest correlation values are located throughout Southeast Anatolia, whereas the lowest correlations have been seen at the Black Sea coastline. The general pattern of the correlation distributions of CLM50 are worse than BATS50 while BATS10 has more improved correlations, especially along the Black Sea coastline.

Although the Gamma QM is mostly preferred in the literature, the results of the best-fitted QM corrections are better than Gamma QM. On the other hand, the season-based QM calculations give better results than QM method. In comparison to all bias correction methods, the month-based MV method has higher correlations to the observations over Turkey. The month-based MV correction methods generate smaller RMSEs than the QM correction methods while the NSE results of the month-based MV methods show a perfect match over Turkey except Mediterranean shorelines. Overall, the month-based MV bias correction method has the best performance especially for the high resolution.

BÖLGESEL İKLİM MODELİNİN FARKLI KONFİGÜRASYONLARIYLA SİMÜLE EDİLMİŞ YAĞIŞ VERİSİNİN TÜRKİYE ÜZERİNDEKİ YANLILIK DÜZELTMESİ

ÖZET

Yağış, kompleks topoğrafyaya sahip bir coğrafya için tahmin edilmesi en zor meteorolojik parametrelerden biridir. Genel sirkülasyon modelleri ve bölgesel iklim modelleri tarafından üretilen yağış simülasyonları, gözlem verileriyle karşılaştırılarak model yanlılığının hesaplanıp düzeltilmesi, model çıktılarının iklim ve hidroloji çalışmalarında kullanılabilmesi için büyük önem taşır.

Bu çalışmanın amacı, farklı konfigürasyonlar ile koşturulan bölgesel iklim modeli ile yağış verisini kaba ve yüksek çözünürlüklü iki domain için modellemek, sonuçlarına yanlılık analizi uygulamaktır. Bu bağlamda bölgesel iklim modeli olarak RegCM4.3 kullanılmıştır. Modelin başlangıç ve sınır koşulları için Avrupa Orta Vadeli Hava Tahmin Merkezi (ECMWF)'den alınan 2.5 derece çözünürlüklü ERA-40 reanaliz veri seti önce kaba çözünürlüklü 50 km, sonra yüksek çözünürlüklü 10 km için koşturulmuştur. Yağış simülasyonları 1971-2000 yılları arasında yapılmış olup, ilk 20 yıl (1971-1990) düzeltme periyodu, son 10 yıl ise (1991-2000) doğrulama periyodu olarak seçilmiştir. İlk 20 yıldan elde edilen düzeltme katsayıları ve parametreleri son 10 yıllık yağış verisine uygulanmıştır. Bölgesel iklim modeli RegCM4.3, iki arazi yüzey modeli (LSM), Biyosfer-Atmosfer Transfer Şeması (BATS) ve Topluluk Arazi Modeli (CLM) ile koşturulmuştur. BATS her iki domain için kullanılırken CLM sadece kaba çözünürlük için kullanılmıştır.

İki arazi yüzey modeli kullanılarak elde edilen yağış simülasyonlarının klimatolojisi, Doğu Anglia Üniversitesi (University of East Anglia)'nden alınan 0.5 çözünürlüklü İklim Araştırma Birim (CRU TS3.10) veri seti ile karşılaştırılmıştır. Ayrıca Meteoroloji Genel Müdürlüğü'nden sağlanan 1971-2000 yılları arasındaki 245 istasyonun yağış gözlemleri ile yağış simülasyonlarındaki model yanlılığı hesaplanmıştır. Arazi yüzey modelinin her iki çözünürlükteki simülasyonları için, istasyon koordinatlarının modele en yakın grid noktaları hesaplanarak yanlılık düzeltme analizleri yapılmıştır. Yanlılık analizi için literatürde yaygın olarak en çok kullanılan ortalama değer yanlılık düzeltmesi (MV) ve dağılımı dengeleme (QM) yöntemleri tercih edilmiştir. Modelin yanlılığını indirgemek için kullanılan bu yöntemler; aylık, mevsimlik ve yıllık bazlarda uygulanmıştır. Dağılımı dengeleme (QM) yöntemi; istasyon gözlemlerine ve modelin ürettiği yağış çıktılarına en iyi uyan dağılım fonksiyonları hesaplanarak uygulanmıştır. En iyi dağılım fonksiyonlarını bulmak için, Uyum İyiliği Testi (GOF) ile Akaike ve Bayesian bilgi kriteri (AIC ve BIC) testleri yapılmıştır. Bunun sonucunda gözlemler için Weibull kümülatif dağılım fonksiyonu, yağış simülasyonları için Genelleştirilmiş Pareto kümülatif dağılım fonksiyonu seçilmiştir. Gamma kümülatif dağılım fonksiyonu yağış parametresini en iyi temsil eden dağılım fonksiyonu olduğu ve literatürde dağılım dengeleme yöntemi uygulamasında çok sık kullanıldığı için ayrıca incelenmiş, sonuçları gözlem ve model çıktılarına en iyi uyan dağılım fonksiyonları ile kıyaslanmıştır. Modelin performansını değerlendirmek için yanlılık

düzeltmesi sonucu elde edilen yağış verilerinin son 10 yıllık periyoduna Spearman Rank Korelasyon, Ortalama Hata Karesinin Kökü (RMSE) ve Nash-Sutcliffe Verim İndeksi (NSE) gibi üç kantitatif doğrulama yöntemi uygulanmıştır.

Model performansı CRU TS3.10 yağış verisinin 30 yıllık mevsimsel ortalamaları ile karşılaştırıldığında, RegCM'in yağış paternlerini genel olarak iyi benzeştirdiği görülmektedir. Modelin pozitif yanlılığı genellikle Türkiye üzerinde ve sarp dağ sıralarının yamaçlarında kış ve ilkbahar mevsimleri boyunca hesaplanmıştır. Kuzey ve güney kıyılardaki benzeştirilen yağış miktarı 600 mm'yi bulmaktadır. Yaz mevsiminin kuraklığı modelin her iki arazi yüzey modeli ile iyi tahmin edilmiştir. Topluluk Arazi Modeli'nin (CLM50) performansı ile Biyosfer-Atmosfer Transfer Şeması'nın (BATS50) performansı arasında çok büyük farklılıklar olmamasına karşın; bahar mevsimi için BATS'ın, CLM'den daha fazla orografik yağış ürettiği gözlenmiştir. Yüksek çözünürlüklü yağış simülasyonlarının dağılımlarının ise topoğrafyayı mimik ettiği görülmektedir. Bununla birlikte en yüksek pozitif yanlılık 300 mm ile ilkbahar mevsiminde gözlenmiştir. Sonbahar mevsimi ise CRU klimatolojisinden daha kurak benzeştirilmiştir.

İlk 20 yılın ortalama değer yanlılık düzeltmesi için hesaplanan düzeltme katsayılarının dağılımına bakıldığında, Karadeniz ve Akdeniz'de bulunan dağların kıyıya paralel uzanması nedeniyle yağış bu bölgelerde az, Ege kıyıları ve Türkiye'nin iç kesimlerinde ise fazla tahmin edilmiştir. İlkbahar mevsimi dışında, modelin genel eğilimi kaba çözünürlük için az yağış tahmini yapma yönündedir. Dağların dik olduğu topoğrafya üzerinde BATS50, CLM50'den daha fazla orografik yağış üretirken, iç kesimlerde CLM50'nin yağışları daha fazla gözlenmiştir. Kıyılardaki sistematik hatalar ise model çözünürlüğünün artması ile küçülmüştür. Düzeltme katsayılarının ortalamalarına bakıldığında BATS50, CLM50 ve BATS10 için sırasıyla; 1.21, 1.36 ve 0.77 olarak hesaplanmıştır. Modelin ürettiği sistematik hatalar Karadeniz ve Akdeniz kıyıları boyunca gözlenmiş olup, bu bölgelerdeki yağış yapılan üç çalışmada da az tahmin edilmiştir. Ege kıyıları ve Türkiye'nin iç kesimlerinde ise RegCM, gözlem verilerinden daha fazla yağış üretmiştir.

Yanlılık düzeltmesi yapılmış yağış simülasyonları ve istasyon gözlemleri arasındaki korelasyonlara bakıldığında; %99 anlamlılık testine göre 0.25 limiti ile değerlendirilen korelasyon hesaplarına göre, en yüksek korelasyonlar Güneydoğu Anadolu'da 0.60 ile 0.90 arasında hesaplanırken, en düşük korelasyonlar Karadeniz kıyılarında 0.25 ile 0.75 değerlerinde gözlenmiştir. Korelasyon dağılımlarının genel paterni göz önüne alındığında, BATS50'nin dağılımı CLM50'den daha iyi iken özellikle Karadeniz bölgesi civarında BATS10 en iyi korelasyonlara sahiptir. Aylık bazda uygulanan ortalama değer (MV) düzeltme yöntemi genellikle Karadeniz, Doğu ve Güneydoğu Anadolu bölgelerindeki korelasyon sonuçlarını düzeltmektedir. Mevsimlik bazda uygulanan dağılımı dengeleme (QM) yönteminin korelasyon sonuçları ise yıllık bazda hesaplanan korelasyonlardan daha yüksektir. Model ve gözlemin dağılımına en iyi uyan dağılım fonksiyonları ile yapılan düzeltme, Gamma kümülatif dağılım fonksiyonu kullanılarak hesaplanan düzeltmeye göre daha iyi sonuçlar vermiştir. Mevsim bazında yapılan yanlılık düzeltmeleri ise yıllık hesaplamalardan daha iyi sonuçlar vermiştir.

En küçük hata değerleri (RMSE) ise aylık bazda uygulanan ortalama değer (MV) yönteminden elde edilmiş olup, hatalar 0-25 mm arasındadır. İç Anadolu' da 0-25 mm civarında hatalar elde edilirken, kıyılarda 150 mm'yi bulmaktadır. Yüksek

çözünürlüklü simülasyonlarda görülen hataların ise kaba çözünürlükten daha düşük olduğu tespit edilmiştir. Nash-Sutcliffe Verim İndeksi hesaplamaları ise aylık bazda uygulanan ortalama değer (MV) yöntemi ile düzeltilen simülasyonların gözlem değerleri ile mükemmel bir uyum sağladığını göstermektedir. Dağılımı dengeleme (QM) yöntemi yağışların dağılımını düzeltse de değişimini düzeltemediği görülmüştür. Kıyıların dışında, batı İç Anadolu ve Güneydoğu Anadolu'da gözlemlerin ortalamasının model sonuçlarından daha belirleyici olduğu ortaya çıkmıştır.

Sonuç olarak; Türkiye üzerinde kantitatif üç doğrulama yöntemine göre, aylık bazda uygulanan ortalama değer (MV) düzeltme yöntemi özellikle yüksek çözünürlüklü simülasyonlarda en yüksek korelasyonlara, en küçük hatalara ve Nash-Sutcliffe Verim İndeksi'ne göre mükemmel uyuma sahiptir.

1. INTRODUCTION

Turkey has very complex topography so that it involves regions with different climatic characteristics. Topographic features and land sea distribution modify the synoptic systems over Turkey, and the complex topography along the coastlines and eastern Anatolia modulates the distribution of precipitation through orographic uplifting and the development of local circulations by regulating the land atmosphere exchanges of heat, water and momentum. Therefore, it is important to represent the effects of complex topography in climate models. Consequently, the regional climate models with high horizontal resolution are necessary to produce realistic climate simulations.

Precipitation is one of the important parameter to be used in climate impact assessments on regional hydrology, agriculture and cryosphere. However, the fields produced by general circulation models are insufficient to be employed directly on these types of studies due to limited representation of orography and relatively poor representation of meso-scale processes [6, 7]. In order to compensate the shortage of the general circulation models and bridge the scale gap between the GCMs and local applications, the GCM outputs are downscaled to higher resolutions by either statistical or dynamical downscaling methods [6, 8] and [9–12]. Both downscaling methods rely on the large-scale information of atmospheric circulation provided by GCMs and each method generates regional details by using different approaches.

Statistical downscaling methods define a transfer function between large-scale observations or reanalysis data and local observations to regionalize large scale climate signal [7, 12, 13]. Then, GCM fields fed into these transfer functions to estimate the corresponding regional climate characteristics. The most important advantage of the statistical downscaling methods is that they require less computational effort than dynamical downscaling so that they are applicable for longer time scales. On the other hand, dynamical downscaling methods are based on simulations of physical and dynamical processes at a fine scale by using limited area atmospheric models. Since statistical downscaling methods are based on the statistical relationships determined

for the present which might not be hold for the future and cannot account for possible systematic changes in regional forcing conditions or feedback processes (IPCC, Scientific Basis, 2007), the dynamical downscaling with regional climate models (RCM) is often favored to empirical statistical downscaling. It has been shown that the downscaling results of regional climate models reveal more realistic climatological distribution compared with the GCM outputs. Besides, they provide spatially detailed and coherent fields since the dynamic model ensures spatial persistence of large-scale atmospheric features [14].

The typical resolutions of the regional climate models range between 30 km and 60 km depending on the resolution of the forcing reanalysis products and general circulation models [6, 8, 9, 15, 16]. However, the regional climate models with these resolutions do not perform well especially over complex topography, and relatively large biases between regional climate models and observations might still be present. Particularly, the small-scale distributions of daily precipitation are highly affected by model resolution and parameterization schemes selected. Therefore, there is a need to have finer resolution simulations to study the impact of the climate change. The general approach is to use double nested simulations.

However, even finer resolution regional climate models are subjected to considerable biases when comparing the simulated climate at present with the corresponding observations. The accuracy of RCM shows seasonal and regional dependences. Biases in products of GCMs and RCMs lead many researchers to avoid direct use of climate model outputs for climate impact studies e.g. in hydrology. If the region of the study has complex topography and land-sea contrast, adjustments of the simulations are required to reproduce local climate characteristics. Therefore, several bias correction methods ranging from simple scaling to sophisticated distribution mapping have been proposed in literature within the last decade. The aim is to correct the biases in the climate model outputs by using statistical properties obtained from observations for the same period of time. Hence the representation of the fields such as precipitation time series generated by regional climate models is further improved [14, 17–19].

In this study, the selected three bias correction approaches were applied to high and low resolution precipitation products of regional climate model, RegCM over Turkey under the recent past climate conditions in daily, monthly and seasonal periods. Then,

the spatial variability of the performance of these bias correction methods are evaluated for the last 10 years of simulations.

This thesis is organized as follows: In the succeeding subsection, the literature survey regarding the objectives of the research is presented and the selection of the methodology is discussed. Section 2 describes the methodology and the data for regional climate modeling and verification. Section 3 and 4 explains the experiment design and the model precipitations climatology for two different resolutions and two different land surface models, respectively. Bias corrections methods and applications to the model simulations are given in Section 5. The last section discusses the results and conclusions.

1.1 Literature Survey

Ju Li-Xia et al. (2006) tested the results of RegCM2 driven by IAP-AGCM GCMs, which is a global grid-point model developed by Institute of Atmospheric Physics, Chinese Academy of Sciences, over East Asia at 60 km resolution. They used different convective parameterizations to study the biases on climate parameters. The surface air temperature and precipitation simulations of two models are compared with CRU observation data. RegCM2 was good at modeling the spatial distribution and seasonal cycle of temperature fileds. However biases in precipitation is relatively larger than the global model [16].

Önol, B. (2012) simulated the annual temperature and precipitation by RegCM3 with 10 km resolution by downscaling 50 km to see high-resolution model performance for the coastal region over Eastern Mediterranean (EM). Due to resolving steep topography over the coasts, strong temperature gradients have been seen in the simulation of high resolution. After comparing the simulations with the coastal meteorological stations over Black Sea and Mediterranean region, both 50 km and 10 km simulations, they showed cold temperature biases when the annual precipitation errors are about 17% and 40% [20].

Zhenming, J. et al (2012) investigated the climate change over the Tibetan Plateau using double-nested dynamically downscaling approaches by RegCM4. Even the simulations of the coarser domain can capture the spatial and temporal distributions,

the nested domain shows more spatial details within the high resolution surface temperature results. Due to solving the topographic conditions well, the nested domain simulated the temperature better than mother domain, when comparing to the observations. However, the model cannot simulate the precipitation as well as temperature [21].

Christensen et al. (2008) simulated an ensemble of thirteen RCMs driven by ECMWF ERA40 over the entire Europe with 25 km high resolution. After the twenty-five percent warmest and wettest months and their climatic conditions are examined, different systematic biases are determined for each model after comparison to the mean of high-resolution gridded observational data set. The model overpredicted warm summers in southeastern Europe, as well as the precipitation is overestimated in northern Europe. The importance and the requirement of the bias correction applications have been emphasized for each individual model depending on the models' performances [22].

Piani et al. (2010) investigated the effectiveness of statistical bias correction for the application of hydrological models. Daily precipitation and temperature simulations of ECHAM5 were used to implement the bias correction methods. To test the approach, the last 50 years of the observed hydrological data set provided by the EU project WATCH was used. After the application of Quantile Mapping correction, the results demonstrated an obvious improvement for both the mean and variance of the variables [13].

Chen et al. (2011) weighted three sources of the uncertainty, such as the selections of the GCMs, future greenhouse gas concentration scenario and the decade to apply the bias correction parameters to demonstrate their inter-annual variability. They focused on total precipitation over ten large catchments, which have different climate. 24 different bias corrected total precipitation and mean temperature variables are evaluated and WATCH bias correction method is performed to generate the future daily precipitation data. When three different uncertainty sources are compared, the selection of bias correction decade approach provided the smallest contribution, whereas the other two sources gave larger contributions. They also indicated that instead of 10 years, if the all period of 40 years were used to correct, the results would be better to reduce the bias [19].

Berg et al. (2012) compared different bias correction methods applied to the dynamically downscaled from the boundary conditions of 50 km coarser domain to 7 km high-resolution RCM COSMO-CLM (COSMO model in CLimate Mode) simulations over Germany and also Alpine mountain region. 1 km gridded HYRAS data set from German Weather Service (DWD), was used as a reference data for bias corrections and to validate the RCM simulations. The annual mean temperature is underestimated for the calibration and validation period. Although MV method corrects the only mean value and expected not to give a good performance for the extreme values, the results of the MV and QM methods are nearly similar for temperature. Precipitation is overestimated for the calibration and validation period. When MV methods corrected the precipitation about 0.4%, QM corrected 2% [23].

Argüeso et al. (2013) compared high resolution (2 km) precipitation simulations of WRF with the gridded and in situ observational data sets over Sydney. The high-resolution domain (2 km) was downscaled by 10 km domain, which was downscaled from 50 km resolution of the mother domain. For each grid point, Quantile mapping method was applied to correct the errors of simulations. They suggest that the gridded data sets were suitable to correct high resolution model at seasonal or monthly timescales, but they were inappropriate to correct at daily timescales. The Quantile mapping method was more efficient at seasonal timescales and it has been proven by this study to reduce the seasonal biases of precipitation significantly [24].

Dobler et al. (2008) used Climate Limited-area Model (CLM) as a dynamical downscaling method (DDM) and two statistical downscaling methods (SDMs) in two domains, Europe and South Asia, to test the performance of the dynamical and statistical models over different orographic and climatological regions. Daily precipitation fields over the European and South Asian regions are simulated using CLM with 50 km resolution forced by ERA-40 re-analysis data. For every observation grid, bias correction methods are applied to CLM simulations namely Local Intensity Scaling (LOCI) and Gamma quantile distribution mapping (GAMMA) which are based on two SDMs. The implementation of the bias correction methods revealed that the performance depends on the model domain. Even though CLM simulations after correction are in good agreement with the observations over European domain, the performance of the correction methods are in question for the South Asia domain. As

a result of bias correction, Gamma quantile distribution mapping method reveals better performance than LOCI [11].

Piani, C. et al. (2010) designed and performed a distribution based bias correction method (quantile mapping) to the ENSEMBLES climate model precipitation data set, which is provided by HIRHAM5 with 25 km spatial resolution, over Europe. Results indicate that the performance of the distribution based bias correction method is well at not only the mean correction, but also at the other moments for drought and heavy precipitation index [25].

Themeßl et al. (2011) attempted to reduce the errors of RCM MM5 daily precipitation simulations, applying the linear and nonlinear empirical-statistical downscaling techniques with bias correction methods. They used seven empirical-statistical downscaling and error correction methods (DECMs) to 10 km high-resolution RCM simulations, which were driven by ERA-40 re-analysis boundary conditions over the Alpine region. They performed direct DECMs, which are Local Intensity Scaling (LOCI) and Quantile Mapping (QM), and Multiple Linear Regression (MLR), Multiple Linear Regression with Randomization (MLRR), the Analogue Method (AM) and the Nearest Neighbor Analogue Method (NNAM) as indirect DECMs, for each observational station separately. As a result, they found that Quantile Mapping indicates the best performance with high percentile and can be favorable for extreme precipitation events [12].

Bordoy et al. (2012) corrected the bias of RegCM3 simulation, which were driven with 25 km resolution in Rhone catchment where is characterized as highly complex orography. Automatic weather station observations provided by MeteoSwiss were used to compare with the simulations of RegCM3 on a monthly basis. The study was about to represent the performance of the nonlinear bias correction method at highly complex orography. In spite of the large spatial and temporal variability, the nonlinear bias correction method significantly improves the mean and the probability distribution for both variables regarding the evaluation period over the entire domain [17].

Chen, J. et al. (2013) evaluated the performance of six bias correction methods for hydrological modeling using four regional climate model simulations which are modeled with 50 km spatial resolution. Four RCMs that Canadian Regional

Climate Model (CRCM), Hadley Regional Model 3 (HRM3), Regional Climate Model 3 (RCM3) and Weather Research & Forecasting model (WRFG) are run by the National Center for Environmental Prediction (NCEP) reanalysis data over North America. Six bias correction methods such as Linear Scaling (LS), LOCI, Daily Translation (DT), Daily Bias Correction (DBC), Quantile Mapping based on Empirical distribution (QME) and Quantile Mapping based on Gamma distribution (QMG) are performed on a monthly basis. As a result, all six bias correction methods, especially distribution-based methods are able to enhance the RCM simulations with the dependency on the choice of watershed locations. They emphasized that the simulation of temporal structure of precipitation is very important particularly at the daily scale [26].

Lafon et al. (2013) compared the performance of four common bias correction techniques, which are linear, nonlinear, gamma-based quantile mapping and empirical quantile mapping, using the daily precipitation simulations of HadRM3-PPE-UK (Hadley Centre Regional Model Perturbated Physics Ensemble) over Great Britain at approximately 25 km resolution. The results showed that, when the distribution of the observed and modeled precipitation data are suitable for gamma distribution, the gamma-based quantile mapping method gives the best accuracy and robustness. Otherwise, the nonlinear correction method is the most effective to reduce the bias, and the linear correction method is the least sensitive to the selection of the calibration period. Meanwhile, the empirical quantile mapping technique is very sensitive to the selection of the calibration period as well, even if it is capable to correct the model results in high accuracy [14].

In this study, double-nested dynamic downscaling method are used and 10 km precipitation simulations are obtained by 50 km. Firstly, the model capability are evaluated by comparing with CRU observational data set. Then, both simulations are corrected with the station-based precipitation observations using two common bias correction methods, which are linear Mean Value (MV) and distribution-based Quantile Mapping (QM) as mostly preferred in the literature. After completing the calibration of first 20 years between 1971-1990, the last 10 years, 1991-2000 are validated. Finally, the three evaluation metrics such as the Spearman rank correlation, the Root Mean Square Error (RMSE) and the Nash-Sutcliffe Efficiency (NSE) are

applied to the modeled, corrected simulations and observed precipitation to be able to interpret the RegCM and correction methods performance.

2. DATA AND METHODOLOGY

2.1 Observation Data

Two observational precipitation data sets were used in this study in order to analyze the performance of the model, to validate precipitation simulations and to statistically correct the precipitations biases for the coarser and the finer domains. They are Climate Research Unit gridded precipitation data set and observed precipitations at the meteorological stations in Turkey.

2.1.1 Climate Research Unit (CRU)

The gridded observational data sets CRU TS3.1 provided by the Climate Research Unit (CRU) of University of East Anglia cover the global land surfaces. The CRU TS3.1 data set has a regular 0.5° grid spacing, includes monthly variables for the period of 1901–2009. These high-resolution data sets contain eight climatic variables; cloud cover, diurnal temperature range, Potential Evapo-Transpiration (PET), daily mean temperature, monthly average daily minimum and maximum temperature, vapor pressure, and precipitation. The CRU TS3.1 data sets are one of the best available consistent long-term gridded observational records used observations of more than 4000 weather stations distributed around the world [27–29]. The stations' coordinates of CRU to generate the gridded data set for the study domain are shown in the Figure 2.4.

2.1.2 Turkish State Meteorological Service (TSMS)

The station-based observational data set taken from Turkish State Meteorological Service, was used in the present study. A total of 245 meteorological stations, shown in Figure 2.5, were selected based on the completeness of the records. At most 20% of the daily precipitation observations are missing in the selected stations. The data for the time periods spanning 1971-1990 (20-year period) are used to estimate the bias

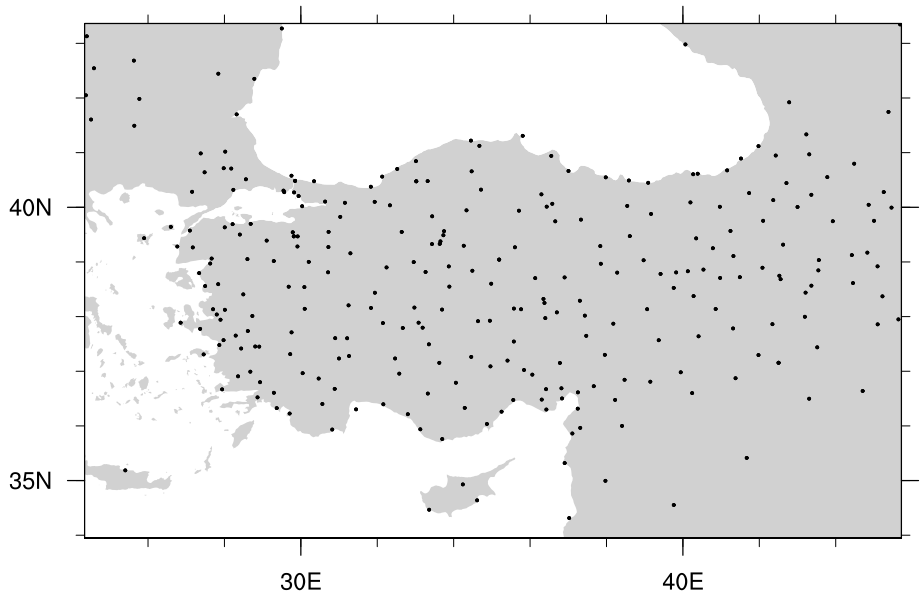

Figure 2.1: Station coordinates of CRU data set.

correction factor and for 1991-2000 (10-year period) to validate the bias correction method.

2.2 Regional Climate Model

The first version of the model, RegCM1, was generated from the Mesoscale Model version 4 (MM4) by the National Center for Atmospheric Research (NCAR), Boulder, Colorado, USA in the late 1980s [30]. RegCM has the dynamical component of MM4 and it is a compressible, finite difference model with vertical σ-coordinates. A split-explicit time integration scheme is used with diminishing horizontal diffusion algorithm of the steep topographical gradients [31]. In the early 1990s, RegCM was upgraded to RegCM2 which was the second generation version of the model [31] and based upon the hydrostatic version of MM5 [32]. The improvements were done on the dynamics of the model and also the physics of the model. In the late 1990s, Giorgi and Mearns upgraded RegCM2 to RegCM2.5 [15] which included with the updates for physical components and a simple aerosol module [33]. The first enterprise of the RegCM was also from the atmospheric component to the other Earth system components [34, 35].

The RegCM system moved to the Earth System Physics Group of the Abdus Salam International Centre for Theoretical Physics (ICTP), in Trieste, Italy in the early 2000s and they improved RegCM2.5 to RegCM3 in the mid-2000s [36]. RegCM3 was easier

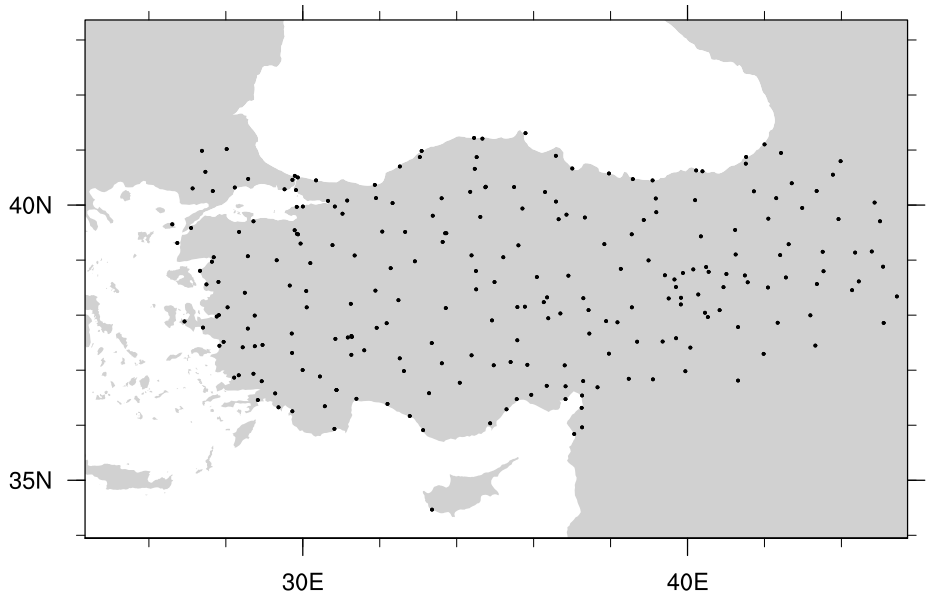

Figure 2.2: Station coordinates of TSMS observations.

to use compared to the previous versions and run in different platforms. And also the increasing use of the new version of the model were targeted for scientific studies in many developing countries [37]. In the latest version, the RegCM (RegCM4) contains interactive user interface for online coupling with chemistry/aerosol, lake, ocean and biosphere model components and also it is more flexible, more portable, and easier to use than the previous versions [2].

Nowadays, the RegCM system developers target the usage of the model in developing countries in spite of the fact that it has been aimed to be a community model at the beginnings [38]. The model has been implemented for wide variety of studies, such as regional climate change projections, paleoclimate studies, land-atmosphere and chemistry/aerosol-climate effects, hydrological studies, agriculture impacts for more than 25 years and in more than 60 countries. Also, the number of publications has been increased during last decade, especially over the domains of developing countries [15, 37].

The RegCM model has been simulated for all land areas, except the polar regions, from sub-regional to continental sizes; from seasonal to centennial periods and the resolutions ranging from 10 to 100 km. The different sets of observational data (ERA40, NCEP, ERA-Interim) and also different GCMs (the MPI-ECHAM5, NCAR-CCSM, HC-HadCM/HadGEM, etc.) outputs can be used as initial and lateral boundary conditions by the model. The new release of RegCM model, which is

RegCM4, can be driven as a new feature in full tropical band mode [39], that means the model can be used for the tropical processes.

The near future plan is improvement of the dynamical core of RegCM since very high resolution applications are needed for the hydrological studies. Nowadays a new non-hydrostatic dynamical core is being developed for the next version of RegCM; furthermore the cloud microphysics and aerosol microphysics are also being improved, as a precondition of very high resolution applications, too. Consequently, a fully coupled Regional Earth System Model with the other components of the climate system, such as biosphere, ocean, hydrology, and human health, is being developed as a long-term purpose of the RegCM system [38].

In this study, two options of Land Surface Model Scheme, Biosphere-Atmosphere Transfer Scheme [40] and Community Land Model [41] are simulated to evaluate the model performace. The biases of both simulations are compared for the mother domain. Land Surface Model Scheme (LSM) is designed to simulate the energy fluxes and the exchange of surface water at soil-atmosphere interface. The LSM resolves the water balances, radiation and energy. Over the past several decades, land surface parametrizations have been improved [42]. When the first generation models have used the aerodynamic bulk transfer formulas to be able to consider the soil moisture variability [43], the second generation models have described the vegetation and its impacts on the radiation, momentum transfer and evapotranspiration [44]. The Biosphere-Atmosphere Transfer Scheme (BATS) [40], is an example of a second-generation model. In the third generation models, such as Community Land Model (CLM) [41], a linked photosynthesis-stomatal conductance model has been added to simulate the observed relationship between photosynthesis and transpiration, realistically.

2.2.1 Biosphere-Atmosphere Transfer Scheme (BATS)

BATS is a default surface package of RegCM, which is designed to define the vegetation such as evapotranspiration, leaf temperature and phenology, and hydrology such as interactive soil moisture, runoff and snow in the surface-atmosphere exchanges of momentum, water vapor and energy [40]. BATS has one vegetation layer, one snow

layer, one surface soil layer of 10 cm thick or root zone layer of 1-2 m thick, and a third deep soil layer of 3 m thick shown in Figure 2.1.

Generalized Deardoff's force-restore (1978) method was used to solve prognostic equations for the soil temperatures. Sensible, radiative and latent heat fluxes are included in the energy balance formulation to be able to diagnose the temperature of the canopy and canopy foliage. In the latest version of RegCM, the subgrid variability of topography and land cover with mosaic-type approach were added to BATS in order to adopt a regular fine-scale surface subgrid for each coarse model grid cell [45]. In RegCM4, two new land use types, urban and sub-urban environments, were added to BATS. Urban development adjusts the surface albedo, changes the surface energy balance and also generates impervious surfaces with large effects in runoff and evapotranspiration [5, 38].

2.2.2 The Community Land Model (CLM)

CLM is the optional land surface model developed by the NCAR as part of the Community Climate System Model (CCSM). Version 3.5 of CLM was coupled to RegCM to obtain more detailed land surface description. CLM is based on BATS and the snow model from Chinese Academy of Sciences Institute of Atmospheric Physics Land Surface Model. In order to describe the land- atmosphere exchanges of water, momentum, energy and carbon, a series of biogeophysically-based parameterizations have been used, illustrated in Figure 2.2. Five possible snow layers, ten unevenly spaced soil layers of temperature, liquid water and ice water in each layer are defined in CLM. To capture the surface heterogeneity, CLM uses a tile or mosaic approach to account land surface complexity within a climate model grid cell. Each CLM grid cell area is divided into five sub-grid hierarchy of land units, which are glacier, wetland, lake, urban and vegetated land cover. Each land units can have a different number of columns (second sub-grid hierarchy, snow/soil columns) and each column can have multiple plant functional types (third sub-grid hierarchy, different vegetation fractions) shown in Figure 2.3. For each land cover type, hydrological and energy balance equations are solved [38].

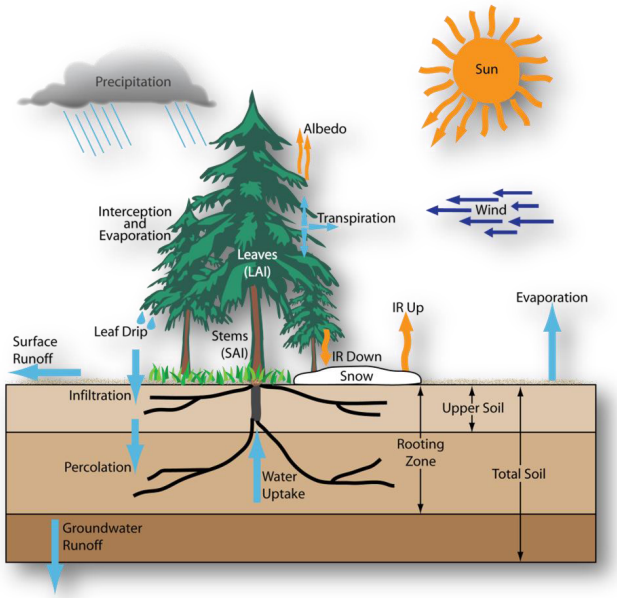

Figure 2.3: Schematic illustration of processes included by BATS model. [3]

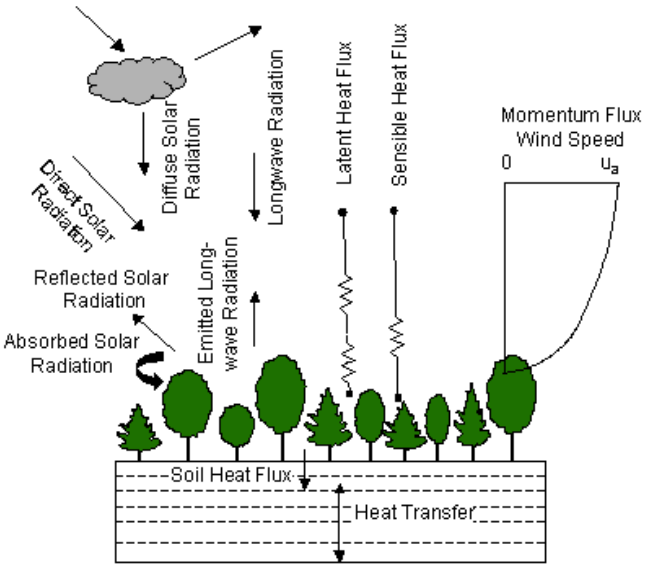

Figure 2.4: Biogeophysics - energy, moisture, momentum. [4]

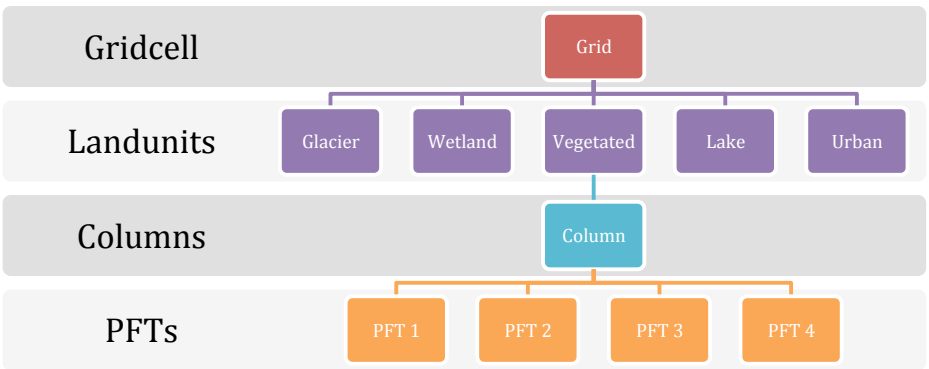

Figure 2.5: CLM sub-grid hierarchies [5].

2.3 Bias Correction

Bias correction methods are frequently applied to global or regional climate model simulations in the climate impact studies to reduce the systematic deviations of the model from observations. Most of the bias correction studies focus on precipitation correction, because the physical characteristics of precipitation make the simulations more difficult. This study presents the implementation of bias correction approaches to RegCM4.3 precipitation simulations for double nested domains with 50 km resolution (mother domain) and 10 km high resolution (nested domain).

In order to correct the errors and the uncertainty of climate models with the coarse spatial resolution, several techniques are applied in the literature [7, 17, 24]. In this study, two direct-point wise techniques are used. Mean Value (MV) Correction [46,47] and Quantile Mapping (QM) Correction [11, 12, 14, 23] methods are implemented independently for each grid cell. Mean Value Corrections are found by using the first 20 years of daily and monthly total precipitation simulations. On the other hand, Quantile Mapping Corrections are found again by using the first 20 years of daily simulations and seasonal precipitation. The applications of both methods are shown in Figure 2.6. For each resolution, the nearest grid point to the station location is selected to compare the simulated and observed precipitation.

2.3.1 Mean Value (MV) bias correction

The simplest method to correct the mean bias of the model is Mean Value Correction. In this approach, it is assumed that the modeled time series is only affected by a linear error. This error can be corrected by simply rescaling the simulations with daily and monthly MV corrections so that the relative change in precipitation as described by the regional climate model is preserved [48]. A multiplicative approach is chosen for the precipitation data to ensure positive precipitation values.

In this approach, the mean values are calculated from daily time series of model $(mod(t_1), mod(t_2), \ldots, mod(t_n))$ and from daily observed values

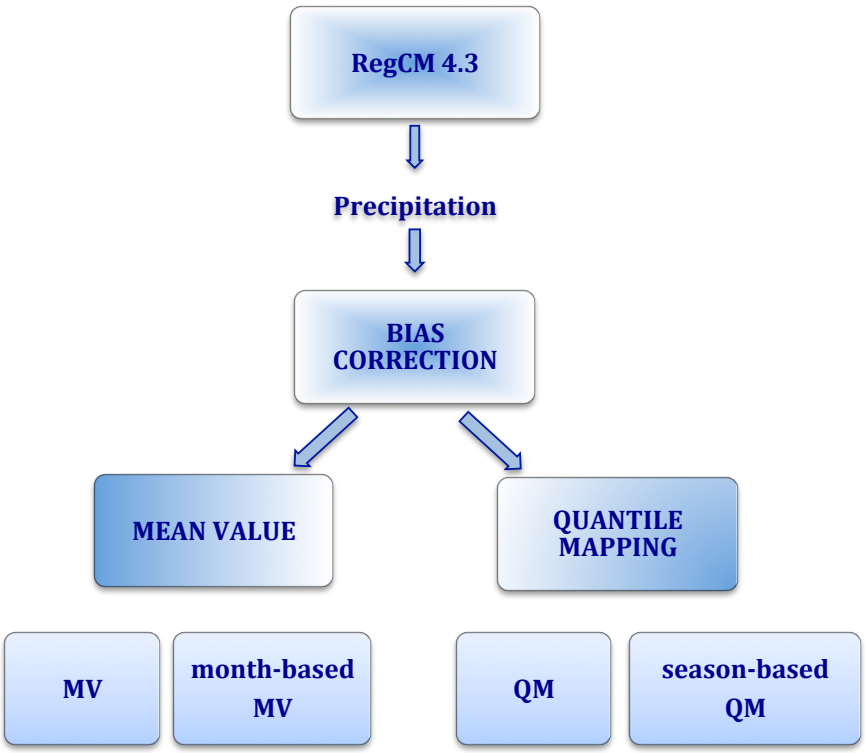

Figure 2.6: Bias correction methods.

$(obs(t_1), obs(t_2), \ldots, obs(t_n))$. After obtained mean values of observation,

$$\overline{obs} = \frac{1}{n}\sum_{t=1}^{n} obs\,(t) \tag{2.1}$$

and model,

$$\overline{mod} = \frac{1}{n}\sum_{t=1}^{n} mod\,(t) \tag{2.2}$$

correction (rescaling) factor (q) is computed by dividing the two mean values.

$$q = \frac{\overline{obs}}{\overline{mod}} \tag{2.3}$$

Then, for each time step, the modeled precipitation value is corrected by multiplying it with the correction factor, q [48].

$$modcor\,(t) = q * mod\,(t) \tag{2.4}$$

To converge the annual variability of the model to the observations, correction (rescaling) factors are calculated for each month separately. For the same time period, every month's correction factors are computed as a ratio of the mean observation to the mean of the model simulation at each station points. Let "mon" denotes $january, february, \ldots, december$, the monthly means of observations and model

simulations are

$$\overline{obs_{mon}} = \frac{1}{n}\sum_{t=1}^{n} obs\left(mon\left(t\right)\right) \tag{2.5}$$

$$\overline{mod_{mon}} = \frac{1}{n}\sum_{t=1}^{n} mod\left(mon\left(t\right)\right) \tag{2.6}$$

and the monthly correction factor (*qmon*) is

$$q_{mon} = \frac{\overline{obs_{mon}}}{\overline{mod_{mon}}} \tag{2.7}$$

Afterward for each month, monthly-corrected value is obtained via

$$modcor\left(mon\right) = q\left(mon\right) * mod\left(mon\right) \tag{2.8}$$

Comprehensibility and applicability are the main advantages of Mean Value Correction method. It also does not require computational effort because the correction factor is only computed ones for each month. Since extreme values contribute to the mean of the time series, the assumption of a linear model error leads to problems in the extreme precipitation. If the simulated precipitations are very low and observations are extremely high at grid points, the correction factor can be extremely high. Then, the application of the multiplicative correction factor results in very high daily precipitation values leading to unrealistic precipitation. In these situations, another correction method, Quantile Mapping has a better response to correct extreme values [48].

2.3.2 Quantile Mapping (QM) bias correction

Quantile mapping correction, which is a popular post-processing approach ([49], also named as quantile matching, cumulative distribution function matching, histogram equalization) is an adaption of the modeled time series frequency distribution to the distribution of the observed values. This method is able to correct errors in variability by correcting the shape of the distribution. However, the quantile-based approach has been recently used for RCMs in order to correct model errors [11,13]. It was originated from the empirical transformation of Panofsky and Brier (1968) and had been applied to the hydrological studies successfully [50,51].

Quantile mapping methods are relied on point-wise and empirical cumulative distribution functions (ecdfs; Wilks, 1995) of modeled and observed data set. To

implement QM method, the best fitted cumulative distribution functions are estimated. Choosing the suitable distribution for each modeled and observed precipitation, Maximum Likelihood Estimation (MLE) and Goodness-Of-Fit (GOF) tests are applied. Most of the QM correction studies usually use only Gamma Cumulative Distribution Function (CDF) without determining the best-fitted distribution functions for precipitation field. Gamma distribution often provides a good fit, because distribution of precipitation variable is characterized by a Gamma distribution for most of the cases. In this study, five different distribution functions are tested to identify best fit: Gamma, Exponential, Weibull and Generalized Pareto. In this study, QM correction method is applied by using both the best fitted distribution and the Gamma Distribution, and the results are compared to each other.

A probability density function (PDF) is mostly associated with the univariate distributions. When X represents the random variable of the model and x stands for a specific time step, the probability density function f_x [52],

$$P[a \leq X \leq b] = \int_a^b f_x(x)\, d_x \tag{2.9}$$

where,

$$f_x(x) \geq 0,$$

$$\int_{-\infty}^{\infty} f_x(x)\, d_x = 1,$$

$$P(a < x < b) = \int_a^b f_x(x) d_x$$

The cumulative distribution function (CDF) $F_x(x)$ of a continuous random variable X with density function $f_x(x)$ is

$$F_x(x) = P(X \leq x) \tag{2.10}$$

$$F_x: \quad R \rightarrow [0,1]$$

The right hand side of the equation shows the probability of the random variable X, which takes a value less than or equal to x. The cumulative distribution function, F_x can also be represented as the integral of its probability density function f_x as [52],

$$F_x(x) = \int_{-\infty}^{x} f_x(t)\, dt \tag{2.11}$$

for $-\infty < x < \infty$ and if f_x is continuous at x, PDF can be determined by deriving of the CDF,

$$P(a < x < b) = F(b) - F(a) \tag{2.12}$$

and

$$f_x(x) = \frac{d}{d_x} F_x(x) \tag{2.13}$$

The empirical distribution functions are obtained by theoretical parametric distributions to compare the modeled and observed data. The probability of the theoretical parametric distribution, $F_x(x)$ is determined via Formula (2.1). In order to calculate related value of the distribution function, the cumulative distribution of observation $F_y(y)$ is compared to the result of the cumulative distribution $F_x(x)$ at the point [52], [48]

$$F_y(y) = F_x(x) \tag{2.14}$$

(see Figure 2.7). Using the probability density function (PDF) for X, the long-term average outcome of a random variable, which is called the Expected Value, can be estimated. Expected Value is a mathematical equivalent of a weighted average of all possible values of X over the long-term. The expected value of X is

$$\mu = E(X) = \int_{-\infty}^{\infty} x f_x(x)\, d_x \tag{2.15}$$

The expected value (mean) of a random variable X, describes where the probability distribution is centered, but it does not give an adequate description of the shape of the distributions. Therefore, the estimation of variability of the random variable X, called variance, becomes more important measure in statistical studies. The variance of the probability distribution of X is

$$\sigma^2 = E\left[(X-\mu)^2\right] = \int_{-\infty}^{\infty} (x-\mu)^2 f_x(x)\, d_x \tag{2.16}$$

The positive square root of the variance gives standard deviation, σ, of X [52].

2.3.2.1 Normal distribution

In statistic, there are countless distribution functions to describe the Cumulative Distribution Function or Probability Density Function. The most important continuous probability distribution, called Normal distribution (or Gaussian distribution) has a special role in meteorological parameters. The mathematical equation for the

probability distribution of the normal variable depends on the two parameters: its expected value (mean) μ and standard deviation σ. The density of the normal random variable X is

$$N(x;\mu,\sigma) = \frac{1}{\sqrt{2\pi\sigma}} \quad e^{-\frac{1}{2\sigma^2}(x-\pi)^2} \tag{2.17}$$

for $-\infty < x < \infty$ where $\pi = 3.14159...$ and $e = 2.71828....$ [52] There are also numerous probability distributions to solve many problems in engineering and science. The Normal, Gamma, Exponential, Weibull and Generalized Pareto probability density functions are also used in this study to estimate the best-fitted distribution.

2.3.2.2 Gamma distribution

For the continuous random variable X, the density function of the gamma distribution with the shape parameter, σ, and the scale parameter, β, is defined by

$$\alpha = \left(\frac{\mu}{\sigma}\right)^2,$$

$$\theta = \frac{\sigma^2}{\mu},$$

$$f(x;\alpha,\beta) = \begin{cases} \frac{x^{\alpha-1}e^{e^{-x}/\beta}}{\beta^{\alpha}\quad \Gamma(\alpha)}, & x > 0 \\ 0, & \text{elsewhere} \end{cases} \tag{2.18}$$

where $\alpha > 0$ and $\beta > 0$.

2.3.2.3 Exponential distribution

The Exponential distribution is the special case of the gamma distribution, when the shape parameter of gamma distribution equal to 1 ($\alpha = 1$), the exponential distribution is

$$f(x;\beta) = \begin{cases} \frac{1}{\beta}e^{-x}/\beta, & x > 0 \\ 0, & \text{elsewhere} \end{cases} \tag{2.19}$$

where $\beta > 0$.

2.3.2.4 Weibull distribution

In recent years, Weibull distribution has been used to deal with such problems. The density function of Weibull distribution is given by

$$f(x;\alpha,\beta) = \begin{cases} \alpha\beta x^{\beta-1}e^{-\alpha x^{\beta}}, & x > 0 \\ 0, & \text{elsewhere} \end{cases} \tag{2.20}$$

where $\alpha > 0$ and $\beta > 0$.

2.3.2.5 Generalized Pareto distribution

Generalized Pareto distribution is used to determine the best fitted distribution. When γ is the location parameter of generalized pareto distribution, the density function is [52]

$$f(x;y,\alpha,\beta) = \left(\frac{1}{\alpha}\right)\left(1+\gamma\left(\frac{(x-\beta)}{\alpha}\right)\right)^{-1-\frac{1}{y}} \tag{2.21}$$

where $\sigma > 0$ and $\beta > 0$ and $\gamma \leq x \leq \gamma$ - α/β when $\beta < 0$.

In order to find possible candidates for a suitable fit, Maximum Likelihood Estimation (MLE) is applied to evaluate the best-fitted distribution parameters. In the use of statistical methods in the atmospheric science, Maximum likelihood estimation is one of the most important approaches [53].

The density function of $x1, x2, .., xn$ of the random variable X, is $f(x1, x2, \ldots xn; \varphi)$. Given values $Xi = xi$, where $i = 1, \ldots, n$, the likelihood of φ as function of $x1, x2, \ldots xn$ is defined as

$$L(\varphi) = f(x1, x2, ...xn; \varphi) \tag{2.22}$$

The maximum likelihood estimate (MLE) of φ is the value of φ that maximizes the likelihood, which makes the data "most likely" (or "most probable").

The density function can be considered as the product of the marginal densities, and the likelihood is

$$L(\varphi) = \prod_{i=1}^{n} f(Xi; \varphi) \tag{2.23}$$

The principle of maximum likelihood provides the estimator of $\hat{\varphi}$ that the most likely data and MLE is [53]

$$L(\hat{\varphi}(x)) = max_{\varphi} L(\varphi, x) \tag{2.24}$$

In order to check the quality of fits, the Goodness-Of-Fit (GOF) tests, Akaike and Bayesian Information Criteria (AIC and BIC) are applied and they are defined as

$$p_{AIC} = 2k - 2\ln(L) \tag{2.25}$$

and

$$p_{BIC} = k\ln(N) - 2\ln(L) \tag{2.26}$$

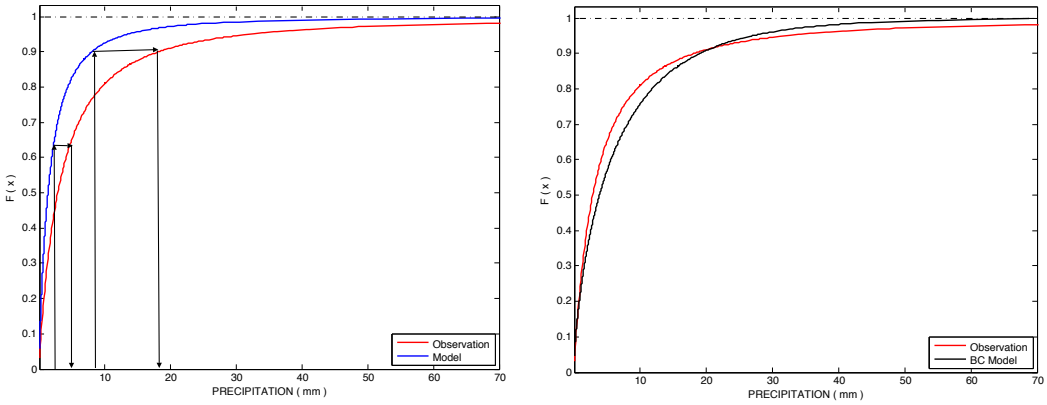

Figure 2.7: Schematic of the Quantile Mapping (QM) bias correction.

respectively, where k is the degrees of freedom, N is the sample length and L is the value of the maximized likelihood function of the estimated model. Finally, the smallest values of AIC or BIC are chosen as the best fitted distributions of model and observation [48].

The AIC criterion results confirm that Generalized Pareto distribution is the best fitted distribution for 172 stations out of 245 stations to the modeled precipitations, whereas Weibull distribution is the best fitted distribution for 187 stations out of 245 to the observed precipitation (The AIC criterion results of modeled and observed stations are illustrated in Appendix A.1). Therefore, for a specific time step t, the modeled precipitation data is corrected with Quantile mapping approach by the relationship given in Formula (2.27)

$$mod_{cor}(t) = F_{obs}^{-1}\left(F_{mod}\left(mod(t)\right)\right) \tag{2.27}$$

where F_{mod} is the Generalized Pareto CDF of modeled variable and F_{obs}^{-1} is the inverse Weibull CDF (or quantile function) corresponding to observed variable.

The CDF functions of modeled data and observation can be determined for each month separately, in order to account the seasonal variations in type and shape of the univariate precipitation distributions. Hence, monthly quantile mapping correction algorithm can compensate the uncertainty of the annual variability of model result.

In different ranks of the data, Quantile Mapping correction is able to correct errors dynamically, well (see Figure 2.7). Even if it has a remarkable advantage, the distribution of model precipitation is changed dramatically [48].

The frequency of extremes of observations and their maximum intensity are limited to the overall maximum in the past observation period. These limitations can create considerable problem for the climate projections, which have adopting the Quantile mapping approach since the frequency of extreme events and their intensity might change in the future climate projections [48].

2.4 Validation Measures

Evaluating the model performance is very important to obtain how well the model simulates the mean and variance of the simulated variables compared to observations. There are numerous measures to quantify this relationship. The most common validation measures are Kendall rank correlation, Spearman rank correlation, Akaike and Bayesian Information Criteria, Pearson Correlation, Absolute mean error and Root Mean Square Error.

After the bias correction calculations, the ability of the RegCM simulations and the efficiency of bias correction methods are tested with three quantitative validation measures for the validation period of 1991 - 2000. The model precipitation simulations, which have been downscaled to the station coordinates, were corrected with the Mean Value and Quantile Mapping correction methods. Afterward, the corrected results are tested using cross-validation techniques for each 245 observational stations. Three validation measures, such as Spearman rank correlation (ρ), Root Mean Square Error (RMSE) and Nash-Sutcliffe Efficiency (NSE) are used in this study and their equations are shown in Table 2.1.

2.4.1 Spearman rank correlation (ρ)

To compare the model and corrected model with station observation data Spearman rank correlation coefficients are calculated. Spearman rank correlation is a measure of the association between two comparable variables. The equation is defined at Table 2.1, where d represents the difference between ranks and n represents the number of observations or model variable. Its range is between +1 and -1, where plus one corresponds to a perfect association of ranks, 0 indicates no association between ranks,

Table 2.1: Validation measures.

Abbreviation	Formula	Range	Perfect Fit
ρ	$1-\frac{6\sum d_i^2}{n(n^2-1)}$	$[-1,1]$	$\lvert\rho\rvert=1$
$RMSE$	$\sqrt{\frac{1}{n}\sum_{i=1}^{n}(o_i-m_i)^2}$	$[0,\infty]$	$RMSE=0$
NSE	$1-\frac{\sum_{i=1}^{n}(o_i-m_i)^2}{\sum_{i=1}^{n}(o_i-\overline{o_i})^2}$	$[-\infty,1]$	$NSE=1$

and -1 indicates a perfect negative association of ranks. The closer ρ is to zero, the weaker the association between the ranks.

2.4.2 Root Mean Square Error ($RMSE$)

Root Mean Square Error is a measure of the average magnitude of the error, which is weighted according to the square of the error. The equation of RMSE is given at Table 2.1. In the RMSE equation, when n symbolizes the number of observations or model variable, o_i and m_i donates the observed and modeled precipitation, respectively. The range of RMSE lies between 0 and infinity, with 0 being a perfect fit.

2.4.3 Nash-Sutcliffe Efficiency (NSE)

Nash-Sutcliffe efficiency (NSE) is one of commonly used criteria as validation measures for hydrological models [54]. NSE is an indicator of the performance of the model to estimate how well the model simulations mimic observations or not. As addressed in RMSE calculations, o_i and m_i stand for observed and modeled precipitation while $\overline{o_i}$ is the mean of the observation. The range of NSE lies between -∞ and 1.0 (perfect fit). When the NSE values are less than zero, the mean value of the observed data are better predictor to use than the model. When NSE values are equal to zero, the modeled data are as accurate as the mean of the observed data. If NSE values are equal to 1, there is a perfect match between the modeled and observed data.

3. EXPERIMENTAL DESIGN

In this study, regional climate model of RegCM is utilized to simulate the present conditions over Turkey and its neighborhood by forcing ERA40 reanalysis data. Two pre-processing steps, Terrain and ICBC, are completed before starting RegCM simulations. Three sets of present conditions are simulated by using different resolutions and land use models.

Terrain is the first step, which defines boundary of the domain with desired grid intervals, and interpolates the elevation and the land use data to the model grids. The United States Geological Survey (USGS) data set was interpolated onto the grid of the mother domain in order to delineate the elevations. Figure 3.1 shows the characteristics of the topography for selected two domains with low and high resolutions.

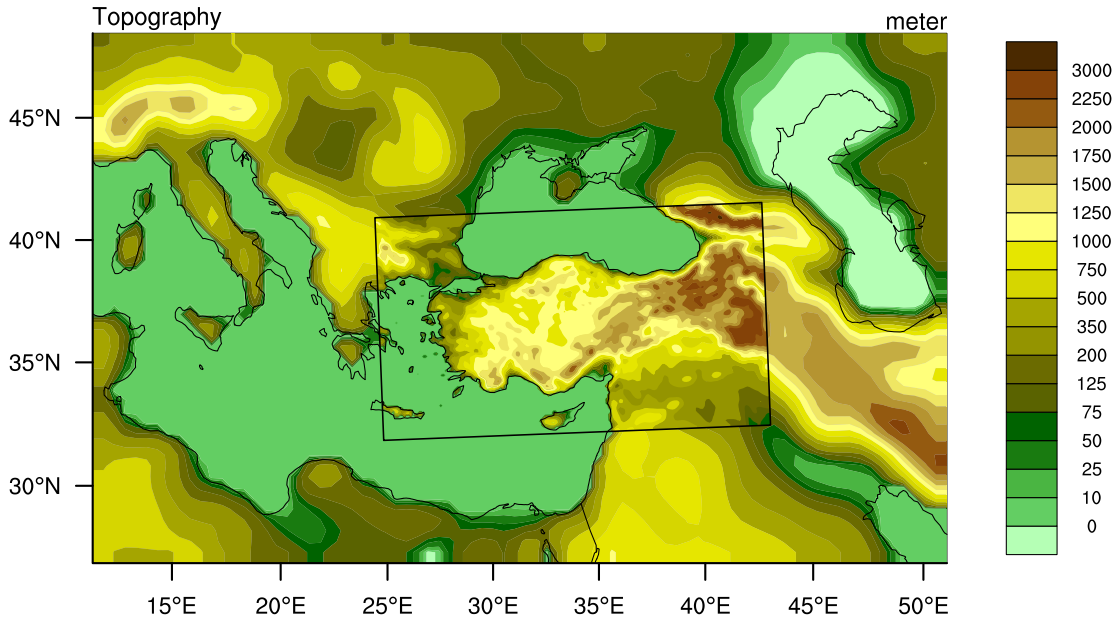

Figure 3.1: Model topography.

For the vegetation/land use data, the mother domain used Global Land Cover Characterization (GLCC) data sets, which were derived from 1 km Advanced Very High Resolution Radiometer (AVHRR) the vegetation/land cover types defined by BATS (Biosphere Atmosphere Transfer Scheme). 22 classes of the land use categories

Table 3.1: Land cover/vegetation classes [1].

1.	Crop mixed farming	
2.	Short grass	
3.	Evergreen needleleaf tree	
4.	Deciduous needleleaf tree	
5.	Deciduous broadleaf tree	
6.	Evergreen broadleaf tree	
7.	Tall grass	
8.	Desert	
9.	Tundra	
10.	Irrigated Crop	
11.	Semi-desert	
12.	Ice cap/glacier	
13.	Bog or marsh	
14.	Inland water	
15.	Ocean	
16.	Evergreen shrub	
17.	Deciduous shrub	
18.	Mixed Woodland	
19.	Forest/Field mosaic	
20.	Water and Land mixture	
21.	Urban	
22.	Sub-Urban	

are used in both mother and nested domains and listed in Table 3.1. Both the elevation and land use data files are available at 60, 30, 10, 5, 3, and 2 minute resolutions. In this study, the topography and land use are interpolated to the model grid points from a global data set at 10 minute resolution.

The second step of the pre-processing is ICBC that generates the initial and boundary conditions from the global data sets. The ICBC program interpolates SST (Sea Surface Temperature) and global re-analysis data to the model grids. For the SST data, the Global Sea-Ice and Sea Surface Temperature (GISST) data were used. GISST is a one-degree monthly gridded data set of sea-surface temperature anomalies and sea-ice coverage fractions covering the period 1947 to 2002 [55]. For the initial and boundary conditions of mother domain, ERA40 data sets with 2.5° x 2.5° grid resolution were utilized. ERA40 is a second-generation re-analysis data set of the global atmosphere and surface conditions produced by the European Centre for Medium-Range Weather Forecasts (ECMWF) in collaboration with many institutions. These input data sets were derived by using many sources of the meteorological observations, such

as radiosonde balloons (since the late 1980s), aircraft observations, ocean-buoyes, satellites-borne instruments (from the 1970s onwards) and scatterometers, and their distribution is shown in the Figure 3.4. RegCM inputs, which are ERA40 re-analysis data sets, cover the period of August 1970 to December 2000 [56]. To drive the model at a higher resolution over subregion, FNEST data that were obtained from the coarse resolution of RegCM simulations were used as initial and boundary conditions.

After pre-processing steps are completed, main model simulations are started using domain file from the Terrain process and ICBC outputs from the ICBC process. When model is run, three main outputs files such as atmosphere, surface and radiation are generated in NetCDF format. The schematic of the model run steps are illustrated in Figure 3.5.

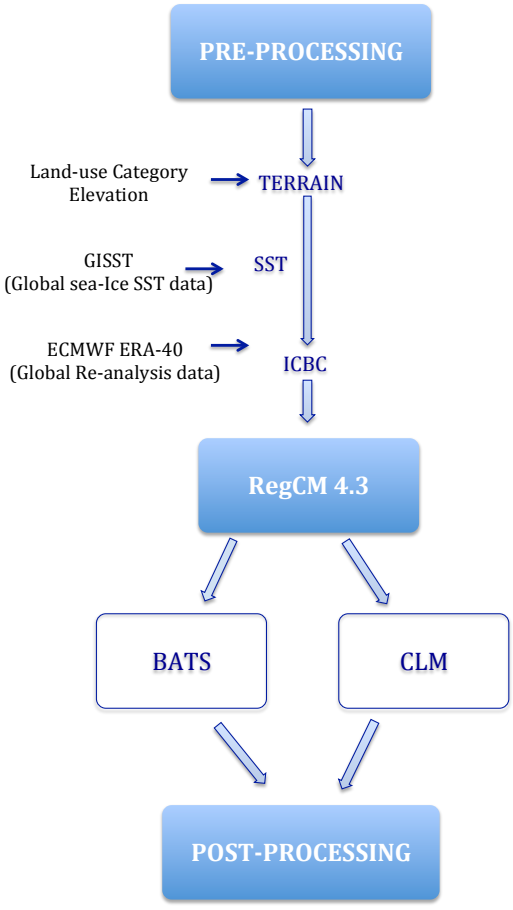

Figure 3.2: Model steps.

In this study, last version of the Regional Climate Model (RegCM 4.3) is adopted using Lambert Conformal projection for two domains. A nest-down approach is applied. The 30-year continuous simulation period ranges from August 1st, 1970 to December 31st, 2000, but analysis of the simulations are started from January

1st of 1971. The first 20-year simulations are chosen as the calibration period and, the last 10-year simulations as the validation period. The physical packages of the model are Holstlag Planetary Boundary Layer (PBL-1990) for the Boundary Layer, Grell (1994) over land and Emanuel over ocean for the Cumulus Convection Scheme, Arakawa&Schubert (1974) for the Grell Scheme Cumulus Closure Scheme, and Explicit Moisture (SUBEX-2000) for the Moisture Scheme, and they are used for both domains. The model options are summarized in Table 3.2.

Table 3.2: Model options available in RegCM4 [2].

Model aspects	**Available options**
Dynamics	• Hydrostatic, σ-vertical coordinate [31]
Radiative transfer	• Modified CCM3 [57]
Planetary Boundary Layer	• Modified Holtslag [58]
	• UW-PBL [59]
Cumulus convection	• Simplified Kuo [30]
	• Grell [60]
	• MIT [61]
	• Tiedtke [62]
Resolved scale precipitation	• SUBEX [63]
Land surface	• BATS [40]
	• Sub-grid BATS [31]
	• CLM [64]
Ocean fluxes	• BATS [40]
	• Zeng [65]
	• Diurnal sea surface temperature [66]
Interactive aerosols	• Organic and black carbon, SO4 [67]
	• Dust [68]
	• Sea salt [69]
Interactive lake	• 1D diffusion/convection [34]
Tropical band	• Coppola et al. [2]
Coupled ocean (not in public version)	• MIT [70]
	• ROMS [71]

3.1 50 km Grid Spacing of Mother Domain

The resolution of first simulation (mother domain) is 50 km, and the cells are distributed in a horizontal grid of 80x50 in longitude and latitude, respectively with 18 vertical sigma levels. The mother domain covers Romania, Czech Republic, Slovakia, Hungary, Austria, Balkans and Italy at North West, Greece at West, Ukraine, South

of Russia and Georgia at North, Azerbaijan and north part of Iran at East, Syria, Iraq and Jordan at South (see Figure 3.3). The coarser domain is centered at 40.00° N and 31.00° E over Turkey.

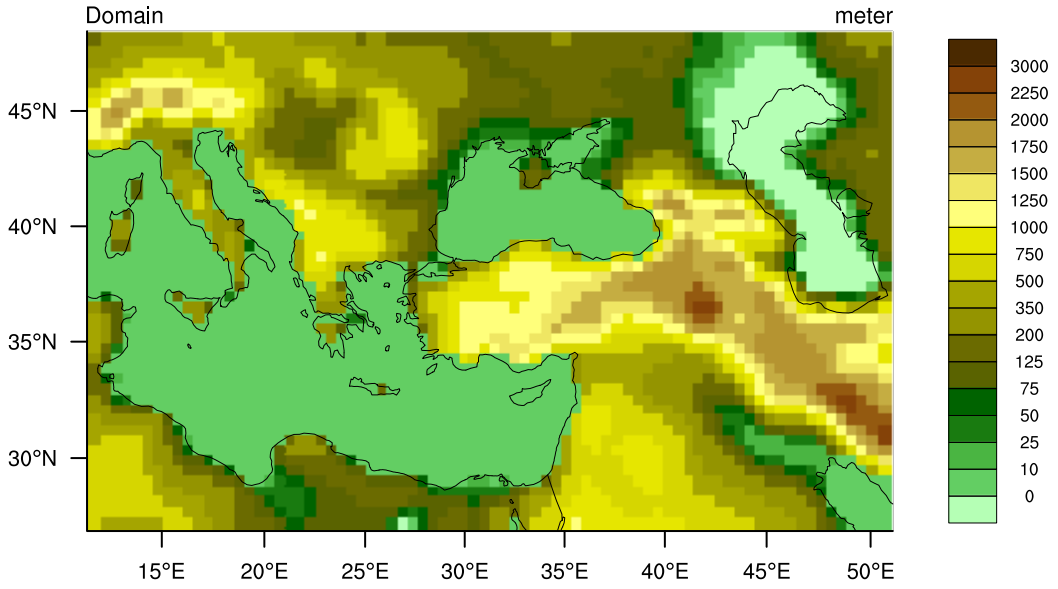

Figure 3.3: Topography of the mother domain.

Each grid cells of the domain has its own coordinates, elevation, land use type. In the Figure 3.3, the elevation characteristics of the domain are defined with a color scale, which is ranging from green to dark brown. The height of the grid cells which are defined with yellow to dark brown, ranges from 1000 meter to 3000 meter above sea level. Figure 3.4 shows the land use types and use of the mother domain with their percentages. There are 22 land use classes as shown in Table 3.2. Each color gives a different type of vegetation and land use. When we look into the usages of land use, the crop/mixed farming has the largest amount with 23.17%, and the ocean that refers offshore has the second largest amount with 21.5%. The desert is the third largest land use type with the percent of 16.67, which has been mostly seen over the north part of Egypt and Libya where the mother domain ends. Afterwards the semi-desert, short grass, inland water, forest/field mosaic land use types follows respectively. The outputs of coarse resolution RegCM4.3 are used to drive the model at a higher resolution over a subregion covering Turkey.

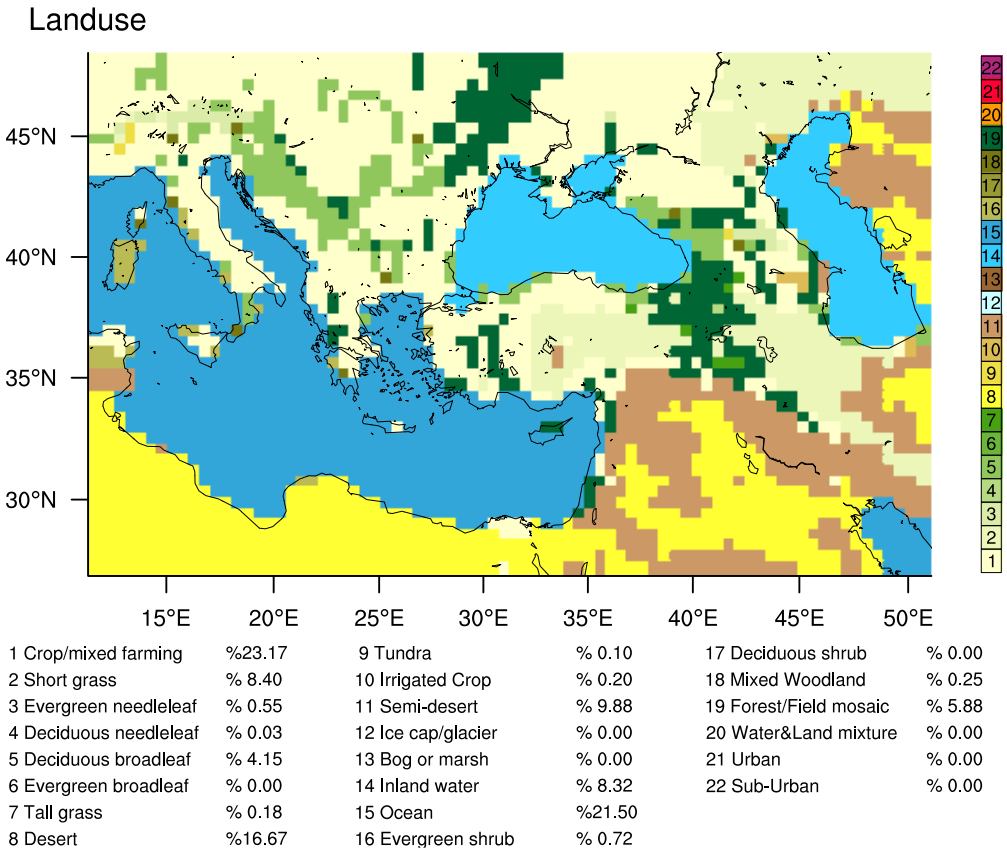

Figure 3.4: Model land use type of the mother domain.

3.2 10 km Grid Spacing of Nested Domain

The model is also driven with a higher resolution of 10 km by nesting the outputs of 50 km resolution simulations, for the same period of the first simulations. The horizontal grid cells are 177x101 with 18 vertical sigma levels. Finer domain covers Turkey, part of Bulgaria at North West, Georgia at North East and Syria at South East. This nested domain is centered at 39.14° N and 34.16° E.

As in the Figure 3.3 of the mother domain, the grid cells and their elevation characteristics are shown in the Figure 3.5. East Anatolian is the highest region of Turkey defined with brown to dark brown color shading in the model topography map. The land use types and their usage with the percentages are illustrated in Figure 3.6. Percentages as follows: desert 2.38%, semi-desert 8.04%, crop/mixed farming 19.77%, ocean (Mediterranean Sea) 19.96%, short grass 9.31%, deciduous needleleaf 0.41%, inland water (Black Sea) 16.38% and forest/field mosaic 13.15%.

The model configuration used for this experiment is summarized in Table 3.3.

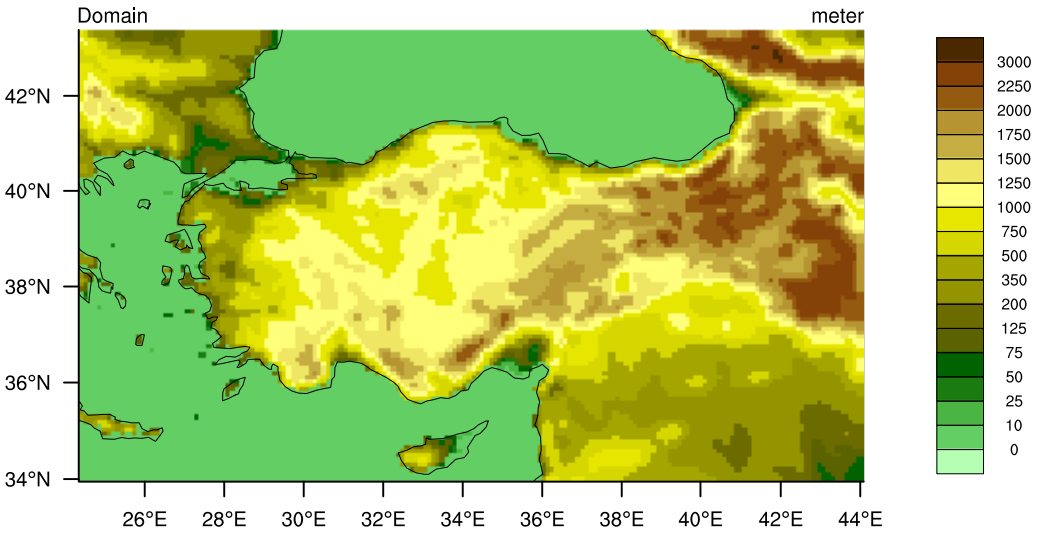

Figure 3.5: Topography of the nested domain.

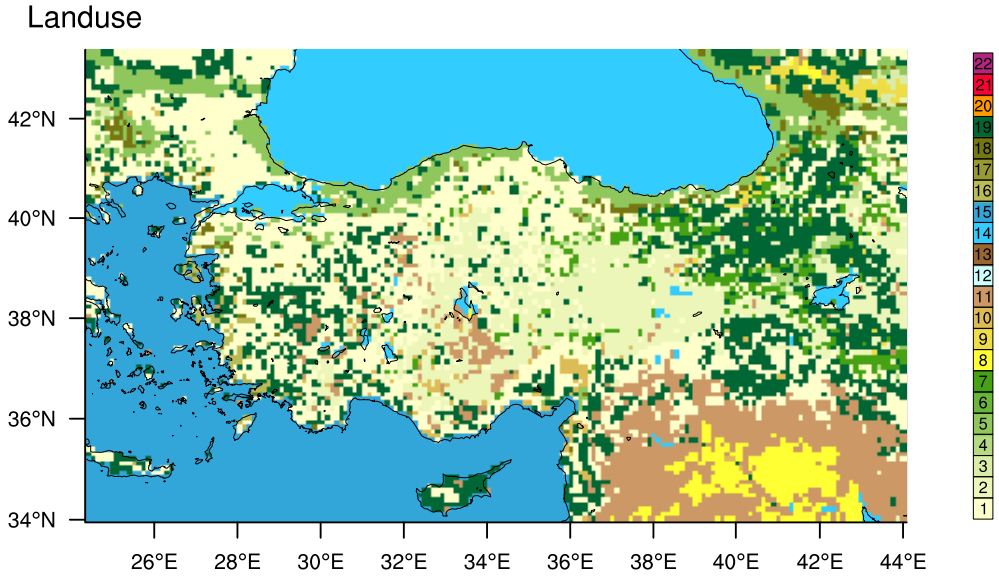

1 Crop/mixed farming	%19.77	9 Tundra	% 0.58	17 Deciduous shrub	% 0.00
2 Short grass	% 9.31	10 Irrigated Crop	% 0.80	18 Mixed Woodland	% 1.14
3 Evergreen needleleaf	% 0.40	11 Semi-desert	% 8.04	19 Forest/Field mosaic	%13.15
4 Deciduous needleleaf	% 0.41	12 Ice cap/glacier	% 0.00	20 Water&Land mixture	% 0.00
5 Deciduous broadleaf	% 4.99	13 Bog or marsh	% 0.00	21 Urban	% 0.00
6 Evergreen broadleaf	% 0.01	14 Inland water	%16.38	22 Sub-Urban	% 0.00
7 Tall grass	% 2.30	15 Ocean	%19.96		
8 Desert	% 2.38	16 Evergreen shrub	% 0.40		

Figure 3.6: Model land use type of the nested domain.

Table 3.3: Summary of the model configuration.

Contents	Mother Domain	Nested Domain
Resolution	50 km	10 km
Projection	Lambert Conformal	Lambert Conformal
Grid Cells	iy=50 and jx=80	iy=101 and jx=177
Vertical Layer	18 σ-layers	18 σ-layers
Central Coordinates	42.00° N and 31.00° E	39.14° N and 34.16° E
Time Interval	3 hours	3 hours
SST Type	GISST	GISST
Data Set Type	ERA-40	FNEST
Boundary Layer Scheme	Holtslag PBL (1990)	Holtslag PBL
Cumulus Convection Scheme over Land	Grell (1994)	Grell
Cumulus Convection Scheme over Ocean	Emanuel (1991)	Emanuel
Grell Scheme Cumulus Closure Scheme	Arakawa Schubert (1974)	Arakawa Schubert
Moisture Scheme	SUBEX (2000)	SUBEX
Variable	Precipitation	Precipitation

4. GEOGRAPHY AND CLIMATE OF TURKEY

Turkey is located in between Asian and European continents at 36-42°N, 26-45 °E between Bulgaria and Georgia, bordering the Black Sea at north, the Aegean Sea at west and the Mediterranean Sea at south. Turkey is situated in temperate zone where the Mediterranean climatic conditions dominate. Due to not only irregular topography, but also sea effects, different types of climate characteristics have been seen [72].

The mountains of the Black Sea and the Mediterranean Sea run parallel to the coastline and that's why the climate of the coastal areas and inland areas are different than each other. The coastal areas have milder climates and have more rainfall than inland parts. However, the mountains of the Aegean Sea extend perpendicular to the coast and it causes sea effect to penetrate to inland areas. Generally, from north to south, the annual temperature average increases uniformly due to increase of the solar radiation intensity. In winter, the minimum temperature has been seen at Northeast where is under the influence of the interaction of atmospheric motions with the high topography, whereas the maximum temperature has been seen at Southeast in summer along the Mediterranean coast.

The annual precipitation amount depends on the geographic regions and the elevation as well. The greatest amount of rainfall has been seen on the eastern part of Black Sea coast throughout the year. Even the Aegean and Mediterranean coasts have cool, rainy winters; summers are hot and moderately dry. In the middle of Turkey the climate is continental, which means, summers tend to be hot and dry; winters are bitterly cold with frequent and heavy snowfall.

The greatest amount of precipitation is observed at winter season over the Black Sea shorelines. The average of annual total 30 years (between 1971-2000) precipitation is approximately 2700 mm. The average of minimum precipitation is measured throughout Central Anatolia with the amount of 600 mm. The smallest change of the precipitation amount has been seen at Southeast Anatolia between the minimum and maximum values of the total 30 years precipitation's averages.

The temperature averages of the 30 years are observed as the minimum, mean and maximum temperature as follows: the coldest minimum and the mean temperatures are occurred at Black Sea with 2.4°C and 6.16°C, respectively whereas the warmest minimum and mean temperature is measured at Mediterranean with 15.4°C and 19.9°C, respectively. When the warmest maximum temperatures have been observed over Mediterranean with 25.13°C, Aegean with 25.24°C and Southeast Anatolia with 25.28°C; the coldest maximum temperatures are measured at Marmara, Black Sea and East Anatolian region, with 9.07°C, 11.08°C, 11.66°C, respectively.

4.1 Model Precipitation Climatology

The precipitation simulations of the coarser domain of BATS and the gridded observational CRU TS3.10 data are analyzed seasonally for the years between 1971 and 2000. In the Figure 4.1 the simulated precipitation for 50 km resolution and the gridded CRU observational precipitation are compared to assess the model performance. RegCM however, tends to overpredict the precipitation over high topography associated with the orographic precipitation. Generally, the precipitation gradient, which is increasing precipitation from inland to coastlines and from central Anatolia to northeastern Anatolia, is well captured by the model. The amount of precipitation is overestimated by RegCM in winter and spring. Besides, the most dramatic differences occur during spring throughout Turkey. The effects of topographic conditions are clearly seen and the model produces more precipitation over high elevations especially over the mountain ranges along the coastlines in Turkey, Alpine region and Zagros Mountains.

In winter, RegCM overpredicts the precipitation along Black Sea, Mediterranean Sea shorelines and Zagros Mountains. Throughout Turkey, the precipitation has been mostly occurred about 200-250 mm. However the model produces excessive amount of precipitation, which is about 500 mm at Caucasus Mountains, 600 mm at Diranic Alps. Less precipitation has been produced by the model on the Aegean Sea coast compared to CRU precipitation data. As mentioned in the previous section, the precipitation data compiled over Turkey from the meteorological stations by CRU does not represent well the high topography areas. These differences between model precipitation and observations might be the result of the misrepresentation of precipitation climatology

by CRU data as much as the deficiency of the model's large scale precipitation parameterization.

The most precipitation is occurred in spring. As addressed in the winter season, there is a similar but more intensive precipitation pattern over Turkey. RegCM overpredicts the precipitation at north and south coastlines where the amount reaches to 600 mm and over the Zagros Mountains approximatelly within 400 mm. Over Caucasus, Diranic, and Apennines Mountains, the model produces more precipitation, as well. The general tendency of the model is to produce excessive precipitation over Eastern Europe, southern parts of Russia and eastern part of Turkey. The overestimation is elevated over the complex topography. In the summer, even if CRU does not show the precipitation more than about 100 mm over Turkey, RegCM generates orographic precipitation the amount ranges about 250-300 mm at the northeast and south shorelines. Throughout the Caucasus, Diranic, and Alpine Mountains, the simulation patterns of summer are similar to the spring season. The precipitation has been underpredicted over the Aegean Sea and Southeast Anatolia region in the autumn. Along the Taurus and North Anatolian Mountains there is an overprediction and the precipitation amount reaches up to 500 mm. Overall, about 200 mm precipitation amounts are generated in the inland areas of Turkey and coincide to the gridded observational data. In general, RegCM performs reasonably well in capturing the general precipitation patterns.

The seasonally averaged precipitation of RegCM with CLM for 50 km, CRU gridded observational data are presented in the Figure 4.2. For winter, CLM produced the same precipitation like BATS and the model overpredicts the precipitation over Turkey. There is an also similar precipitation pattern with BATS in summer and autumn seasons. For the spring season, BATS generates more orographic rainfall than CLM generally over Turkey. At very steep mountain barriers along the Black Sea and Mediterranean Sea coasts the precipitation is overpredicted. The precipitation estimations by RegCM-CLM are very close to BATS observations throughout Turkey.

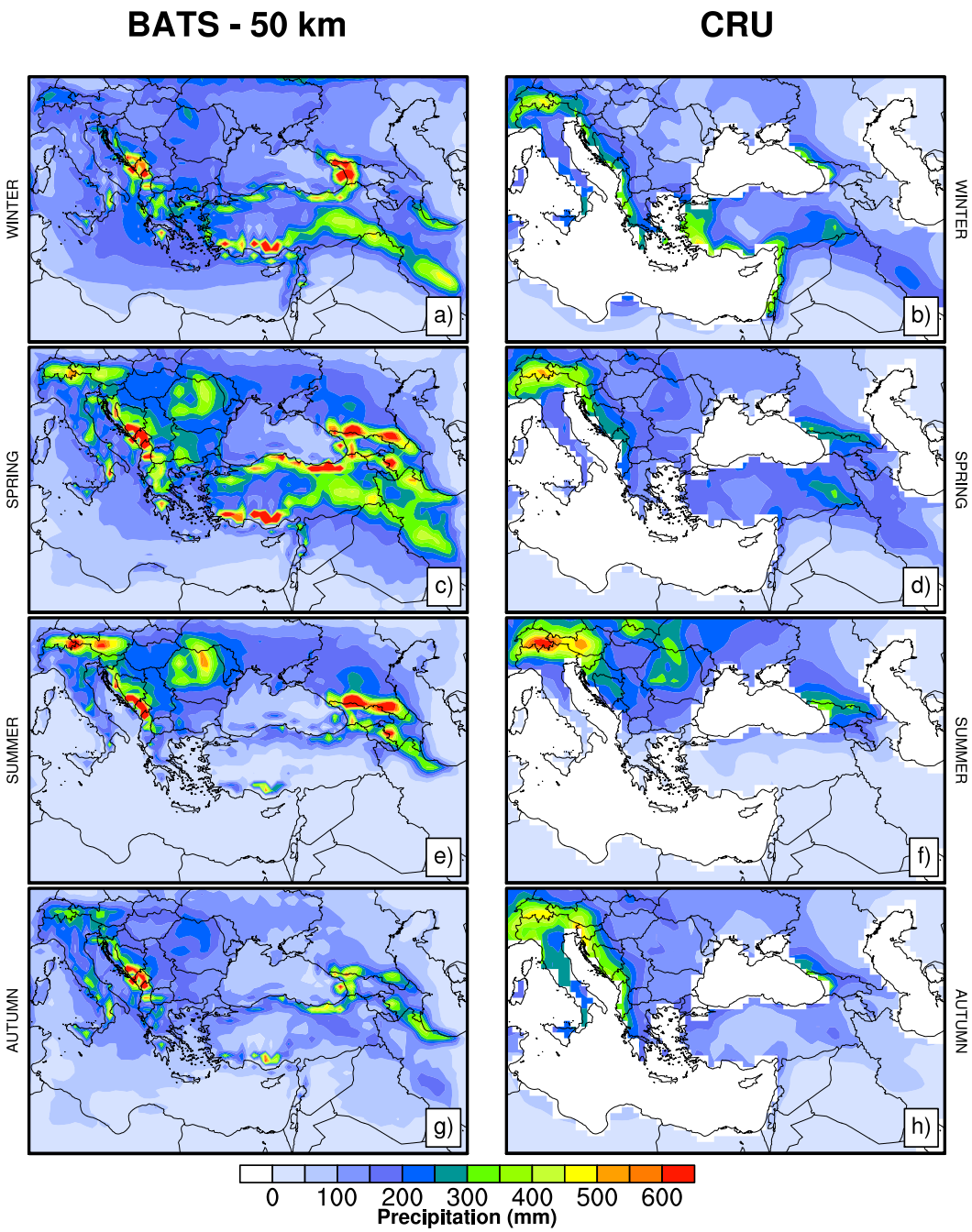

Figure 4.1: The comparison of BATS 50 km and CRU.

In the Figure 4.3, the seasonal averages of RegCM-BATS precipitations of nested domain (10 km resolution) and gridded observational CRU are evaluated. In the winter, RegCM produces excessive precipitation amount reaches up to 600 mm over east of the North Anatolian, Taurus and Zagros Mountains. Along the Aegean and Black Sea coasts, the precipitation amount is about 450 mm, while CRU observations indicate the range of precipitation of 200-350 mm over Black sea coast and more than 300 mm precipitation over the Aegean and Mediterranean shorelines and southeast of Turkey. Areas that have relatively less precipitation are located with a noticeable exception

over the shorelines and eastern Turkey. However, there is a tendency for the model to simulate excessive precipitation except summer and autumn season.

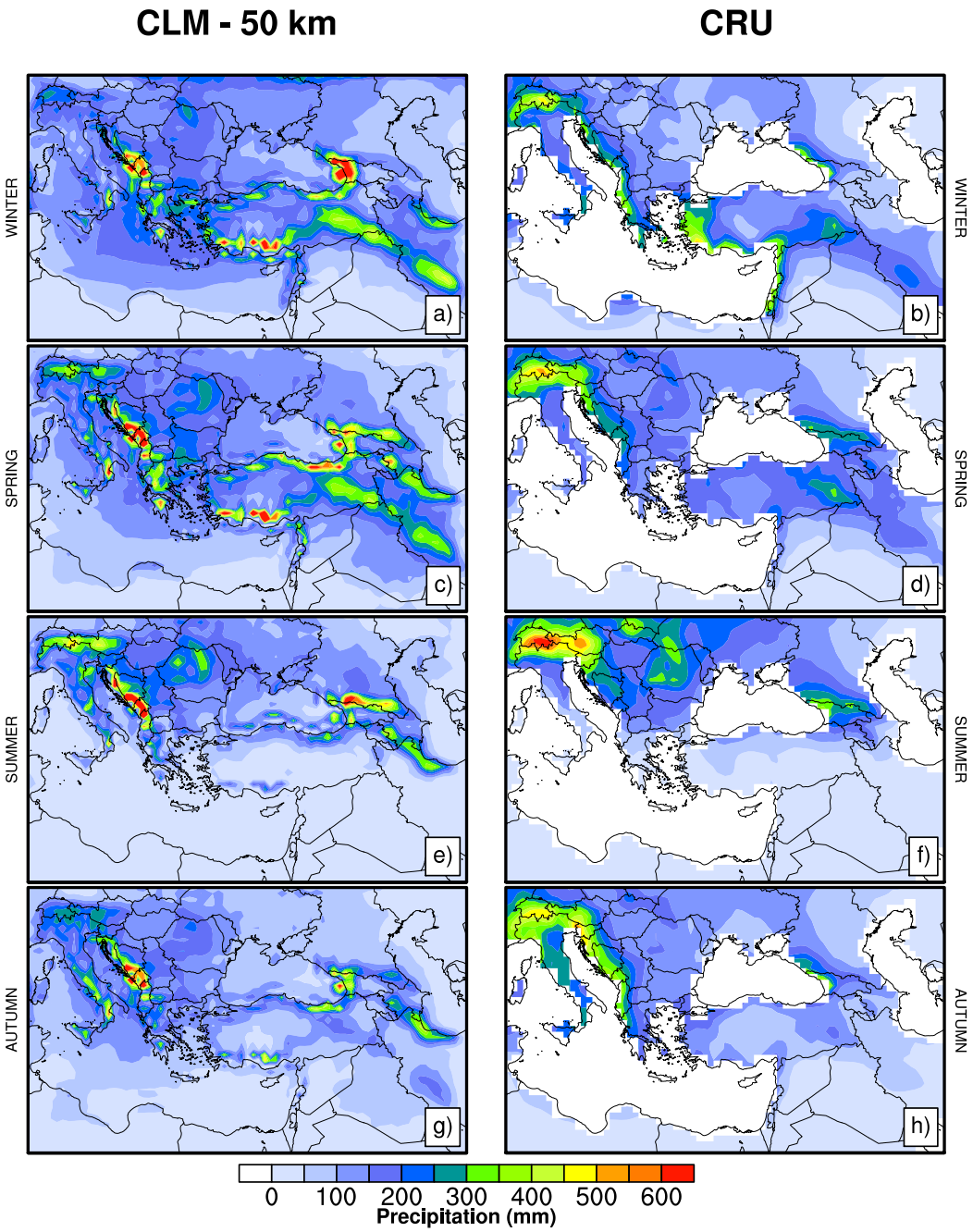

Figure 4.2: The comparison of CLM 50 km and CRU.

The nested domain precipitation distribution is highly similar to the mother domain in summer and autumn, which has about 100-200 mm precipitations over most of Turkey. Eastern Black Sea coast receives more than 300 mm precipitation which coincides with the station observations even though it is not revealed in relatively coarse resolution CRU field. The most precipitation is occurred in the spring season over Turkey. The precipitation distribution mimics the topography in high resolution. The high

topographic conditions, because of the steep mountains along the coastlines and beginning of the Zagros Mountains, lead to generate more precipitation as addressed in 50 km domain's results. Even though, there is no more than 250 mm rainfall along the shorelines and inland region of Turkey for spring average in CRU observations, the modeled high resolution precipitation fields reveal up to 600 mm precipitation over North Anatolian (Pontic) and Zagros Mountains. Overall, long-term precipitation patterns are strongly controlled by topography.

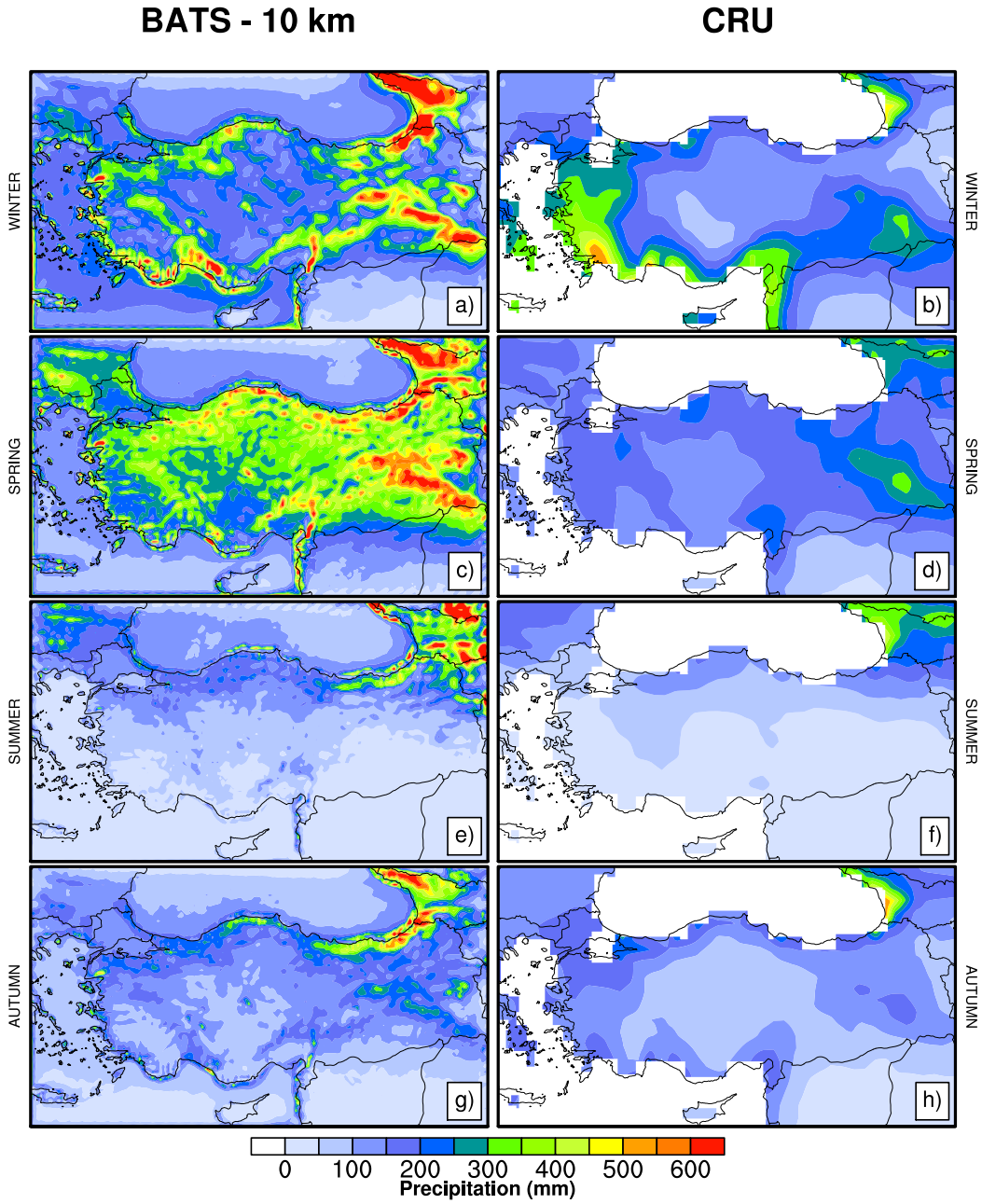

Figure 4.3: The comparison of BATS 10 km and CRU.

5. BIAS ANALYSIS

5.1 The Biases in Comparison to CRU Precipitation

The first column of Figure 5.1 shows the precipitation bias between 50 km RegCM-BATS simulation and the gridded CRU TS3.10 data set with 0.5° grid spacing. The precipitation biases are evaluated from the analyses of the seasonal averages of the period 1971-2000 as in the previous section of the model and observation comparison.

Mostly, the positive biases have been seen over the mountain ranges because of two reasons: The first one is that CRU precipitation data set which is constructed by the interpolation of station observations to a coarse-resolution grid, is underestimated precipitation in topographically complex regions due to an underrepresentation of station locations at high elevations [73]. The second one is, the model tends to produce more precipitation over mountainous areas as a result of imperfect parameterization of some climate processes.

Taking into account for the general pattern, the precipitation amount of the summer season is quite similar to CRU precipitation distritheevenly diIn gtobution. The model overestimates the precipitation between the amounts of 60-180 mm, at the north and south coastlines of Turkey; however, there is almost no bias in the central Anatolia. Generally, RCMs accuracy are diminished at representing spring precipitation than winter precipitation, due to the difficulties in modeling convective rainfall [74]. Spring has the highest positive bias ranging from 60 to 300 mm, particularly throughout Aegean sea region, Zagros, North Anatolian and Taurus Mountains. In the autumn, the negative bias amounts reveal up to 180 mm, along the Mediterranean coastlines of the Syria and Israel. Over the Aegean part, Southeast Anatolia region of Turkey and Alpine Mountains, the negative bias is the range of 60-180 mm while the positive bias has been observed with 60 -180 mm throughout Antalya Bay, North Anatolian and Caucasus Mountains. The bias does not occur over the Central Anatolia region in the summer and autumn.

The comparison of the 50 km RegCM-CLM simulation and the gridded CRU data has been demonstrated in the second column of Figure 5.1. As reviewed in the previous section, the difference of the precipitation simulated by using BATS and CLM land surface models are noteworthy only in the spring season over Turkey. The CLM bias in comparison to BATS is reduced along the central part of Turkey and also throughout Ukraine.

The similar precipitation bias patterns are observed over Turkey for the 10 km simulations of RegCM-BATS with respect to CRU data, illustrated in the third column of Figure 5.1. While the least positive biases are seen in the summer with the amount of 60-180 mm at the north shorelines of Turkey, the most positive biases are occurred up to 300 mm over high elevations in the spring. Winter bias distribution is very similar to the mother domain, except the increase of positive bias distribution over the Central Anatolia. However, the positive precipitation bias is increased in the autumn for the high resolution simulation.

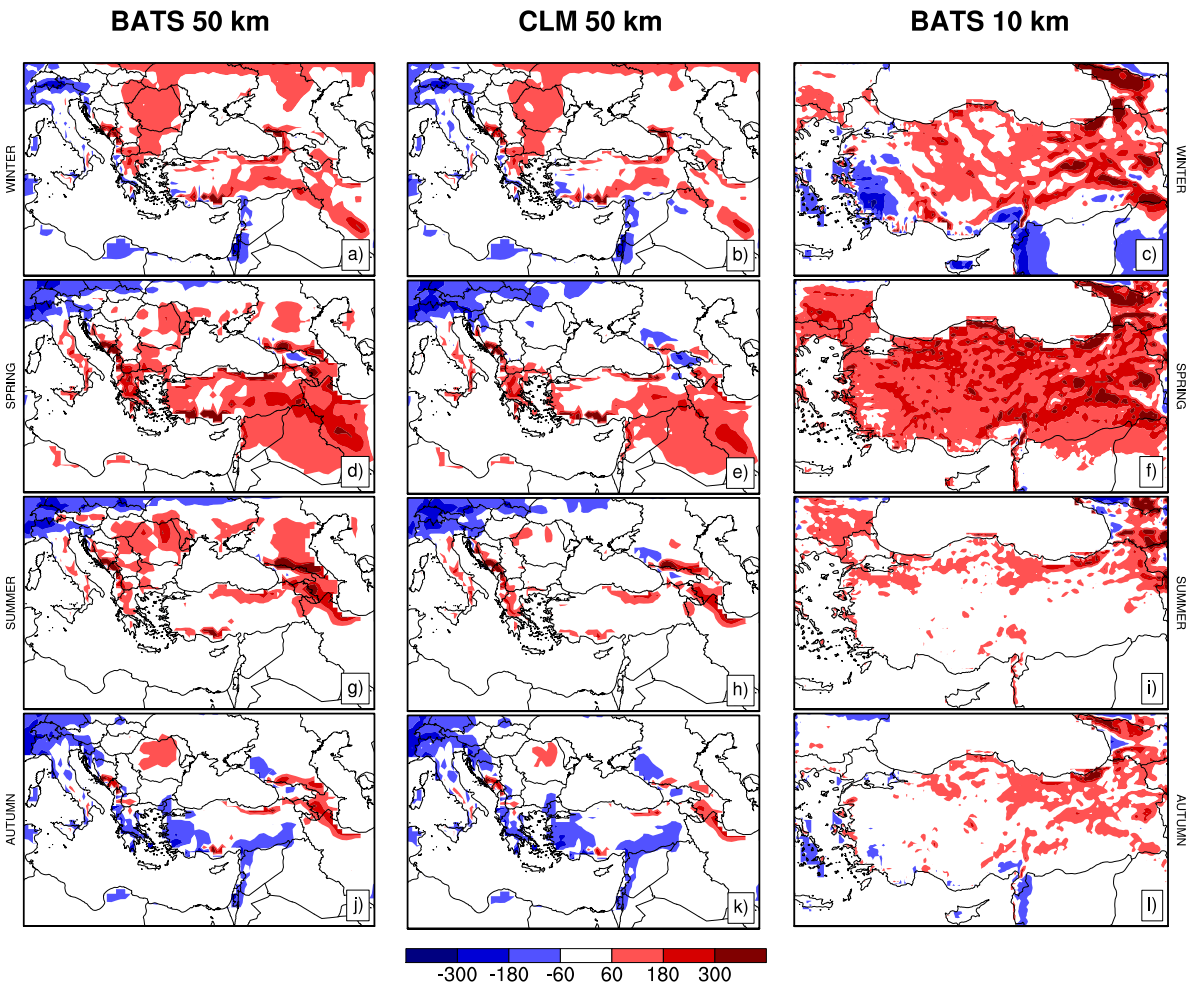

Figure 5.1: Bias analysis of RegCM and CRU data set.

5.2 The Biases in Comparison to Station Precipitation Observations

In this section, the biases of the precipitations have been calculated using station observations which are taken from TSMS. In Figure 5.2, the location of the station points have been demonstrated along with the locations of the 50 and 10 km domains' grids. Here, red circles represent the station coordinate pairs, the coordinates of 50 and 10 km are represented with black and white circles, respectively.

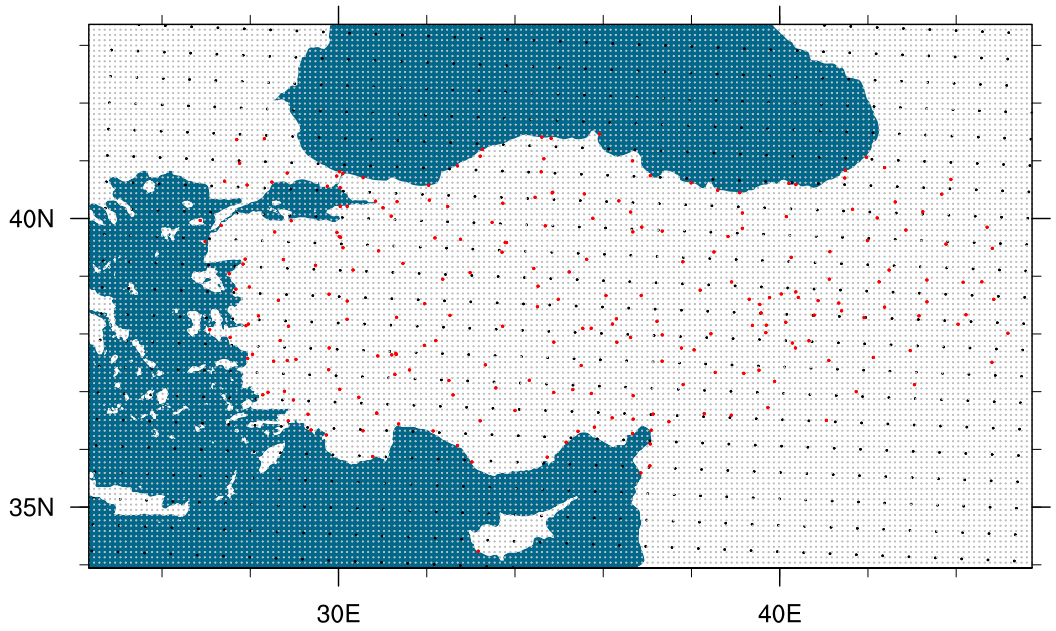

Figure 5.2: Station grids.

After the modeled precipitations are gridded to the stations coordinates, the bias corrections are performed as explained in the Section 2. In the next part, the applications of the bias correction methods have been presented for chosen three stations.

5.2.1 Application

To apply the bias correction methods, three stations are randomly selected from three distinct groups in which the modeled precipitation is in good agreement with the observed precipitation (17270 Sanliurfa-Merkez), the modeled precipitation is able to represent the observations but not in a good agreement (17606 Kastamonu-Bozkurt) and the modeled precipitation do not agree with the observation (17630 Kocaeli-Kartepe).

To apply the MV method, only one correction factor is calculated for each station, from the first 20 years and then the last 10 years are validated multiplying by the correction factors. The mean of the observed and modeled precipitation and their ratios are given in Table 5.1 with the elevations of the model and stations.

Table 5.1: MV correction.

Stations	17270 Sanliurfa Merkez	17606 Kastamonu Bozkurt	17630 Kocaeli Kartepe
$\overline{obs}$	1.24	3.64	1.45
$\overline{mod}$	1.25	3.95	1.92
q	0.99	0.92	0.75
Model elevations (m)	475.8	952.5	771.8
Station elevations (m)	550.0	167.0	1320.0

MV bias correction method is also carried out with the month-based approach. After calculating the correction factors for the each month of the first 20 years, the last 10 years of modeled precipitations are multiplied by every month's correction factor. For 3 stations, the monthly averages of the observed and modeled precipitation and the monthly correction factors are shown in Table 5.2.

Table 5.2: Month-based MV correction.

	17270			17606			17630		
	$\overline{obs}$	$\overline{mod}$	q_{mon}	$\overline{obs}$	$\overline{mod}$	q_{mon}	$\overline{obs}$	$\overline{mod}$	q_{mon}
January	30.2	26.2	1.2	44.7	29.7	1.5	6.7	18.3	0.4
February	24.1	19.9	1.2	39.1	29.5	1.3	6.5	24.5	0.3
March	21.7	20.1	1.1	34.8	50.5	0.7	10.9	29.2	0.4
April	13.8	20.5	0.7	17.9	79.7	0.2	17.5	31.6	0.6
May	11.7	14.4	0.8	20.5	73.8	0.3	25.1	25.9	0.9
June	1.2	4.1	0.3	20.9	37.3	0.6	32.5	13.1	2.5
July	0.006	0.07	0.09	19.4	25.4	0.8	18.8	8.5	2.2
August	0.9	0.004	216.3	22.1	21.4	1.1	15.8	8.5	1.8
September	0.9	1.5	0.6	34.6	21.7	1.6	12	10.1	1.2
October	6.4	8.3	0.8	63.9	40.5	1.6	11.7	18.8	0.6
November	15.3	16.2	0.9	59.3	33.9	1.7	8.8	18.5	0.5
December	25.2	21.6	1.2	66.1	37.7	1.8	10.2	26.9	0.4

After month-based MV bias corrections, the monthly sums of modeled, observed and corrected precipitation simulations are illustrated for the validation period in Figure 5.3.

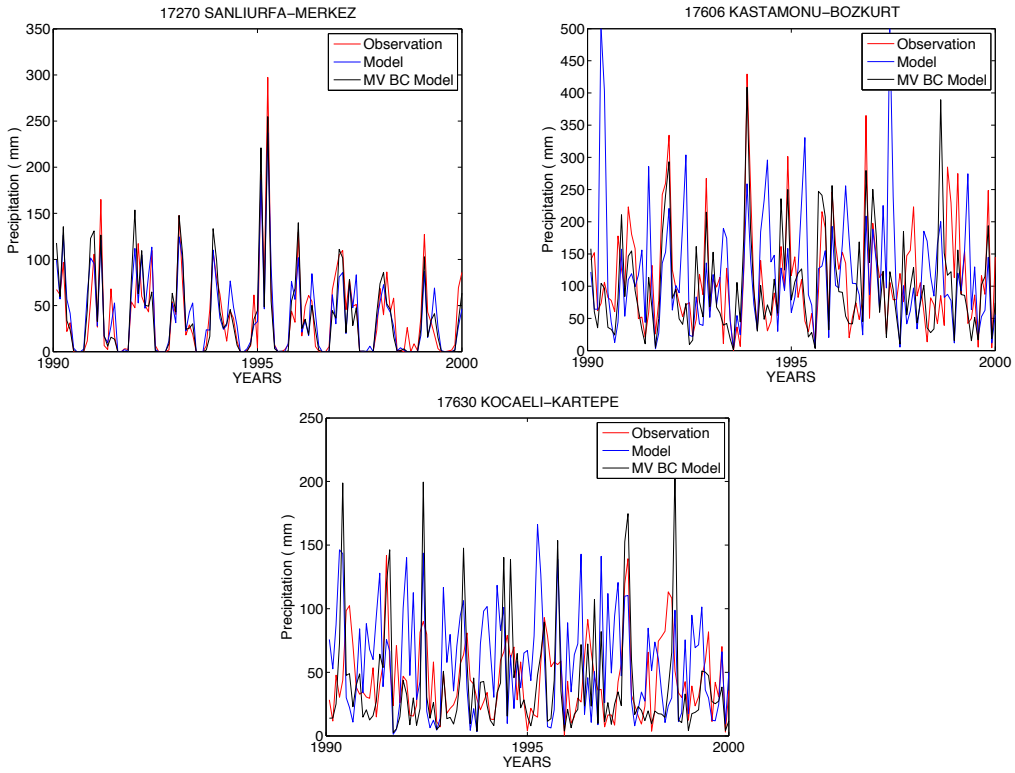

Figure 5.3: The comparison of the observed, modeled and corrected precipitation simulations using month-based MV.

To see the frequency of the modeled and observed precipitations, Figure 5.4 is demonstrated below for 3 stations. The red and blue color symbolize the frequency of the observations and the simulations, respectively. As seen from the frequency distributions, the model is not able to simulate the precipitations near tails of the distribution. It produces more precipitation in the range of 0-2 mm for all cases than the observations while it cannot capture the extreme precipitation higher than 40 mm.

For the application of the Quantile Mapping (QM) bias correction, the parameters of Gamma CDF are firstly used as preferred in many studies of bias corrections. In Figure 5.5, the cumulative distributions of the modeled and observed precipitations are shown. Red, blue and black lines represent the observed, simulated and bias corrected precipitation, respectively. It is clearly seen from the figure that, the GAMMA CDF could not adjust the shape of the distribution of the modeled precipitation. Figure 5.6 shows the observed, modeled and corrected precipitations as the monthly sums of the last 10 years.

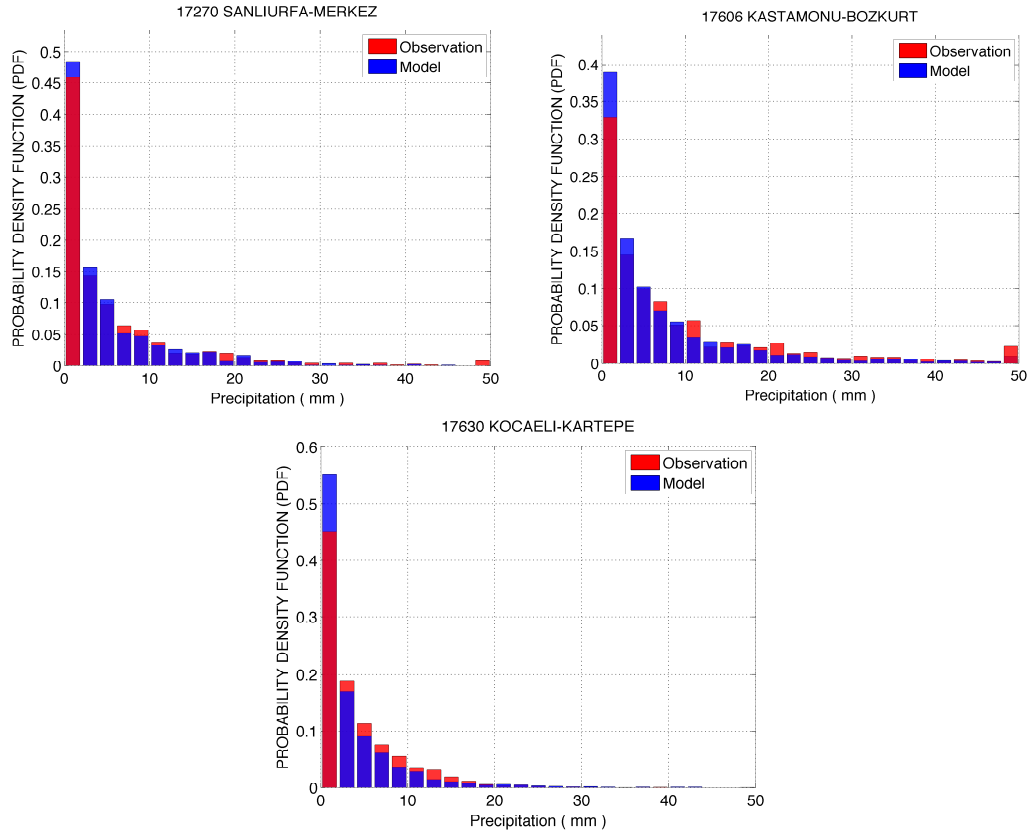

Figure 5.4: The frequency of the modeled and observed precipitation.

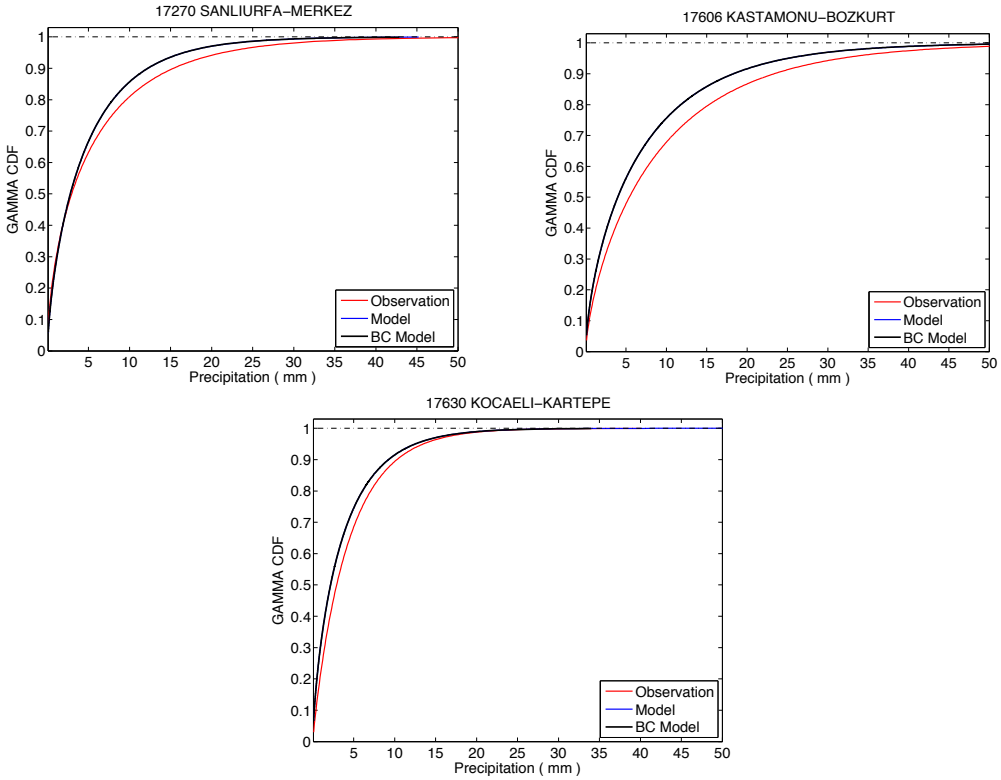

Figure 5.5: Gamma CDFs of the modeled and observed precipitation.

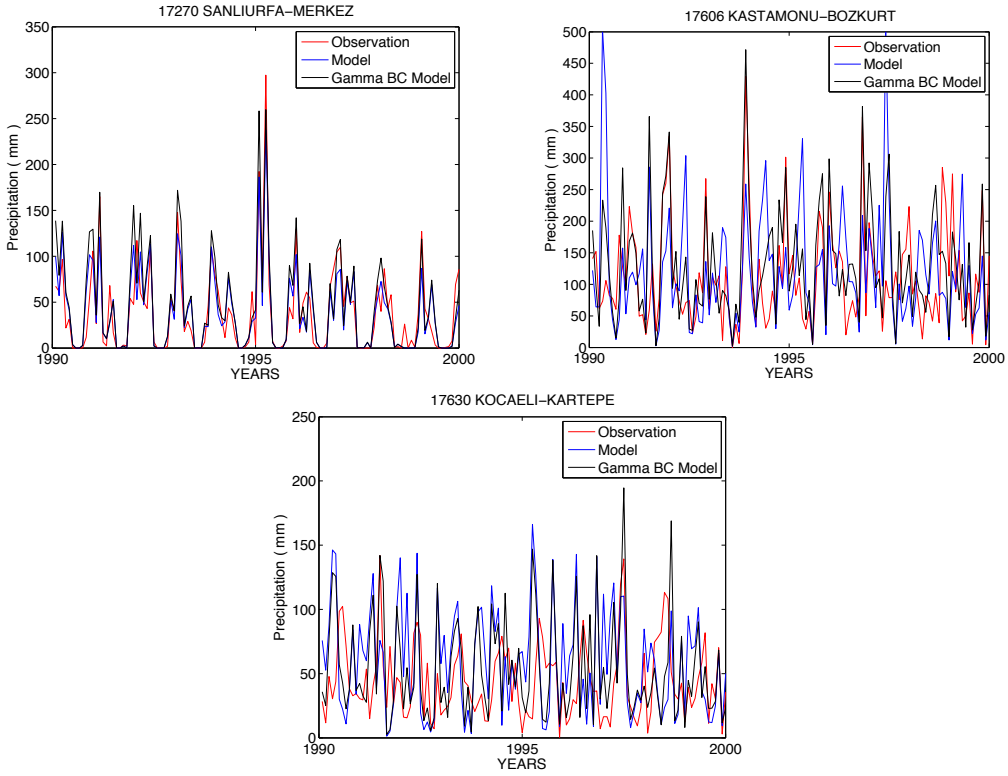

Figure 5.6: The comparison of observed, modeled and corrected precipitation simulations with Gamma CDF.

Instead of commonly preferred in the literature, QM bias correction methods are also performed to the simulations of RegCM using best-fitted CDF parameters, as Weibull CDF to observed precipitation and Generalized Pareto CDF to modeled precipitation. To estimate the best-fitted CDF parameters, Maximum Likelihood and Akaike Information Criteria are used (see Table 5.3). The smallest values of AIC indicate the best fitted CDFs (bold ones) to apply QM bias correction.

Table 5.3: The Maximum Likelihood and Akaike Information Criteria results of the observed and the modeled precipitations.

	Normal	Weibull	Gamma	G.Pareto	Exponential
17270					
LLE obs	2776.6	2035.4	2047.6	2060.4	2152.5
LLE mod	3114.9	2370.8	2385.6	2368.7	2437.1
AIC obs	5557.2	**4074.7**	4099.3	4126.8	4306.9
AIC mod	6233.8	4745.7	4775.3	**4743.5**	4876.2
17606					
LLE obs	5644.3	4529.3	4548.8	4528.9	4618.8
LLE mod	7597.7	5791.9	5831.4	5788.5	5981.9
AIC obs	11292.5	**9062.6**	9101.5	9063.8	9239.6
AIC mod	15199.5	11587.9	11666.8	**11582.9**	11965.7
17630					
LLE obs	3654.3	2993.7	2997.4	2990.1	3000.6
LLE mod	5931.8	4258.8	4299.9	4218.9	4383.8
AIC obs	7312.7	5991.3	5998.9	**5986.1**	6003.1
AIC mod	11867.6	8521.5	8603.7	**8443.8**	8769.6

The cumulative distribution functions of RegCM and station observations are shown in Figure 5.7 (Weibull CDF) and Figure 5.8 (Generalized Pareto CDF). In the all figures, the red lines represent the CDFs of the observed precipitation, the blue lines represents the CDFs of the modeled and black lines represents the corrected precipitation simulations. The best cumulative distribution correction has been seen at second station, which is Kastamonu. The QM correction methods could not correct the distribution of 3rd station, Kocaeli. The monthly sum of the observed, modeled and corrected precipitations are compared in Figure 5.9 for last 10 years.

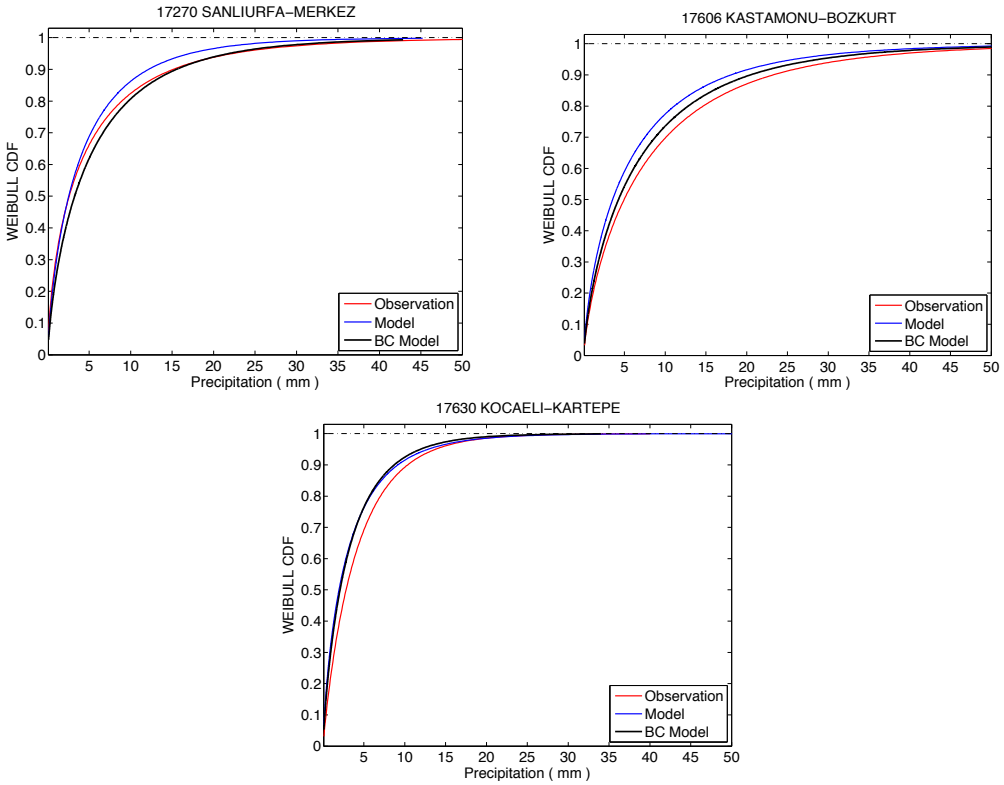

Figure 5.7: Weibull CDFs of the modeled and observed precipitation.

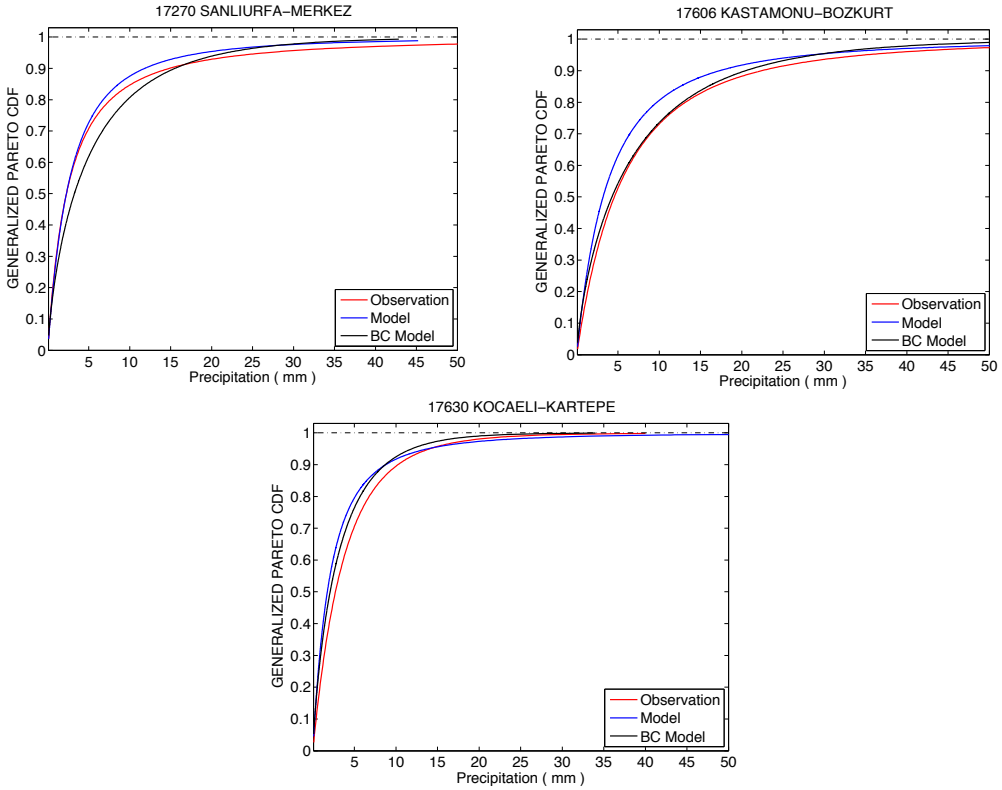

Figure 5.8: G.Pareto CDFs of the modeled and observed precipitation.

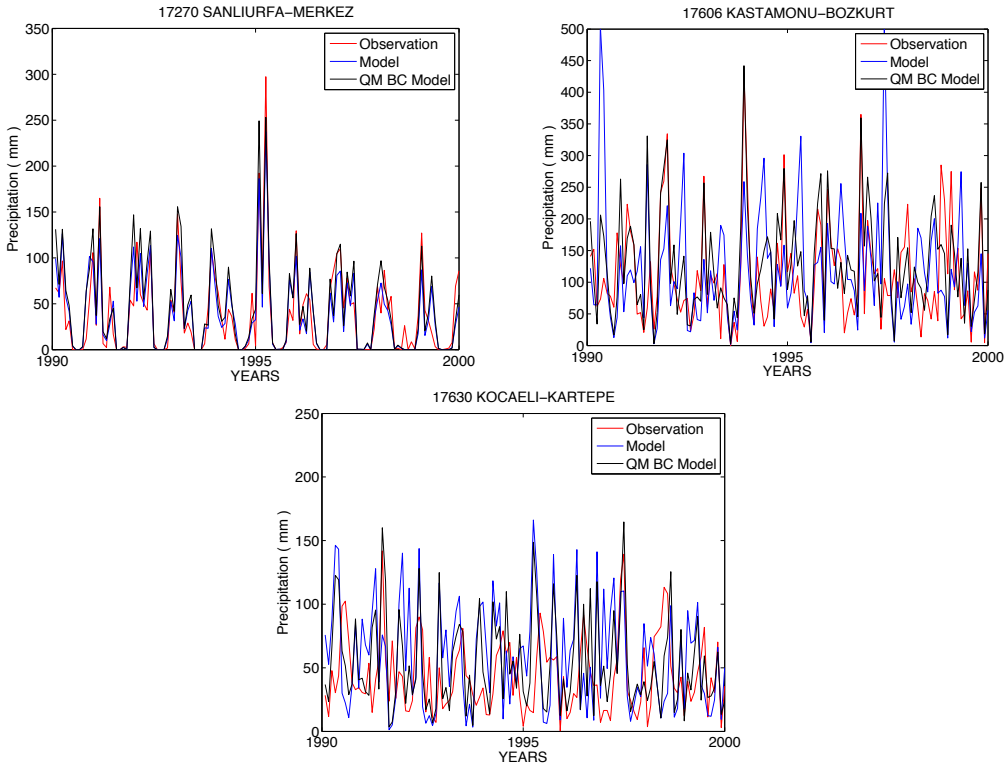

Figure 5.9: The comparison of observed, modeled and corrected precipitation simulations with best-fitted CDFs.

Table 5.4: Quantitative results of the 3 selected stations for coarse and high resolution domain.

50 km	**17270**			**17606**			**17630**		
	r	***RMSE***	***NSE***	***r***	***RMSE***	***NSE***	***r***	***RMSE***	***NSE***
WC	0.86	23.27	0.83	0.26	110.25	0.23	0.03	52.05	-0.06
MV	0.86	23.36	0.83	0.26	98.62	0.38	0.03	40.71	0.35
MV-M	**0.89**	**22.87**	**0.84**	**0.65**	**61.62**	**0.76**	**0.54**	39.62	0.39
QM Gam	0.86	29.66	0.72	0.27	130.84	-0.08	0.02	60.01	-0.41
QM-S Gam	0.87	27.61	0.76	0.55	73.27	0.66	0.35	41.81	0.32
QM	0.86	27.82	0.76	0.29	120.01	0.09	0	58.49	-0.34
QM-S	0.87	25.79	0.79	0.57	67.03	0.72	0.38	**38.33**	**0.43**
10 km	**17270**			**17606**			**17630**		
	r	***RMSE***	***NSE***	***r***	***RMSE***	***NSE***	***r***	***RMSE***	***NSE***
WC	0.84	33.24	0.65	0.43	81.73	0.58	0.13	113.83	-4.06
MV	0.84	28.02	0.75	0.43	75.29	0.64	0.13	**38.47**	**0.42**
MV-M	**0.89**	**24.11**	**0.82**	**0.69**	68.77	0.7	**0.56**	40.48	0.36
QM Gam	0.84	39.06	0.52	0.44	94.48	0.44	0.14	62.3	-0.52
QM-S Gam	0.86	35.69	0.6	0.56	75.19	0.64	0.42	43.87	0.25
QM	0.84	37.65	0.55	0.45	88.95	0.5	0.14	60.89	-0.45
QM-S	0.86	34.23	0.63	0.6	**60.41**	**0.77**	0.46	42.61	0.29

WC: without correction, MV-M: month-based MV, QM Gam: Gamma CDF fitted QM, QM-S Gam: Season-based Gamma CDF fitted QM, QM: Best-fitted QM, QM-S: Season-based best-fitted QM

In the Table 5.4, the quantitative results of validation measures are demonstrated for 3 selected stations. As a result, the month-based MV method generally have the best results for both resolutions.

5.2.2 Bias correction results

Two bias correction methods, Mean Value (MV) bias correction and Quantile Mapping (QM) correction, are applied in this study to RegCM4.3 precipitation simulations of two nested domain, simulated with two land use models BATS and CLM which is used only for the mother domain.

Mean Value bias correction method is performed by following two approaches. In the first approach, only one correction factor, which is named as the MV correction factor, is calculated for each station by using the model precipitations and observations within the first 20 years of simulations between 1971 and 1990. In the second approach, the month-based correction factors are estimated from each month of the correction period for each station. Biases of the simulated precipitations in the last 10 years are corrected by using these correction factors. The correlation, RMSE and NSE results of the correction models will be discussed in the next section.

MV corrections are calculated from division of the mean of the observed precipitation by the mean of the modeled precipitation. For each station, the only one correction factor is found and then multiplied by last 10 years simulations (validation period) day by day. The distributions of the correction factors, which are obtained for BATS and CLM simulations, are demonstrated over 50 and 10 km topography in Figure 5.10.

The colors are ranging from dark blue to dark red. The blue colors represent the correction factors smaller than one and show that the RegCM overpredicts the precipitation. The red colors signify the correction factors larger than 1, which means model underestimate the precipitation at the station.

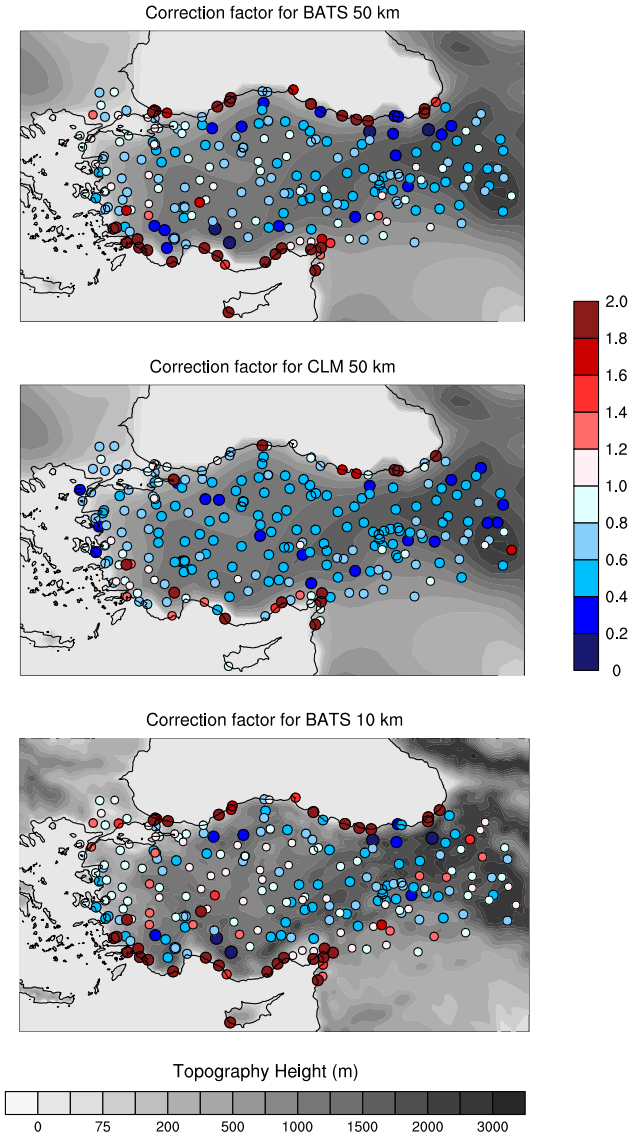

Figure 5.10: Correction factors for MV bias correction.

The correction factor 1 corresponds to equal means of the model and observation. When the errors increase or are further away from 1, the sizes of the correction factors

become larger for blue and red circles in the all figures. Similarly, when the errors decrease or are getting closer to 1, the sizes of the correction factors get smaller. Here, it is accepted that there is no over or underprediction of precipitation at the stations if the correction factor is around 1+- 0.2.

Since the mountains of the Black Sea and the Mediterranean Sea run parallel to the coastline, the precipitation is underpredicted over the Black Sea and Mediterranean Sea shorelines for all three experiments (Figure 5.10). It might be as a result of the misrepresentation of the topographic slopes so that their influence on the airflow patterns are unresolved. Along the Aegean Sea and inland part of Turkey, RegCM overestimates the precipitation.

Generally, CLM produces more rain over Turkey, except some stations throughout the north and south coastlines. BATS simulation results for 10 km are not so different than 50 km distribution along the coastlines. However, the higher resolution of 10 km significantly increase the accuracy of the precipitation inland stations from west to east. Over the highest elevation region of Turkey and the inland parts of Aegean region, BATS 10 km results changes from overestimations to underestimation with the increasing resolution. The average of the correction factors for BATS50, CLM50 and BATS10 are 1.21, 1.36 and 0.77, respectively. And their standard deviations are 2.19, 2.44 and 0.78.

The distributions of the month-based linear correction factors of RegCM-BATS are shown for each month over the 50 km grid spacing topography of Turkey in Figure 5.11 and Figure 5.12. The correction factors are found by dividing the mean of the observed precipitation to the mean of the modeled precipitation for each month.

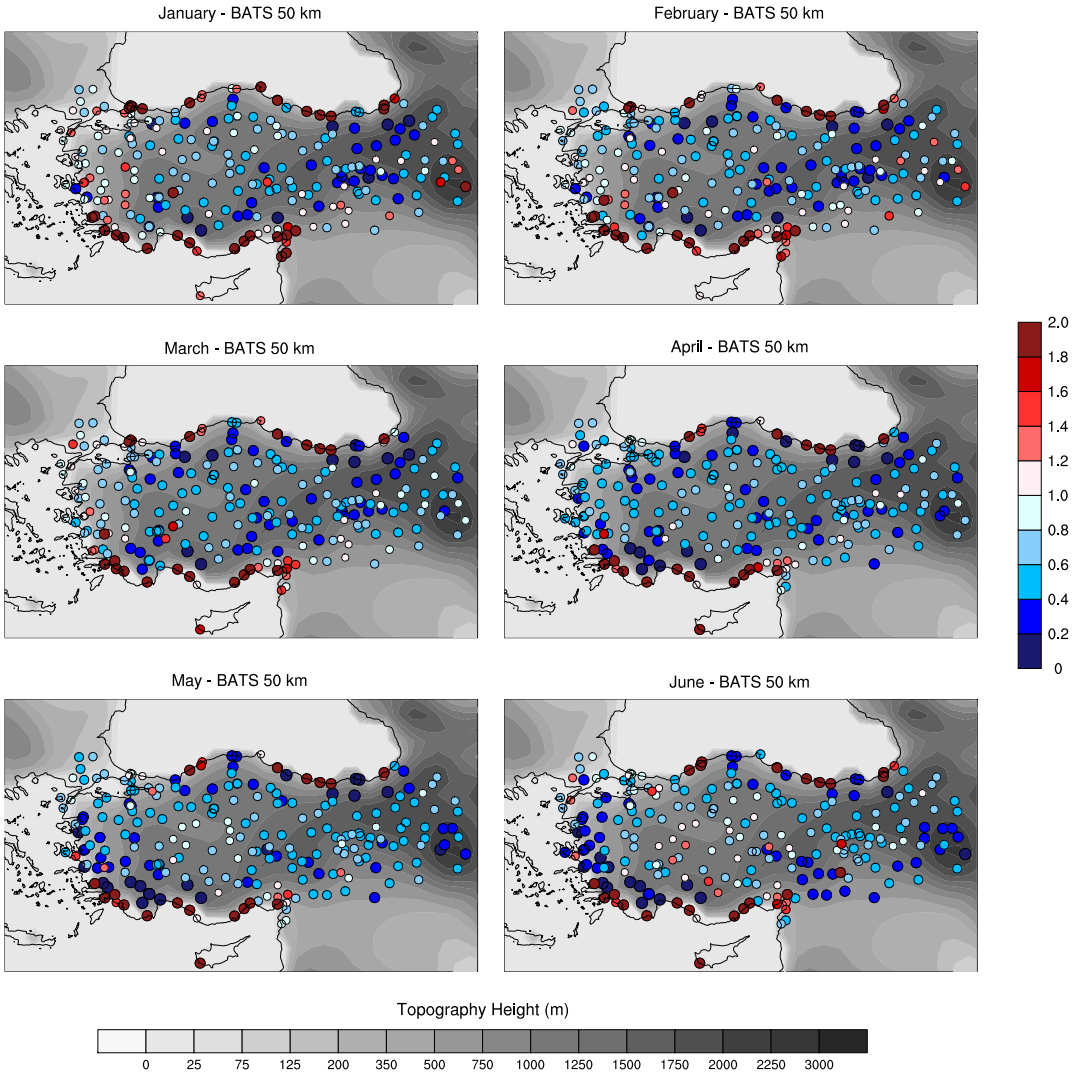

Figure 5.11: The distribution of correction factors for BATS 50 km.

In the light of this information, for the winter season, there is an underprediction along the Black Sea, Mediterranean Sea and the south of the Aegean Sea shorelines, where the correction factors' colors are dark red. At the inland part of Turkey, the station observations underestimate precipitation. The high topographic conditions lead to increase the errors along Agrı, Palandöken and Southeast Taurus Mountains where are situated at the highest region of Turkey. The errors over Istanbul are decreasing in the spring. The underestimations have been still occurred at the shorelines, when the overpredictions are increasing along the Taurus and North Anatolian Mountains. Until May, the model overestimates less precipitation and the errors are reduced at the inland parts especially over the high topography of Northeast region.

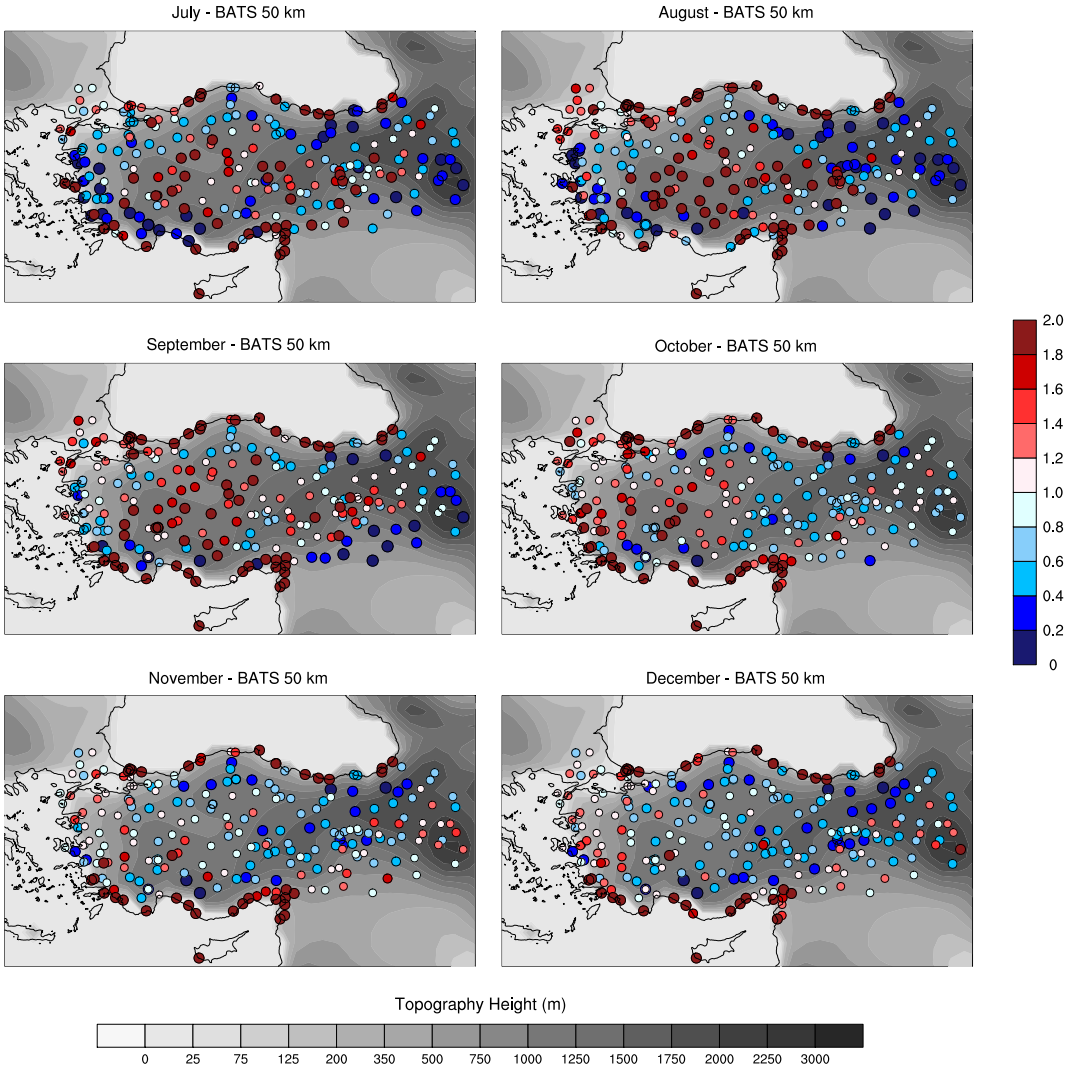

Figure 5.12: The distribution of correction factors for BATS 50 km.

In the summer, the precipitation is underpredicted at the Central Anatolia and along the coastlines. Over the highest elevation of Turkey and the Aegean region, more precipitation has been produced by the model that is demonstrated with blue colors. In the beginning of the autumn, RegCM tends to generate less precipitation. This distribution has been changed until the end of the autumn, and the model overestimates the precipitation throughout the inland part, whereas the modeled precipitation is underestimated over the shorelines. The errors are also decreased at the highest mountainous regions of Turkey. The averages of the correction factors range between 1.02 and 1.22 in winter while they are increased to 1.55-1.64 from July to October. Except spring season, the general tendency of RegCM-BATS at 50 km resolution is the underestimate the precipitation. Underestimation is elevated starting from the end of the summer months through autumn.

The correction factors of the mother domain RegCM-CLM simulations are given in Figure 5.13 and Figure 5.14. CLM has the similar bias pattern in the winter when comparing to BATS results. In the spring the errors are reduced along the inland part of Turkey, however the underestimations are still at the north and south shorelines. On May, the underprediction increases over west Central Anatolia and in the summer, as well. Generally, precipitations are underestimated over Turkey, except Aegean Sea coastline, the inland parts of the Black Sea and southeast of Turkey. In the autumn, the systematic errors at the shorelines and the underestimations of the precipitations have been continued as in the BATS results. Winter averages of the correction factors are in between 1.27 and 1.42 which are larger than the RegCM-BATS at the same resolution. Standard deviations of the correction factors are smallest in April (1.13) and largest in August (2.73)

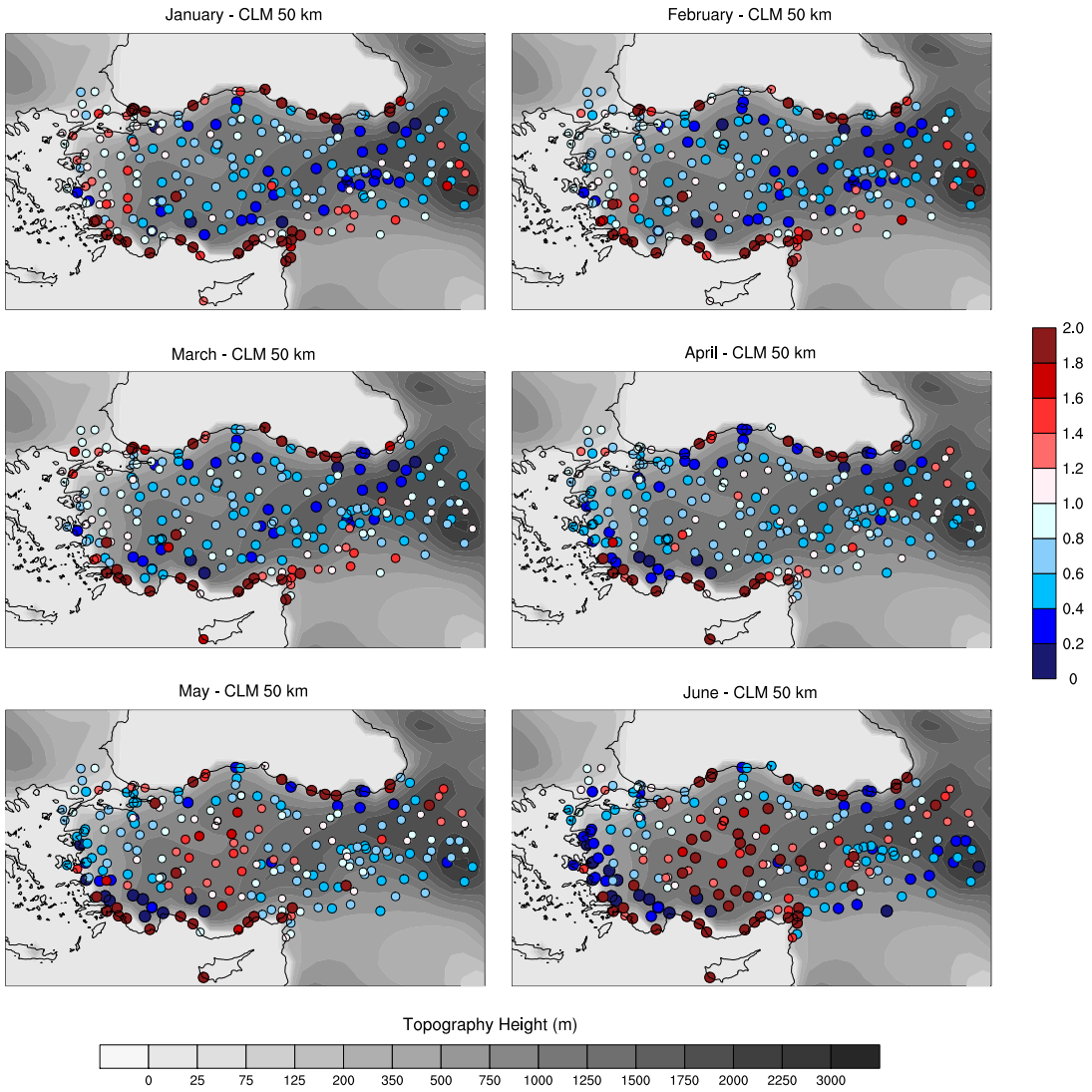

Figure 5.13: The distribution of correction factors for CLM 50 km.

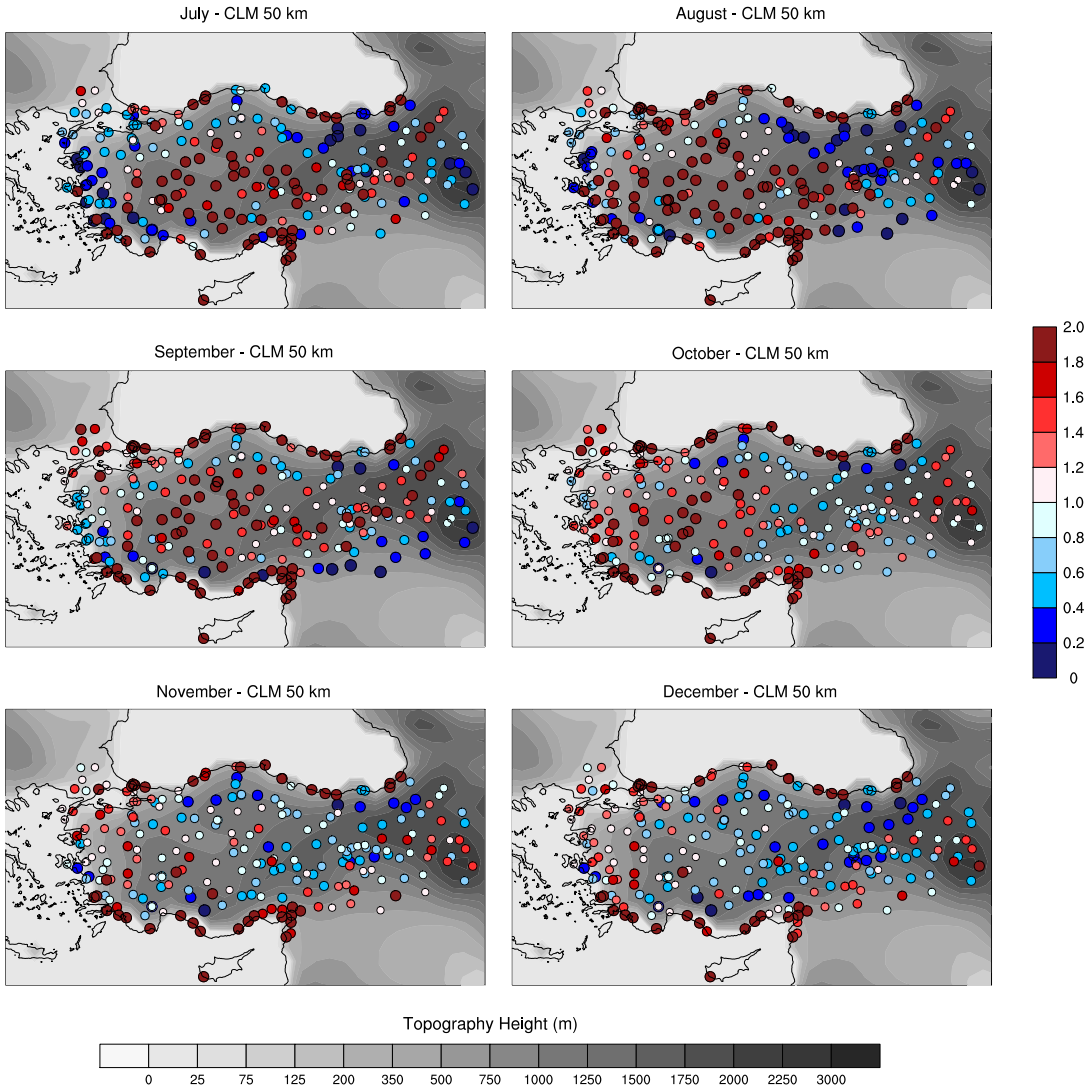

Figure 5.14: The distribution of correction factors for CLM 50 km.

In the Figure 5.15 and Figure 5.16, the correction factors of the high resolution RegCM-BATS simulations are shown over the 10 km grid spacing topography. Winter correction factor distribution is similar with the simulation of the 50 km resolution; however the systematic errors over the coastlines are getting smaller than mother domain errors. The precipitation is mostly overestimated by the model in the spring season and on June and the sizes of errors are increasing, as well. On July, August and September, the errors have been reduced along the Central Anatolia and nearly East Anatolia parts and the averages of the corrections factors vary between 1.05 and 1.26. The systematic precipitation underpredictions are still continuing at the shorelines of north and south. In the autumn, the model produces more precipitation with less error over the inland regions, whereas the precipitation is underpredicted along the coastlines

as BATS 50 km and CLM 50 km results. The general tendency of the RegCM-BATS at 10 km resolution is to produce less precipitation.

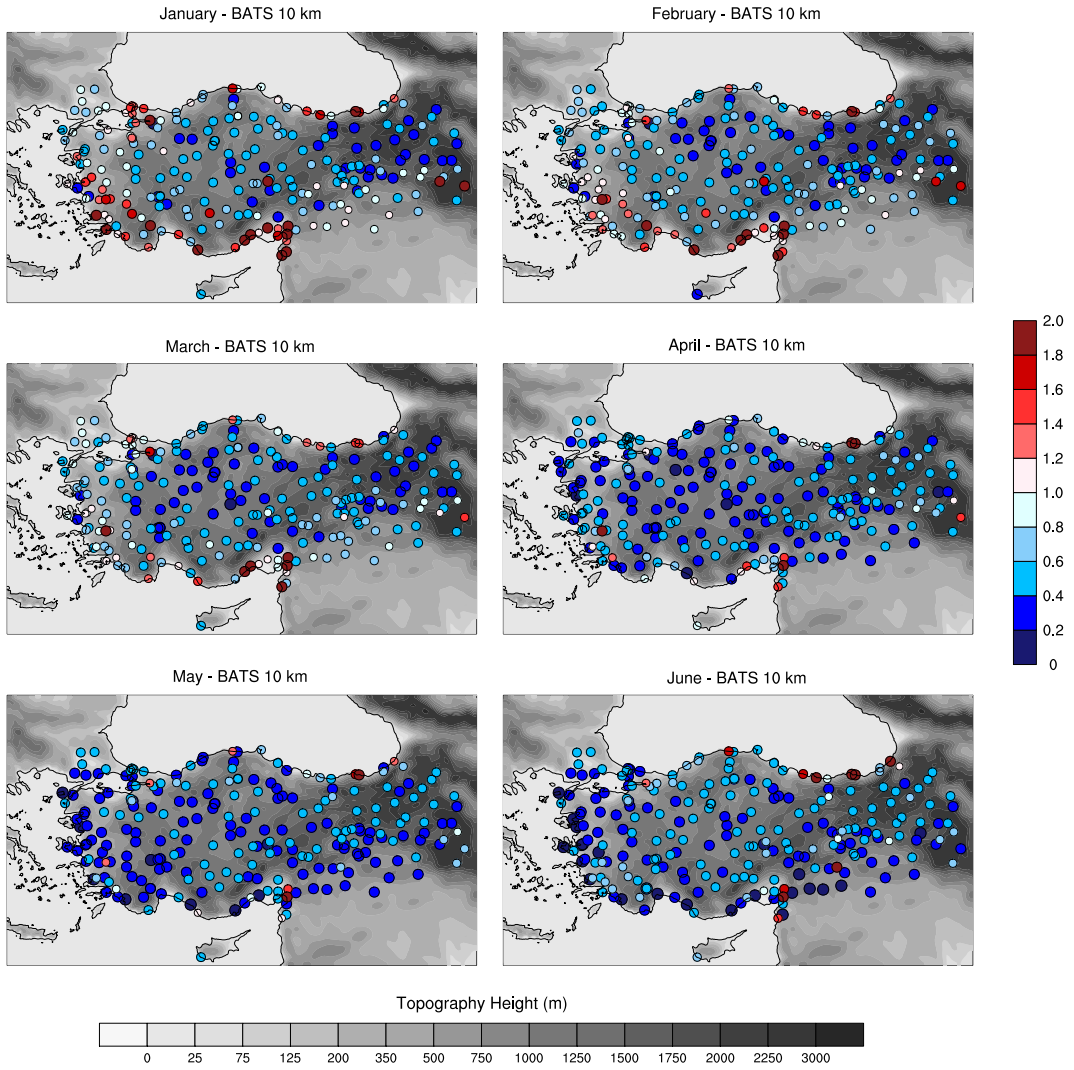

Figure 5.15: The distribution of correction factors for BATS 10 km.

The distribution of Spearman rank correlation between daily BATS50, CLM50 and BATS10 precipitation simulations and observations are shown for each station at Figure 5.17, Figure 5.18 and Figure 5.19, respectively. In the all figures, the color range changes from dark green to dark red. Beginning from the yellow, which means the correlations are equal to 0.25, which coincides to 99% confidence level. If the correlation values increase from 0.25 to 1, the colors change from yellow to red. When the correlation values are under the specified confidence interval, the colors turn dark green from light green.

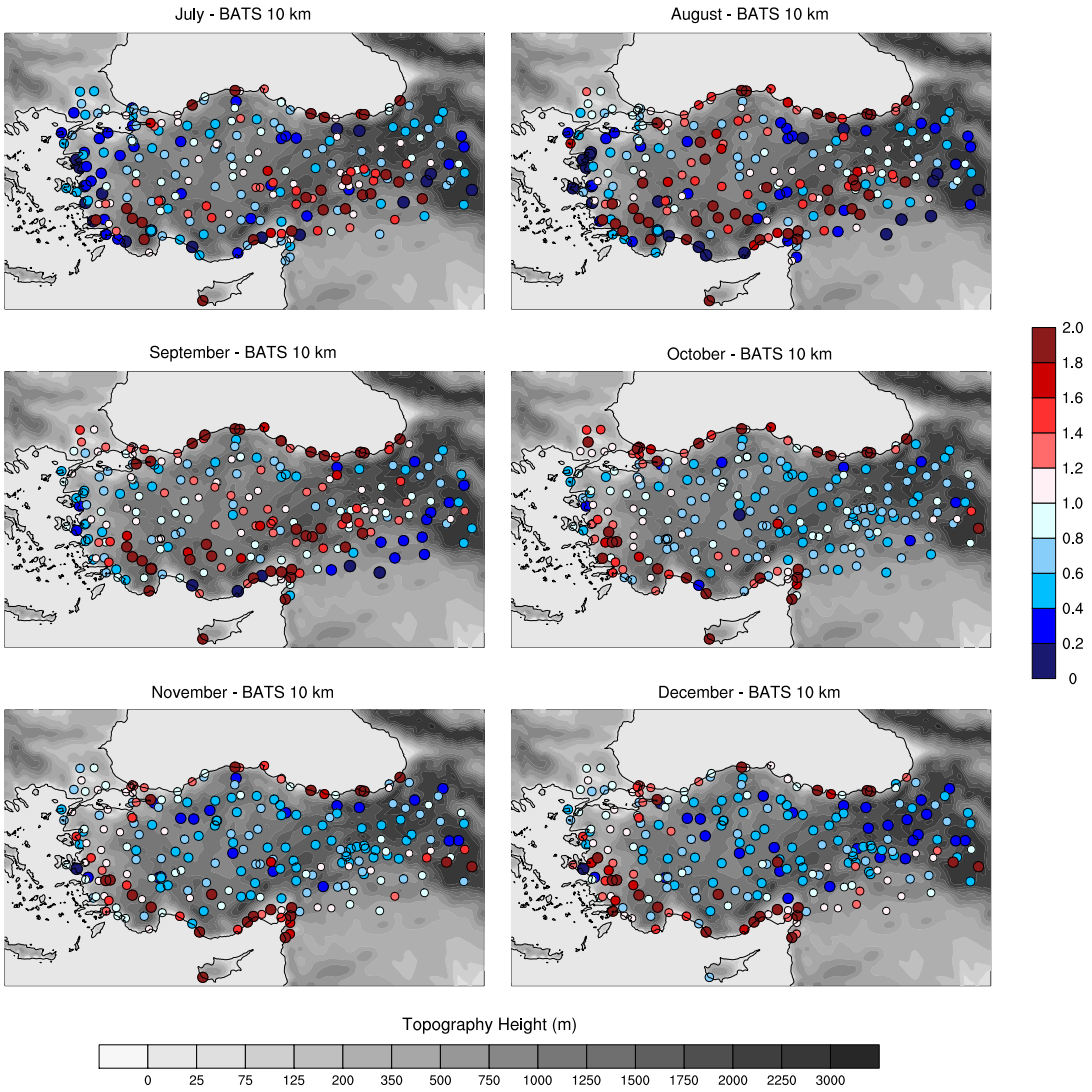

Figure 5.16: The distribution of correction factors for BATS 10 km.

The first Figure 5.17 represents the correlation distributions of RegCM-BATS simulations for the mother domain over 50 km topography. The lowest correlations between the model and observation are located at Black Sea coastline for the uncorrected precipitation. The month-based MV correction generally improves the correlations over Black Sea, East and Southeast Anatolia.

Most studies use Quantile Mapping approaches with Gamma Cumulative Distribution Function (CDF), which is most appropriate distribution function for precipitations. In this study, we also compared QM method with Gamma CDF and the best-fitted CDFs for the model (Generalized Pareto CDF) and observation (Weibull CDF). After Gamma CDF and best-fitted CDF QM correction, the lowest correlations are still calculated at the Black Sea shoreline. However, the season-based QM correction methods improve

the correlations over the shorelines. The best-fitted CDF QM correction results are better than Gamma CDF QM.

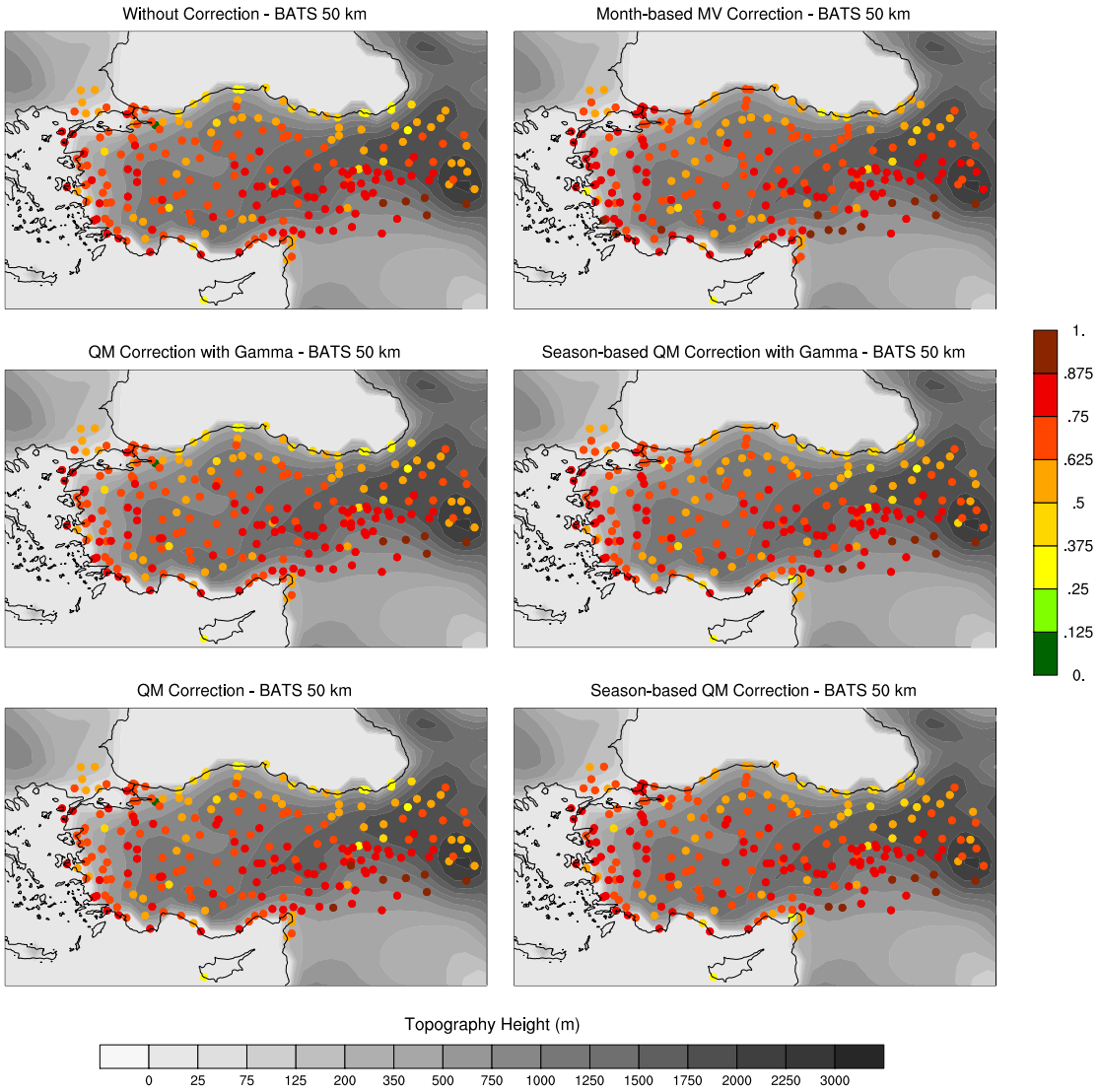

Figure 5.17: BATS 50 km Spearman rank correlation distribution.

As indicated in Figure 5.17, the season-based QM correlations also give better results than QM correction method. Overall, the month-based MV corrected precipitations are the best corrected ones. The correlations over the Black Sea coastline are between 0.25 and 0.75 when from 0.50 to 0.87 at the Aegean and Mediterranean coastlines. Along the Southeast Anatolia, the correlations are calculated as the highest values, which are between 0.60 and 0.90. Over the inland parts of Turkey, the correlations vary between 0.40 and 0.80.

The correlation distributions of the mother domain, which is simulated for CLM, are demonstrated at Figure 5.18. The general of the correlation distributions are worsened than BATS correlation results. The range of correlation values are generally the same

with BATS 50 km results, instead of east Black Sea region, where the correlations are between 0.24 and 0.40. The correlation results of the season-based QM method are mostly better than QM.

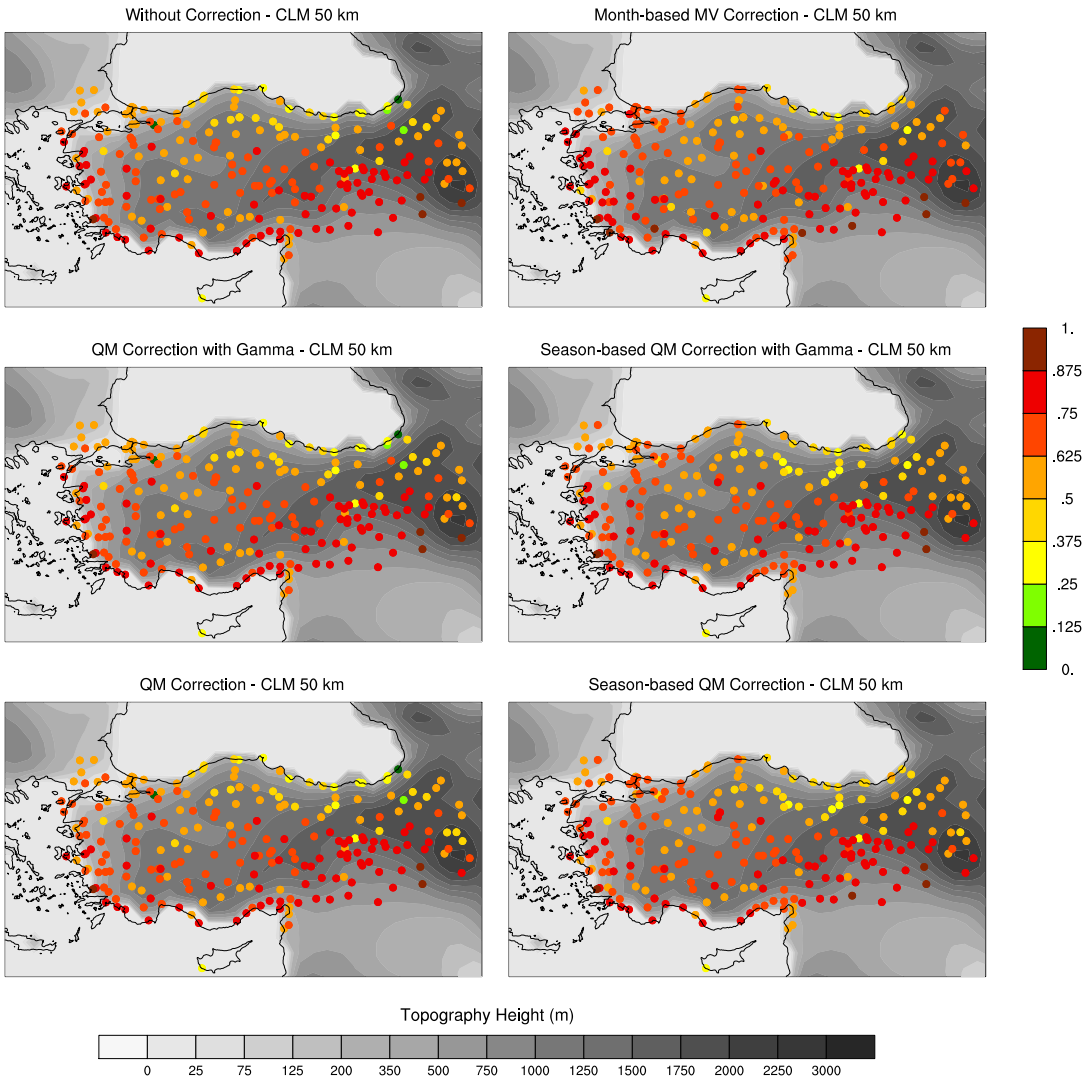

Figure 5.18: CLM 50 km Spearman rank correlation distribution.

In the Figure 5.19, RegCM-BATS correlation results are shown for 10 km grid spacing domain over high resolution topography. The correlations of the high resolution BATS simulations are generally better than the simulations of the coarser resolution, especially at the Black Sea coastline.

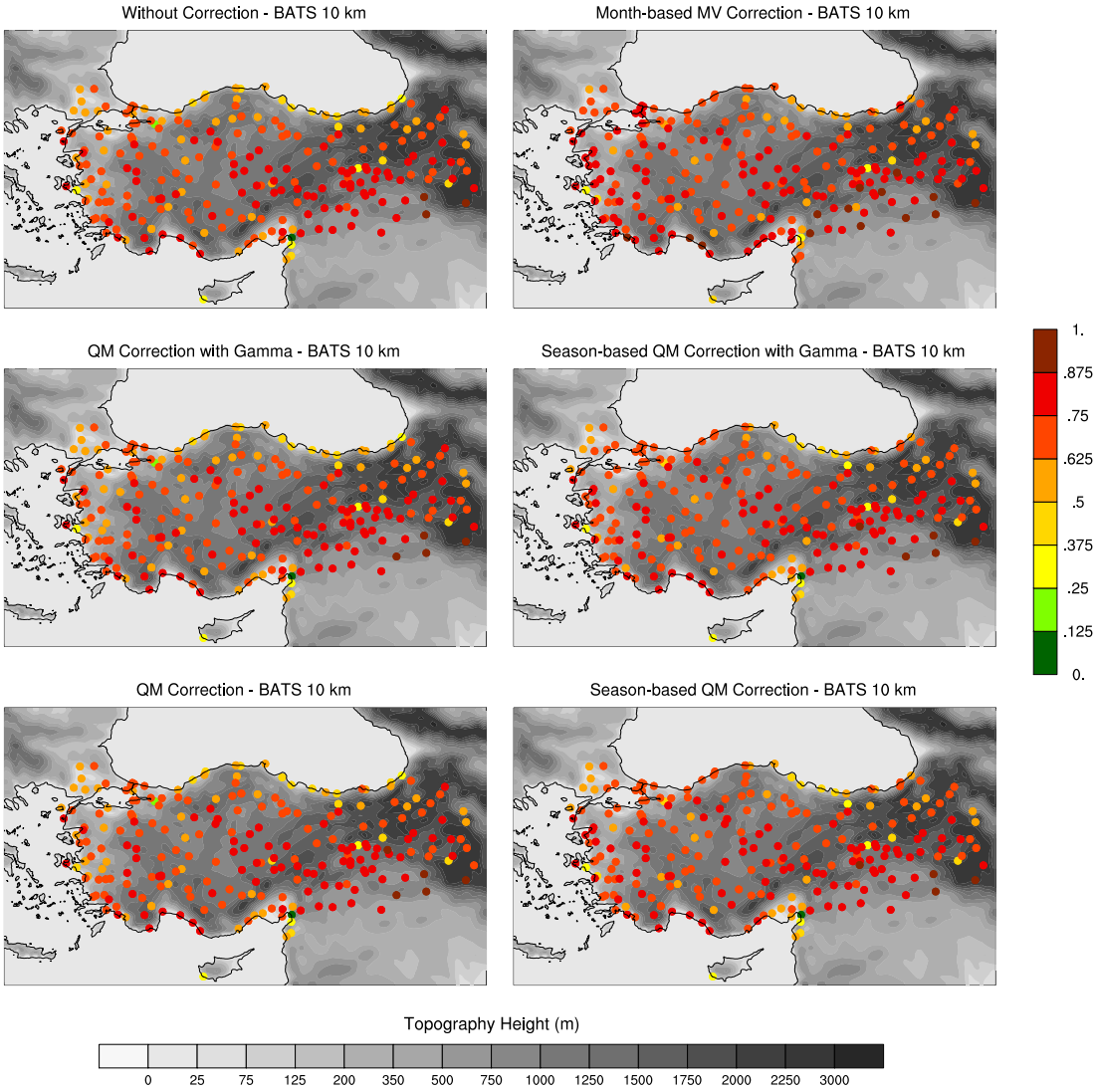

Figure 5.19: BATS 10 km Spearman rank correlation distribution.

When the results of BATS 50 km and 10 km are compared, the modeled precipitations are more improved throughout Turkey. The high resolution BATS precipitations have not been simulated well along the bay of Iskendurun, where the correlations values decrease to 0. That's why the correlations results of high resolution are worse than coarse resolution at Iskenderun Bay. Even the MV method has a quite good performance over Iskenderun, the QM bias correction methods could not correct the precipitations over there. On the whole the figures of the bias correction methods, the correlations are generally between 0.36 to 0.90, which are corresponds to %99 confidence interval.

Before correction, for the mother domain of RegCM simulations, the Black Sea shoreline has big root mean square errors (RMSEs), while they are small at the inland part of Turkey. The smallest errors are calculated from the month-based MV corrected

precipitation simulations. Over the Central Anatolia, the RMSEs are about 0-25 mm and they also reach up to 150 mm at the coastlines. For comparison of the QM correction methods, the RMSE of the season-based QM correction results are better (smaller) than QM approach and also RMSE results for the best-fitted CDF parameters are better than Gamma CDF parameters.

The RMSEs results of the high resolution domain are smaller than the coarse resolution along the Black Sea coastlines. The month-based MV correction method has the smallest RMSE for the mother domain. The best-fitted season-based QM corrected precipitation has the smallest errors when compare to other methods of QM, especially over the Black Sea coasts.

Before correction, the NSE results are close enough to perfect fit, throughout the west coasts and over the inland part of Turkey. That means there is a perfect match between the modeled and observed precipitation. Using the correction of the month-based MV, almost perfect match can easily be seen, except the Mediterranean shorelines. Even the QM methods correct the distribution of the simulations, it is not capable of correcting the variability. Instead of the coastlines, west Central Anatolia and Southeast Anatolia, the mean of the observations are better predictor than the model.

The figures of the RMSE and the NSE are given in the Appendix A.2 section.

6. CONCLUSIONS

The aim of this study is to analyze the performance of RegCM model for different configurations. The simulations are conducted for the period of 1971-2000. The biases of the regional climate model in precipitation are investigated and the performance of different bias correction methods to reproduce the observed precipitation are tested over Turkey. Since simulation period is only 30 years, the first 20 years are selected to build the correction model and the last 10 years are used to validate the correction methodology.

In this study, the precipitation simulations are carried out by using RegCM coupled with two Land Surface Models, BATS and CLM for 50 km coarse resolution and BATS for 10 km high resolution. The biases in daily precipitation simulations are modeled by means of two different methodology and 245 station observations taken from TSMS for 1971 -1990.

First, overall performances of two Land Surface Models (BATS and CLM) and two resolutions are evaluated in the calibration period between 1971 and 1990, to obtain the correction factors and correction parameters. Second, each LSM and the domain are tested for the validation period of 1991 to 2000 using cross-validation methods, such as Spearman rank correlation, RMSE and NSE.

• When comparing the modeled precipitation with CRU data set, the positive biases have been seen over the mountainous regions. This might be explained by either the deficiency of the physical parameterization packages of the model or the gridded observations since the CRU data use the meteorological station network which is not evenly distributed over the low and high altitudes.

• In general, the performance of RegCM is good at capturing the general precipitation patterns. The long-term precipitation patterns are strongly controlled by topography. The best performance has been occurred in the summer. The highest

positive bias is estimated in the spring season and the dryness of the summer season is very well captured by two land surface models.

• Along the Black Sea and the Mediterranean mountains that run parallel to the coastlines, the precipitation is underpredicted for BATS50, CLM50 and BATS10 experiments, whereas the precipitation is generally overpredicted throughout the Aegean Sea and inland part of Turkey. Even the winter correction factor distribution of BATS50 is similar to BATS10, the systematic errors are becoming smaller with the increasing resolution over the shorelines. Generally, CLM produces more precipitation throughout inland, whereas BATS generates more precipitation over high topography.

• The correlations results between the modeled and observed precipitations show that the correlations of CLM50 are worse than BATS50 correlations while BATS10 has more improved correlations, especially along the Black Sea coastline. Overall, according to the validation measures, the correction results of the month-based MV method has the highest correlations, the smallest errors and the perfect matches according to NSE over Turkey especially for the high resolution.

As a consequence, this study investigates the performance of bias correction methods to RegCM simulations, especially for the evaluation of climate and hydrology studies. All bias correction approaches are capable to improve the simulated precipitation. The previous studies found that Quantile Mapping method has better performance than MV to correct the model precipitation biases Dobler et al., 2008 [11]; Piani et al., 2010 [25], [13]; Themeßl et al., 2011 [12]; Argüeso et al., 2013 [24]; Chen et al., 2013 [26]; Lafon et al., 2013 [14]. However, the result of this work illustrates that the month-based MV method show the best performance over Turkey to reduce the precipitation biases.

REFERENCES

[1] **Giorgi, F.**, **Elguindi, N.**, **Cozzini, S. and Giuliani, G.**, (2011). Regional Climatic Model RegCM User's Guide Version 4.3, The Abdus Salam International Centre for Theoretical Physics, Trieste, Italy.

[2] **Giorgi, F.**, **Coppola, E.**, **Solmon, F.**, **Mariotti, L.**, **Sylla, M.B.**, **Bi, X.**, **Elguindi, N.**, **Diro, G.T.**, **Nair, V.**, **Giuliani, G.**, **Turuncoglu, U.U.**, **Cozzini, S.**, **Güttler, I.**, **O'Brien, T.A.**, **Tawfik, A.B.**, **Shalaby, A.**, **Zakey, A.S.**, **Steiner, A.L.**, **Stordal, F.**, **Sloan, L.C. and Brankovic, C.** (2012). RegCM4: model description and preliminary tests over multiple CORDEX domains, *Clim Res*, ***52***, 7–29.

[3] **Hostetler, S.W.**, **Alder, J.R. and Allan, A.M.** (2011). Dynamically downscaled climate simulations over North America: Methods, evaluation and supporting documentation for users, **Technical Report**, U.S. Geological Survey Open-File Report.

[4] **Bonan, G.B.** (2002). Ecological Climatology: Concepts and Applications., **Technical Report**, Cambridge University Press, Cambridge.

[5] **Oleson, K.W.**, **Dai, Y.**, **Bonan, G.B.**, **Bosilovichm, M.**, **Dickinson, R.E.**, **Dirmeyer, P.A.**, **Hoffman, F.**, **Houser, P.R.**, **Levis, S.**, **Niu, G.**, **Thornton, P.**, **Vertenstein, M.**, **Yang, Z. and Zeng, X.a.** (2004). Technical Description of the Communty Land Model (CLM), **Technical ReportTN-461+ STR**, NCAR, Boulder, Colorado.

[6] **Marinucci, M.R.**, **Giorgi, F.**, **Beniston, M.**, **Wild, M.**, **Tschuck, P.**, **Ohmura, A. and Bernasconi, A.** (1995). High Resolution Simulations of January and July .Climate over the Western Alpine Region with a Nested Regional Modeling System, *Theor. Appl. Climatol.*, ***51***, 119–138.

[7] **Schmidli, J.**, **Goodess, C. M. amd Frei, C.**, **Haylock, M.R.**, **Hundecha, Y.**, **Ribalaygua, J. and Schmith, T.** (2007). Statistical and dynamical downscaling of precipitation: An evaluation and comparison of scenarios for the European Alps, *J. Geophys. Res.*, ***112***(D04105).

[8] **Giorgi, F. and Mearns, L.O.** (1991). Approaches to the simulation of regional climate change- a review, *Reviews of Geophysics*, ***29***(2), 191–216.

[9] **Giorgi, F. and Mearns, L.O.** (1999). Introduction to special section: regional climate modeling revisited, *J. Geophys. Res.*, ***104***, 6335–6352.

[10] **Mearns, L.**, **Giorgi, F.**, **Whetton, P.**, **Pabon, D.**, **Hulme, M. and Lal, M.** (2004). Guidelines for use of climate scenarios developed from regional climate

model experiments. Data Distribution Centre of the Intergovernmental Panel on Climate Change, **Technical Report**, Data Distribution Centre of the Intergovernmental Panel on Climate Change.

[11] **Dobler, A. and Ahrens, B.** (2008). Precipitation by a regional climate model and bias correction in Europe and South Asia, *Meteorologische Zeitschrift*, ***17***(4), 499–509.

[12] **Themeßl, M.J.**, **Gobiet, A. and Leuprecht, A.** (2011). Empirical statistical downscaling and error correction of daily precipitation from regional climate models, *Int. J. Climatol.*, ***31***, 1530–1544.

[13] **Piani, C.**, **Weedon, G.**, **Best, M.**, **Gomes, S.**, **Viterbo, P.**, **Hagemann, S. and Haerter, J.** (2010b). Statistical bias correction of global simulated daily precipitation and temperature for the application of hydrological models, *J. Hydrology*, ***395***, 199–215.

[14] **Lafon, T.**, **Dadson, S.**, **Buys, G. and Prudhomme, C.** (2013). Bias correction of daily precipitation simulated by a regional climate model: a comparison of methods, *Int. J. Climatol*, ***33***, 1367–1381.

[15] **Giorgi, F. and Mearns, L.O.** (1999). Introduction to special section: regional climate modeling revisited., *J. Geophys. Res.*, ***104***, 6335–6352.

[16] **Li-Xia, J. and Wang, H.** (2006). A regional climate model nested in a global gridpoint general circulation model., *Chinese Journal of Geophysics*, ***49***(1), 49–58.

[17] **Bordoy, R. and Burlando, P.** (2012). Bias Correction of Regional Climate Model Simulations in a Region of Complex Orography, *Journal of Applied Meteorology and Climatology*, ***52***.

[18] **Perkins, S.E.**, **Pitman, A.J.**, **Holbrook, N.J. and McAneney, J.** (2007). Evaluation of the AR4 climate models' simulated daily maximum temperature, minimum temperature, and precipitation over Australia using probability density functions, *J. Climate*, ***20***(8154), 4356–4376.

[19] **Chen, C.**, **Haerter, J.**, **Hagemann, S. and Piani, C.** (2011). On the contribution of statistical bias correction to the uncertainty in the projected hydrological cycle, *Geophys Res. Lett.*, ***38***(L20403), pp6.

[20] **Önol, B.** (2012). Effects of coastal topography on climate: high-resolution simulation with a regional climate model, *Clim. Res.*, ***52***, 159–174.

[21] **Zhenming, J. and Shichang, K.** (2012). Double-Nested Dynamical Downscaling Experiments over the Tibetan Plateau and Their Projection of Climate Change under Two RCP Scenarios, *Journal Atmos. Sci.*, ***70***.

[22] **Christensen, J.H.**, **Boberg, F.**, **Christensen, O.B. and Lucas-Picher, P.** (2008). On the need for bias correction of regional climate change projections of temperature and precipitation., *Geophys Res. Lett.*, ***35***(L20709), 6pp.

[23] **Berg, P.**, **Feldmann, H. and Panitz, H.J.** (2012). Bias correction of high resolution RCM data, *Journal of Hydrology*.

[24] **Argüeso, D.**, **Evans, J.P. and Fita, L.** (2013). Precipitation bias correction of very high resolution regional climate models., *Hydrol. Earth Syst. Sci. Discuss.*, ***10***, 8145–8165.

[25] **Piani, C.**, **Haerter, J.O. and Coppola, E.** (2010). Statistical bias correction for daily precipitation in regional climate models over Europe, *Theor. Appl. Climatol.*, ***99***, 187–192.

[26] **Chen, J.**, **Brissette, F.P.**, **Chaumont, D. and Braun, M.** (2013). Finding appropriate bias correction methods in downscaling precipitation for hydrologic impact studies over North America, *Water Resources Research*, ***49***, 4187–4205.

[27] **Jones, P. and Harris, I.**, CRU TS3.10: Climatic Research Unit (CRU) Time-Series (TS) Version 3.10 of High Resolution Gridded Data of Month-by-month Variation in Climate (Jan. 1901-Dec. 2009), `http://badc.nerc.ac.uk/view/badc.nerc.ac.uk__ATOM__ACTIVITY_fe67d66a-5b02-11e0-88c9-00e081470265`.

[28] **Harris, I.**, **Jones, P.D.**, **Osborn, T.J. and Lister, D.H.** (2013). Updated high-resolution grids of monthly climatic observations, *Int. J. Climatology*.

[29] **Mitchell and Jones** (2005). An improved method of constructing a database of monthly climate observations and associated high-resolution grids, *Int. J. Climatology*, ***25***, 693–712.

[30] **Anthes, R.A.**, **Hsie, E.Y. and Kuo, Y.H.** (1987). Description of the Penn State/NCAR Mesoscale Model Version 4 (MM4), **Technical ReportTN-282 + STR**, NCAR, Boulder, Colorado.

[31] **Giorgi, F.**, **Bates, G.T. and Nieman, S.J.** (1993a). The multi-year surface climatology of a regional atmospheric model over the Western United States, *J. Climate*, ***6***(75-95).

[32] **Grell, G.A.**, **Dudhia, J. and Stauffer, D.R.** (1994). Description of the fifth generation Penn State/NCAR Mesoscale Model (MM5), **Technical ReportTN-398+STR**, NCAR, Boulder, Colorado.

[33] **Qian, Y. and Giorgi, F.** (1999). Interactive coupling of regional climate and sulfate aerosol models over eastern Asia., *J Geophys Res*, ***104***, 6477–6499.

[34] **Hostetler, S.W.**, **Bates, G.T. and Giorgi, F.** (1993). Interactive nesting of a lake thermal model within a regional climate model for climate change studies., *J Geophys Res*, ***98***, 5045–5057.

[35] **Small, E.E.**, **Sloan, L.C.**, **Hostetler, S.W. and Giorgi, F.** (1999). Simulating the water balance of the Aral Sea with a coupled regional climate-lake model., *J Geophys Res*, ***104***, 6583–6602.

[36] **Pal, J.S.**, **Giorgi, F.**, **Bi, X.Q.**, **Elguindi, N.**, **Solmon, F.**, **Rauscher, S.A.**, **Gao, X.**, **Francisco, R.**, **Zakey, A.S.**, **Winter, J.**, **Ashfaq, M.**, **Syed, F.S.**, **Sloan, L.C.**, **Bell, J.L.**, **Diffenbaugh, N.S.**, **Karmacharya, J.**, **Konaré, A.**, **Martinez, D.**, **Rocha, R.P. and Steiner, A.L.** (2007). Regional climate modeling for the developing world: the ICTP RegCM3 and RegCNET., *Bull Am Meteorol Soc*, ***88***, 1395–1409.

[37] **Giorgi, F.**, **Pal, J.S.**, **Bi, X.Q.**, **Sloan, L.C.**, **Elguindi, N. and Solmon, F.** (2006). Introduction to the TAC special issue: the RegCNET network., *Theor Appl Climatol*, ***86***, 1–4.

[38] **Giorgi, F. and Anyah, R.O.** (2012). The road towards RegCM4, *Clim. Res.*, ***52***, 3–6.

[39] **Coppola, E.**, **Giorgi, F.**, **Mariotti, L. and Bi, X.** (2012). RegT-Band: a tropical band version of RegCM4., *Clim. Res.*, ***52***(115-133).

[40] **Dickinson, R.E.**, **Henderson-Sellers, A. and Kennedy, P.** (1993). Biosphere-atmosphere transfer scheme (BATS) version 1e as coupled to the NCAR community climate model., **Technical ReportTN-387+STR**, NCAR, Boulder, CO.

[41] **Dai, Y.J.**, **Zeng, X.**, **Dickinson, R.E.**, **Baker, I.**, **Bonan, G.B.**, **Bosilovich, M.G.**, **Denning, A.S.**, **Dirmeyer, P.A.**, **Houser, P.R.**, **Niu, G.**, **Oleson, K.W.**, **Schlosser, C.A. and Yang, Z.** (2003). The common land model, *Bull. Am. Meteorol. Soc.*, ***84***.

[42] **Sellers, P.J.**, **Dickinson, R.E.**, **Randall, D.A.**, **Betts, A.K.**, **Hall, F.G.**, **Berry, J.A.**, **Collatz, G.J.**, **Denning, A.S.**, **Mooney, H.A.**, **Nobre, C.A.**, **Sato, N.**, **Field, C.B. and Henderson-Sellers, A.** (275). Modeling the exchanges of energy, water and carbon between continents and the atmosphere, *Science*, ***1997***, 502–509.

[43] **Manabe, S.** (1969). Climate and ocean circulation. I. The atmospheric circulation and the hydrology of the earth's surface, *Mon Weather Rev.*, ***97***, 739–774.

[44] **Steiner, A.L.**, **Pal, J.**, **Giorgi, F.**, **Dickinson, R.E. and Chameides, W.L.** (2005). The coupling of the Common Land Model (CLM0) to a regional climate model (RegCM), *Theor. Appl. Climatol.*, ***82***, 225–243.

[45] **Giorgi, F.**, **Francisco, R. and Pal, J.S.** (2003). Effects of a sub-grid scale topography and landuse scheme on surface climate and hydrology. I. Effects of temperature and water vapor disaggregation., *J. Hydrometeorology*, ***4***, 317–333.

[46] **Kunstmann, H.**, **Schneider, K.**, **Forkel, R. and Knoche, R.** (2004). Impact analysis of climate change for an Alpine catchment using high resolution dynamic downscaling of ECHAM4 time slices, *Hydrology and Earth System Sciences*, ***8***(6), 1030–1044.

[47] **Jung, G. and Kunstmann, H.** (2007). High-resolution Regional Climate Modelling for the Volta Basin of West Africa,, *J. Geophys. Res.,*, ***112***(D23108).

[48] **Vogl, S. and Kunstmann, H.** (2013). Lokale Verfeinerung und Bias-Korrektur von regionalen Klimaszenarien, **TUF01UF 32722**, Universität Augsburg, Augsburg and Garmisch-Partenkirchen.

[49] **Gudmundsson, L.**, **Bremnes, J.B.**, **Haugen, J.E. and Engen, S.T.** (2012). Technical Note: Downscaling RCM precipitation to the station scale using quantile mapping – a comparison of methods, *Hydrol. Earth Syst. Sci. Discuss.*, ***9***, 6185–6201.

[50] **Dettinger, M.**, **Cayan, D.**, **Meyer, M. and Jeton, A.** (2004). Simulated hydrologic responses to climate variations and change in the Merced, Carson, and American river basins, Sierra Nevada, California, 1900-2099., *Climatic Change*, ***62***, 283–317.

[51] **Wood, A.W.**, **Leung, L.**, **Sridhar, V. and Lettenmaier, D.** (2004). Hydrological implications of dynamical and statistical approaches to downscaling climate model outputs., *Climatic Change*, ***62***, 189–216.

[52] **Walpole, R.E.**, **Myers, R.H.**, **Myers, L.S. and Ye, K.** (2011). *Probability & Statistics for Engineers & Scientists*, Pearson, ninth edition.

[53] **Rice, J.A.** (2007). *Mathematical Statistics and Data Analysis*, Thomson Higher Education, Belmont, CA, third edition.

[54] **Gupta, H.V.**, **Kling, H.**, **Yilmaz, K.K. and Martinez, G.F.** (2009). Decomposition of the mean squared error and NSE performance criteria: Implications for improving hydrological modeling., *Journal of Hydrology*, ***377***(1-2), 80–91.

[55] (2006), Met Office, Hadley Centre. HadISST 1.1 - Global sea-Ice coverage and SST (1870-Present), `http://badc.nerc.ac.uk/view/badc.nerc.ac.uk__ATOM__dataent_hadisst`.

[56] **Uppala, S.M.**, **KÅllberg, P.W.**, **Simmons, A.J.**, **Andrae, U.**, **Da Costa Bechtold, V.**, **Fiorino, M.**, **Gibson, J.K.**, **Haseler, J.**, **Hermandez, A.**, **Kelly, G.A.**, **Li, X.**, **Onogi, K.**, **Saarinen, S.**, **Sokka, N.**, **Allan, A.M.**, **Andersson, E.**, **Arpe, K.**, **Balmaseda, M.A.**, **Beljaars, A.C.M.**, **Van De Berg, L.**, **Bidlot, J.**, **Bormann, N.**, **Caires, S.**, **Chevallier, F. an Dethof, A.**, **Dragosavac, M.**, **Fisher, M.**, **Fuentes, M.**, **Hagemann, S.**, **Hólm, E.**, **Hoskins, B.J.**, **Isaksen, L.**, **Janssen, P.A.E.M.**, **Jenne, R.**, **Mcnally, A.P.**, **Mahfouf, J.F.**, **Morcrette, J.J.**, **Rayner, N.A.**, **Saunders, R.W.**, **Simon, P.**, **Steri, A.**, **Trenberth, K.E.**, **Untch, A.**, **Vasiljevic, D.**, **Viterbo, P. and Woollen, J.** (2005). The ERA-40 re-analysis, *Q. J. R. Meteorol. Soc.*, ***131***(612), 2961–3012.

[57] **Kiehl, J.**, **Hack, J.**, **Bonan, G.**, **Boville, B.**, **Breigleb, B.**, **Williamson, D. and Rasch, P.** (1996). Description of the NCAR Community Climate Model (CCM3)., **Technical ReportTN-420+ STR**, NCAR, Boulder, Colorado.

[58] **Holtslag, A.**, **Bruijn, E. and Pan, H.L.** (1990). A high resolution air mass transformation model for short-range weather forecasting., *Mon Weather Rev.*, ***118***, 1561–1575.

[59] **Bretherton, C.S.**, **McCaa, J.R. and Grenier, H.** (2004). A new parameterization for shallow cumulus convection and its application to marine subtropical cloud-topped boundary layers. I. Description and 1D results., *Mon Weather Rev.*, ***132***, 864 – 882.

[60] **Grell, G.** (1993). Prognostic evaluation of assumptions used by cumulus parameterizations., *Mon Weather Rev*, ***121***, 764 –787.

[61] **Emanuel, K.A. and Zivkovic-Rothman, M.** (1999). Development and evaluation of a convection scheme for use in climate models., *Journal Atmos. Sci.*, ***56***, 1766–1782.

[62] **Tiedtke, M.** (1989). A comprehensive mass-flux scheme for cumulus parameterization in large-scale models., *Mon Weather Rev*, ***117***, 1779–1800.

[63] **Pal, J.**, **Small, E. and Eltahir, E.** (2000). Simulation of regional-scale water and energy budgets: representation of subgrid cloud and precipitation processes within RegCM., *J Geophys Res.*, ***105***, 29579–29594.

[64] **Steiner, A.L.**, **Pal, J.S.**, **Rauscher, S.A.**, **Bell, J.L.**, **Diffenbaugh, N.S.**, **Boone, A.**, **Sloan, L.C. and Giorgi, F.** (2009). Land surface coupling in regional climate simulations of the West Africa monsoon., *Clim. Dyn.*, ***33***, 869–892.

[65] **Zeng, X.**, **Zhao, M. and Dickinson, R.E.** (1998). Intercomparison of bulk aerodynamic algorithms for the computation of sea surface fluxes using TOGA COARE and TAO data., *J. Climate*, ***11***, 2628–2644.

[66] **Zeng, X. and Beljaars, A.** (2005). A prognostic scheme of sea surface skin temperature for modeling and data assimilation., *Geophys Res Lett*, ***32***(L14605).

[67] **Solmon, F.**, **Giorgi, F. and Liousse, C.** (2006). Aerosol modeling for regional climate studies: application to anthropogenic particles and evaluation over a European/African domain., *Tellus Ser. B. Chem. Phys. Meterol.*, ***58***, 51–72.

[68] **Zakey, A.S.**, **Solmon, F. and Giorgi, F.** (2006). Implementation and testing of a desert dust module in a regional climate model., *Atmos Chem Phys*, ***6***, 4687–4704.

[69] **Zakey, A.**, **Giorgi, F. and Bi, X.** (2008). Modeling of sea salt in a regional climate model: fluxes and radiative forcing., *J Geophys Res*, ***113***(D14221).

[70] **Artale, V.**, **Calmanti, S.**, **Carillo, A.**, **Dell'Aquila, A.**, **Hermann, M.**, **Pisacane, G.**, **Ruti, P.M.**, **Sannino, G.**, **Struglia, M.V.**, **Giorgi, F. and Bi, X. Rauscher, S.** (2010). An atmosphere-ocean regional climate model for the Mediterranean area: assessment of a present climate simulation., *Clim Dyn*, ***35***, 721–740.

[71] **Ratnam, J.V.**, **Giorgi, F.**, **Kaginalkar, A. and Cozzini, S.** (2009). Simulation of the Indian monsoon using the RegCM3-ROMS regional coupled model., *Clim. Dyn.*, ***33***, 119–139.

[72] **Kadıoğlu, M.** (2000). Regional Variability of Seasonal Precipitation over Turkey, *Int. J. Climatol.*, ***20***, 1743–1760.

[73] **Adams, J. and Lettenmaier, D.** (2003). Adjustment of global gridded precipitation for systematic bias, *J. Geophys. Res.*, ***108***(4257).

[74] **Maraun, D.**, **Wetterhall, F.**, **Ireson, A.M.**, **Chandler, R.E.**, **Kendon, E.J.**, **Widmann, M.**, **Brienen, S.**, **Rust, H.W.**, **Sauter, T.**, **Themeßl, M.J.**, **Venema, V.K.C.**, **Chun, K.P.**, **Goodess, C.M.**, **Jones, R.G.**, **Onof, C.**, **Vrac, M. and Thiele-Eich, I.** (2010). Precipitation downscaling under climate change: Recent developments to bridge the gap between dynamical models and the end user, *Reviews of Geophysics.*, ***48***(Rg3003).

APPENDICES

APPENDIX A.1 : Akaike Information Criteria results
APPENDIX A.2 : RMSE and NSE results

APPENDIX A.1

Table A.1: Akaike Information Criteria results of the observed precipitation.

sta	Normal	Gamma	Exp	Weibull	G.Pareto	sta	Normal	Gamma	Exp	Weibull	G.Pareto
1	11273.3	8638.0	8862.7	8589.8	8613.8	**61**	5817.1	4208.4	4341.4	4173.1	4173.8
2	12542.3	9533.6	9930.2	9483.6	9573.8	**62**	6973.8	5129.8	5279.9	5093.8	5103.2
3	11244.4	8575.6	8910.4	8529.6	8598.4	**63**	6587.5	4889.0	5022.8	4862.7	4887.9
4	9119.0	7013.8	7172.1	6985.4	7024.6	**64**	5513.2	4217.9	4285.6	4198.6	4203.2
5	10442.0	7359.9	7722.4	7284.9	7309.0	**65**	5850.1	4402.0	4492.4	4374.7	4373.0
6	11918.7	9048.2	9324.1	8996.4	9036.3	**66**	8440.1	6845.7	6999.2	6835.3	6904.5
7	13260.6	9956.6	10378.1	9894.0	9970.9	**67**	8599.2	6748.1	6903.6	6719.7	6751.5
8	11123.3	8126.6	8450.5	8061.9	8092.1	**68**	7803.6	6350.1	6398.9	6329.9	6324.0
9	15428.5	12338.8	12706.3	12297.3	12400.2	**69**	6998.6	5756.8	5825.2	5750.6	5782.8
10	14882.0	11951.6	12307.3	11920.8	12038.1	**70**	5764.7	4525.6	4674.5	4509.6	4554.2
11	9324.1	7230.5	7310.2	7194.4	7167.9	**71**	5270.7	4008.0	4179.3	3984.9	4020.7
12	7279.0	5246.5	5585.8	5211.4	5294.3	**72**	5070.4	4141.7	4226.2	4138.8	4182.7
13	6686.3	4936.1	5139.9	4897.8	4918.3	**73**	5310.5	4352.4	4419.5	4348.5	4383.6
14	8393.3	5586.4	6100.0	5509.5	5548.1	**74**	6560.9	4844.2	5080.2	4811.2	4857.2
15	7127.5	5169.4	5402.9	5123.5	5145.0	**75**	5797.1	4369.2	4490.4	4347.2	4372.7
16	9014.5	6859.1	7092.5	6823.1	6869.5	**76**	6416.5	4703.6	4904.0	4671.8	4708.6
17	9511.8	7153.2	7408.6	7112.1	7161.9	**77**	5358.4	3681.7	3830.0	3634.4	3615.0
18	8676.0	6434.2	6727.2	6399.4	6475.9	**78**	4855.6	3597.8	3708.2	3574.9	3590.4
19	10350.6	7743.5	8031.5	7701.8	7767.3	**79**	4758.9	3579.5	3643.7	3560.4	3564.1
20	10133.4	7800.9	7966.7	7764.9	7787.6	**80**	5741.4	4207.1	4328.6	4176.9	4183.3
21	9160.2	6737.9	6917.7	6694.1	6709.9	**81**	6435.6	5308.0	5408.6	5304.6	5359.1
22	10290.1	7952.5	8130.7	7919.6	7955.7	**82**	6306.3	5022.9	5124.9	5009.8	5044.4
23	8194.5	5862.6	6019.7	5806.7	5778.9	**83**	6740.0	5329.7	5518.7	5322.4	5407.0
24	6295.9	4826.5	4890.8	4802.7	4799.6	**84**	5557.2	4099.3	4307.0	4074.7	4126.8
25	7131.4	5272.7	5391.5	5236.1	5231.4	**85**	5672.8	4676.8	4714.9	4668.6	4677.5
26	7454.4	5162.0	5419.5	5105.4	5119.2	**86**	5744.0	4440.5	4579.6	4427.7	4480.7
27	6836.1	5072.3	5195.6	5041.2	5051.1	**87**	5585.1	4536.8	4570.6	4528.2	4539.0
28	7184.6	5362.9	5501.9	5333.5	5355.6	**88**	6594.0	5472.9	5493.4	5461.3	5454.3
29	7248.1	5465.2	5574.0	5438.2	5454.0	**89**	5527.6	4344.9	4480.2	4331.3	4374.2
30	7298.2	5525.3	5628.5	5499.7	5514.3	**90**	7889.0	6041.8	6340.6	6008.8	6074.6
31	6471.1	4790.1	4923.6	4764.9	4792.6	**91**	6069.4	4927.5	5057.1	4916.6	4963.5
32	7574.6	5077.3	5380.5	5014.4	5028.5	**92**	5876.2	4681.5	4826.4	4663.3	4698.3
33	7100.2	5595.8	5620.6	5582.8	5579.8	**93**	7222.0	5538.5	5747.6	5502.4	5531.8
34	7679.6	5985.8	6040.6	5962.7	5955.7	**94**	6882.7	5063.0	5405.1	5007.2	5026.9
35	4507.5	3333.9	3374.0	3314.5	3305.2	**95**	7351.7	5638.7	5966.1	5618.5	5722.2
36	6622.9	4930.7	5204.9	4893.8	4938.1	**96**	6675.0	5090.4	5362.9	5063.8	5128.1
37	5229.9	3952.9	4129.2	3933.8	3981.8	**97**	4788.9	3679.5	3821.0	3662.8	3701.2
38	6149.1	4538.7	4768.0	4506.9	4551.5	**98**	5569.0	4126.9	4390.3	4105.0	4178.1
39	8261.5	5972.3	6210.8	5921.9	5943.3	**99**	6275.5	4687.9	4890.4	4654.8	4686.3
40	7911.7	6186.5	6353.5	6171.6	6235.4	**100**	7537.1	5699.8	5929.3	5669.4	5723.9
41	8678.0	6656.6	6827.2	6619.2	6635.1	**101**	6318.5	4883.9	5122.4	4863.6	4931.1
42	7307.8	5480.5	5610.2	5450.1	5465.7	**102**	5022.8	4196.2	4200.8	4189.7	4179.8
43	6541.0	4863.4	5017.1	4843.1	4894.2	**103**	10441.8	8254.6	8355.1	8211.7	8184.1
44	6350.3	4745.4	4823.9	4725.4	4737.9	**104**	11292.5	9101.5	9239.5	9062.6	9063.8
45	6339.8	4464.3	4629.6	4424.5	4435.5	**105**	6880.9	5156.2	5352.6	5113.3	5121.0
46	8219.0	6224.1	6407.0	6188.8	6216.7	**106**	9944.8	7514.8	7682.6	7460.7	7442.8
47	6203.0	4771.8	4985.6	4754.3	4823.6	**107**	11346.8	8671.8	8842.0	8613.0	8589.9
48	5040.0	3802.3	3951.8	3784.4	3827.5	**108**	10759.0	6905.6	7400.5	6791.1	6774.6
49	7867.7	5720.0	5969.7	5675.5	5707.2	**109**	9852.7	7712.9	7867.6	7675.7	7686.6
50	6745.6	4747.2	5006.1	4704.8	4740.7	**110**	9534.3	7348.2	7511.4	7314.4	7339.5
51	6065.8	4624.5	4677.0	4600.7	4590.9	**111**	11998.3	9257.1	9489.2	9201.6	9212.8
52	7923.4	6394.0	6548.8	6386.2	6459.7	**112**	10027.1	7290.1	7573.3	7214.9	7190.5
53	6077.9	4428.5	4580.3	4390.8	4391.9	**113**	14604.7	11546.1	11986.3	11510.0	11647.3
54	6173.7	4568.9	4805.1	4537.8	4588.4	**114**	7312.7	5998.9	6003.1	5991.3	5986.1
55	5309.9	4212.4	4296.4	4197.6	4218.7	**115**	6692.3	4948.3	5223.5	4910.4	4951.4
56	5403.5	4296.0	4399.2	4286.3	4327.0	**116**	7142.9	5562.2	5699.2	5529.8	5538.4
57	6114.0	4724.8	4920.9	4706.6	4765.0	**117**	8082.8	6077.3	6269.8	6042.4	6075.4
58	6566.4	5110.8	5248.3	5097.7	5149.5	**118**	8388.2	6402.8	6530.8	6361.9	6353.8
59	6790.1	5050.9	5216.2	5022.1	5056.4	**119**	7627.2	5384.0	5502.3	5327.7	5277.8
60	5168.1	3949.3	3992.6	3924.0	3900.0	**120**	7029.7	5317.5	5414.2	5292.2	5305.1

Table A.2: Akaike Information Criteria results of the observed precipitation.

sta	Normal	Gamma	Exp	Weibull	G.Pareto	sta	Normal	Gamma	Exp	Weibull	G.Pareto
121	7366.5	5538.7	5667.6	5509.1	5529.2	**183**	5433.2	4577.5	4577.6	4579.5	4570.8
122	5473.8	4296.6	4312.9	4278.7	4253.7	**184**	8680.6	6563.0	6774.4	6533.4	6586.3
123	6077.2	5107.0	5119.2	5117.4	5119.9	**185**	4987.3	3998.7	4073.6	3985.6	4004.8
124	9154.8	7008.4	7206.5	6966.7	6984.2	**186**	5323.1	4281.1	4366.8	4272.5	4309.0
125	8216.4	6419.6	6480.9	6397.0	6395.8	**187**	5734.5	4522.1	4593.6	4501.9	4506.5
126	8124.5	6022.5	6248.3	5982.4	6016.6	**188**	6747.2	5272.8	5399.5	5250.3	5274.8
127	6926.7	5405.0	5443.3	5385.8	5376.9	**189**	6656.8	5185.2	5293.0	5160.2	5173.7
128	6324.1	4834.4	4868.7	4810.2	4785.4	**190**	7614.0	5438.5	5708.5	5385.6	5404.9
129	7553.9	5683.9	5903.1	5649.2	5690.1	**191**	6499.9	4720.0	4910.4	4677.4	4685.1
130	10808.9	8946.8	9061.4	8930.9	8969.8	**192**	6112.7	4727.4	4773.6	4705.5	4694.4
131	3079.3	2590.6	2593.9	2593.3	2597.4	**193**	5586.9	4249.1	4312.6	4228.7	4229.0
132	6292.1	4700.4	4846.6	4678.7	4718.9	**194**	6974.8	4933.1	5110.1	4878.7	4856.4
133	7586.1	5420.1	5602.8	5368.6	5360.9	**195**	7673.5	5842.3	5960.9	5813.6	5829.3
134	7950.3	6387.0	6428.4	6369.6	6371.3	**196**	5347.1	3986.5	4030.1	3961.8	3940.7
135	6366.9	4900.6	4947.6	4876.9	4860.0	**197**	6275.6	4979.5	5014.1	4951.7	4915.4
136	6368.8	4998.4	5045.3	4980.9	4980.5	**198**	7037.2	5789.1	5887.7	5778.7	5819.4
137	7078.3	5468.5	5533.9	5445.9	5447.6	**199**	6955.2	5577.1	5723.5	5566.5	5626.2
138	7214.5	5481.0	5585.7	5455.7	5468.5	**200**	9359.4	7657.7	7790.7	7644.7	7694.9
139	6337.4	4781.6	4851.1	4758.6	4761.4	**201**	5513.7	4399.6	4503.9	4389.8	4431.8
140	8194.4	6518.9	6576.3	6505.2	6523.5	**202**	5845.3	4670.7	4684.9	4653.0	4627.0
141	7556.2	6295.3	6324.9	6287.4	6300.3	**203**	5381.6	4362.4	4483.4	4359.1	4421.8
142	6780.0	5239.5	5376.2	5221.1	5264.7	**204**	5615.7	4451.9	4578.8	4443.6	4497.1
143	7646.9	5684.9	5780.8	5650.9	5641.1	**205**	5775.4	4608.3	4676.4	4602.1	4637.6
144	6766.7	5186.3	5246.3	5162.9	5161.0	**206**	6032.5	5124.4	5130.8	5119.9	5122.1
145	7544.1	6054.6	6114.5	6042.1	6063.2	**207**	6865.9	5398.9	5491.8	5375.5	5385.1
146	5766.8	4642.3	4652.9	4631.5	4619.2	**208**	6066.6	4623.5	4733.8	4597.2	4609.5
147	5002.9	3949.7	3947.7	3946.3	3930.3	**209**	5554.8	4321.4	4370.2	4302.6	4299.2
148	5652.6	4431.0	4568.3	4414.5	4455.1	**210**	5906.0	4806.3	4855.1	4799.2	4817.3
149	6467.7	4846.3	4981.5	4825.3	4863.5	**211**	6541.0	5412.3	5490.6	5407.2	5446.6
150	6311.6	4626.2	4770.6	4595.8	4616.8	**212**	6561.9	4954.8	5037.5	4919.0	4892.3
151	6455.2	4876.4	4967.4	4846.8	4841.5	**213**	7473.5	5578.1	5891.5	5546.2	5622.5
152	5683.9	4272.9	4359.1	4246.9	4246.1	**214**	5500.7	4491.4	4594.7	4486.4	4538.2
153	6225.6	4853.4	4887.9	4835.0	4826.5	**215**	6257.1	4762.4	4946.8	4737.7	4781.0
154	7218.4	6004.5	6069.5	6001.8	6040.7	**216**	5850.0	4416.4	4574.8	4385.7	4401.1
155	4854.9	4280.3	4278.3	4280.2	4282.3	**217**	5769.2	4378.1	4509.0	4353.1	4372.2
156	6242.9	5202.9	5202.2	5198.2	5188.3	**218**	6028.4	4467.4	4617.3	4433.5	4443.9
157	5705.0	4559.7	4677.3	4552.5	4605.9	**219**	9761.8	6194.5	7168.6	6088.1	6113.4
158	7660.7	5838.8	6077.7	5814.2	5883.9	**220**	5116.5	3724.5	3831.4	3694.8	3694.4
159	6414.6	5153.3	5216.0	5140.7	5160.1	**221**	4905.2	3513.5	3633.9	3483.7	3489.9
160	7117.4	4922.0	5202.1	4870.1	4897.1	**222**	5292.4	3980.3	4049.3	3956.8	3954.8
161	6174.0	4635.1	4777.1	4613.7	4652.9	**223**	7251.9	5690.3	5848.1	5674.0	5728.9
162	6958.6	5100.4	5275.2	5060.2	5071.8	**224**	5914.5	4838.4	4904.2	4835.6	4870.0
163	6323.1	4615.8	4746.4	4583.5	4593.0	**225**	7563.2	6045.5	6143.2	6022.5	6036.0
164	6131.0	4763.3	4777.7	4745.8	4719.0	**226**	6899.5	5446.0	5631.0	5428.7	5489.7
165	7659.0	6133.1	6264.9	6115.3	6157.4	**227**	4998.1	3687.4	3818.5	3661.6	3678.9
166	6369.9	5131.8	5169.6	5120.4	5124.9	**228**	6386.2	5144.2	5203.6	5124.8	5125.8
167	6440.0	5375.0	5387.6	5368.2	5371.1	**229**	7242.0	5635.8	5851.7	5615.5	5682.9
168	3898.8	3182.7	3231.4	3179.8	3206.7	**230**	4718.2	3701.0	3764.5	3681.6	3679.7
169	7114.7	5793.9	5844.6	5785.6	5806.4	**231**	5965.5	4839.8	4914.8	4825.4	4842.9
170	7883.6	6361.4	6439.4	6348.4	6375.8	**232**	5355.6	4103.8	4237.8	4083.8	4114.1
171	6848.6	5726.1	5727.0	5721.0	5713.2	**233**	6833.9	5505.4	5692.5	5495.7	5571.0
172	6381.1	5123.1	5154.9	5110.5	5113.1	**234**	5340.3	4032.5	4232.4	4007.7	4049.3
173	5174.8	4270.6	4270.5	4272.5	4265.5	**235**	6487.3	5088.5	5243.4	5068.1	5108.5
174	6308.0	5206.4	5206.2	5201.1	5188.9	**236**	8184.9	6337.2	6546.2	6301.9	6336.6
175	5476.5	4273.3	4411.9	4259.4	4306.2	**237**	6603.7	5403.4	5471.2	5388.7	5403.5
176	5290.3	4253.9	4309.7	4239.7	4250.1	**238**	4699.9	3634.1	3714.0	3620.6	3642.4
177	6233.3	4588.5	4743.7	4561.9	4596.6	**239**	4019.0	3104.7	3139.8	3091.6	3091.7
178	6745.9	5052.8	5185.3	5024.9	5043.9	**240**	6577.1	5230.5	5411.3	5215.6	5277.3
179	7833.1	5250.8	5649.4	5186.8	5220.0	**241**	5680.5	4437.1	4520.5	4416.0	4422.8
180	5275.7	4172.4	4195.7	4160.3	4156.4	**242**	7037.1	5393.7	5585.2	5358.4	5379.5
181	6301.8	5071.5	5125.6	5057.5	5069.9	**243**	6368.5	4963.3	5122.0	4932.3	4945.9
182	7577.5	6370.2	6416.7	6363.2	6385.9	**244**	7965.3	6319.5	6514.9	6298.5	6357.7
						245	7699.4	5843.2	6082.1	5817.9	5889.8

Table A.3: Akaike Information Criteria results of the modeled precipitation.

sta	Normal	Gamma	Exp	Weibull	G.Pareto	sta	Normal	Gamma	Exp	Weibull	G.Pareto
1	7906.1	5748.6	5937.4	5690.0	5662.7	**61**	8468.7	5788.9	5990.2	5707.0	5637.3
2	5594.1	3846.8	3902.4	3801.9	3739.7	**62**	9945.0	7139.0	7323.0	7061.6	6995.8
3	14973.3	11473.3	11728.3	11397.9	11383.3	**63**	10450.6	7169.0	7395.5	7068.5	6970.9
4	7188.7	4942.5	5062.1	4867.6	4769.9	**64**	9972.3	7869.6	8021.9	7841.6	7880.0
5	14775.9	11609.6	11961.1	11555.4	11622.7	**65**	10177.6	8106.2	8260.5	8082.2	8130.2
6	6330.0	4264.6	4335.9	4204.4	4117.6	**66**	11860.9	9447.2	9587.6	9413.9	9437.6
7	6337.8	4413.8	4436.2	4378.9	4313.8	**67**	11562.8	9488.5	9624.5	9472.3	9529.3
8	18860.0	15228.6	15532.3	15176.4	15236.9	**68**	11576.7	9354.9	9474.4	9333.7	9372.5
9	12693.7	9891.4	10059.0	9843.4	9846.7	**69**	10618.9	8568.7	8685.5	8542.7	8566.8
10	13901.8	10880.0	11116.3	10824.8	10843.7	**70**	6587.1	4821.1	5043.9	4773.2	4775.1
11	13901.8	10880.0	11116.3	10824.8	10843.7	**71**	8198.3	5913.9	6114.3	5844.7	5796.3
12	11139.3	7516.1	7957.6	7377.6	7267.4	**72**	7455.4	5621.1	5851.0	5573.7	5580.9
13	11002.7	7499.9	7843.0	7375.3	7270.0	**73**	7676.1	5440.1	5784.8	5370.8	5371.2
14	11050.2	7768.3	8087.1	7657.8	7572.6	**74**	6556.4	4470.0	4721.9	4393.7	4339.8
15	8387.5	5839.8	5995.2	5765.0	5693.0	**75**	10641.8	7114.9	7579.8	6967.2	6824.9
16	8756.8	6211.4	6368.9	6138.0	6070.7	**76**	10664.0	7875.0	8310.6	7804.5	7840.2
17	8756.8	6211.4	6368.9	6138.0	6070.7	**77**	9422.3	6505.7	6680.3	6414.0	6309.3
18	11197.0	8430.8	8670.9	8375.3	8395.6	**78**	8105.7	5233.8	5473.0	5116.6	4981.9
19	12317.4	9079.6	9301.0	8998.7	8951.4	**79**	9551.7	6400.8	6776.1	6281.4	6185.0
20	12613.9	9601.2	9777.2	9539.4	9514.8	**80**	10442.1	7659.6	7841.6	7589.3	7543.1
21	15593.0	11928.1	12260.1	11842.7	11837.1	**81**	8914.9	6765.8	6929.0	6720.9	6719.5
22	14318.9	11056.2	11323.2	10988.7	10993.2	**82**	7206.5	5517.2	5645.0	5482.2	5482.6
23	13512.9	9960.2	10102.2	9880.7	9799.2	**83**	9807.8	7721.3	7864.6	7693.5	7727.3
24	12835.3	9249.8	9411.5	9166.7	9090.6	**84**	6233.8	4775.3	4876.2	4745.6	4743.5
25	12367.9	9176.7	9315.1	9114.5	9073.1	**85**	7183.6	5476.9	5611.5	5439.8	5437.2
26	10527.0	7048.8	7202.9	6947.1	6818.3	**86**	8795.5	6887.8	7058.9	6858.0	6895.3
27	11681.5	8886.6	8998.2	8839.8	8815.6	**87**	9890.5	7918.9	8073.6	7892.5	7931.4
28	13366.0	9534.4	9713.0	9437.2	9336.8	**88**	12074.7	9267.6	9557.9	9211.5	9245.5
29	18880.1	15338.4	15521.1	15293.2	15313.8	**89**	6111.2	4297.4	4449.2	4245.0	4213.0
30	12682.8	8455.0	8626.1	8330.0	8161.4	**90**	9926.5	7600.6	7974.7	7548.4	7602.0
31	13416.0	10143.4	10284.5	10083.2	10049.1	**91**	5817.8	3921.4	4165.0	3851.3	3806.0
32	14294.7	10277.6	10478.3	10177.0	10081.0	**92**	1985.0	1235.2	1266.4	1210.6	1173.2
33	12212.4	8726.3	8824.7	8661.4	8595.8	**93**	4594.4	3097.8	3188.6	3044.0	2973.9
34	11159.4	7717.4	7924.3	7624.1	7542.8	**94**	10447.4	8379.9	8599.3	8350.3	8403.9
35	9526.8	6363.7	6461.3	6284.0	6171.0	**95**	3105.0	2037.6	2120.1	2000.8	1964.2
36	10679.3	7461.1	7747.7	7350.0	7249.4	**96**	992.7	574.1	576.2	564.5	543.0
37	9154.8	6180.2	6355.0	6085.5	5983.5	**97**	3418.8	2163.3	2210.7	2124.4	2072.4
38	9154.8	6180.2	6355.0	6085.5	5983.5	**98**	3336.6	1880.2	1915.7	1828.3	1723.2
39	10719.5	8063.6	8249.5	8004.0	7984.5	**99**	8302.8	5411.9	5808.1	5272.6	5127.9
40	14272.3	10494.1	10925.6	10390.3	10378.1	**100**	6282.5	4396.2	4623.6	4334.1	4306.7
41	11531.5	8152.1	8470.1	8044.6	7974.4	**101**	3745.2	2450.8	2536.3	2407.3	2365.2
42	11392.3	7366.9	7698.6	7222.7	7080.3	**102**	5807.5	3869.5	3917.1	3828.1	3775.4
43	11392.3	7366.9	7698.6	7222.7	7080.3	**103**	7906.1	5748.6	5937.4	5690.0	5662.7
44	11392.3	7366.9	7698.6	7222.7	7080.3	**104**	15199.5	11666.8	11965.7	11587.9	11583.0
45	9975.6	6453.8	6616.8	6345.8	6205.3	**105**	9980.5	7050.4	7443.0	6954.7	6914.2
46	10651.5	7124.3	7368.8	7007.3	6883.4	**106**	9065.0	6424.3	6567.3	6350.8	6276.6
47	10129.8	6618.6	7243.7	6470.5	6362.2	**107**	14318.9	11056.2	11323.2	10988.7	10993.2
48	11187.5	7696.1	8100.9	7577.5	7506.1	**108**	15199.5	11666.8	11965.7	11587.9	11583.0
49	11333.7	7836.2	8026.0	7737.3	7638.5	**109**	8756.8	6211.4	6368.9	6138.0	6070.7
50	9494.5	6494.0	6704.9	6401.6	6316.4	**110**	5075.7	3271.5	3332.4	3216.2	3131.1
51	11989.9	8943.8	9162.4	8883.5	8887.2	**111**	4405.7	2861.3	2929.0	2809.2	2731.8
52	12023.7	9580.0	9725.8	9549.1	9580.2	**112**	18860.0	15228.6	15532.3	15176.4	15236.9
53	12630.8	9070.1	9307.8	8969.8	8883.7	**113**	7389.5	5240.3	5403.5	5168.9	5099.3
54	11431.3	7756.3	8024.8	7625.2	7485.8	**114**	11867.6	8603.7	8769.6	8521.5	8443.8
55	10071.5	6822.5	7483.7	6703.3	6667.6	**115**	9760.3	6617.5	6811.4	6513.4	6390.6
56	9543.9	6630.3	6985.9	6538.5	6501.2	**116**	10166.5	7140.9	7547.7	7040.6	6997.9
57	6587.1	4821.1	5043.9	4773.2	4775.1	**117**	9370.6	6877.8	7049.1	6818.0	6790.4
58	7283.7	5354.8	5508.0	5308.5	5295.4	**118**	14272.3	10494.1	10925.6	10390.3	10378.1
59	9297.4	6196.5	6494.2	6083.6	5972.7	**119**	15066.3	11366.1	11585.6	11285.3	11245.3
60	8103.4	5361.1	5599.6	5263.1	5160.6	**120**	14614.5	10551.8	10802.1	10440.2	10343.0

Table A.4: Akaike Information Criteria results of the modeled precipitation.

sta	Normal	Gamma	Exp	Weibull	G.Pareto	sta	Normal	Gamma	Exp	Weibull	G.Pareto
121	12835.3	9249.8	9411.5	9166.7	9090.6	**183**	13036.1	9118.4	9335.2	9010.1	8903.1
122	12597.8	9258.5	9428.3	9187.4	9143.2	**184**	8770.0	6363.2	6717.2	6290.1	6277.3
123	12212.4	8726.3	8824.7	8661.4	8595.8	**185**	6675.2	5042.1	5250.2	5010.6	5047.9
124	11531.5	8152.1	8470.1	8044.6	7974.4	**186**	7254.8	5322.0	5500.5	5277.8	5281.1
125	11867.6	8603.7	8769.6	8521.5	8443.8	**187**	10641.8	7114.9	7579.8	6967.2	6824.9
126	13012.6	8966.1	9255.7	8840.7	8727.2	**188**	7985.2	5108.0	5232.3	5007.2	4848.2
127	20313.3	16893.2	17081.2	16871.8	16946.4	**189**	9632.8	6624.0	6820.2	6525.5	6413.3
128	15633.9	11538.2	11717.7	11450.4	11375.6	**190**	452.8	282.8	285.7	277.6	270.5
129	11967.3	8054.2	8426.9	7904.1	7763.0	**191**	12268.9	8761.9	9148.7	8654.2	8598.8
130	14272.3	10494.1	10925.6	10390.3	10378.1	**192**	12143.5	8569.8	8923.0	8461.4	8402.4
131	11214.0	7608.7	7911.7	7484.3	7363.4	**193**	12143.5	8569.8	8923.0	8461.4	8402.4
132	10531.9	6905.2	7192.9	6775.2	6640.3	**194**	11734.4	8253.1	8612.0	8147.1	8091.8
133	12049.7	8260.2	8438.4	8153.0	8030.0	**195**	13007.1	9637.7	10050.8	9567.7	9625.7
134	13606.4	9999.8	10168.4	9927.6	9885.8	**196**	9972.3	7869.6	8021.9	7841.6	7880.0
135	12049.7	8260.2	8438.4	8153.0	8030.0	**197**	8589.6	6903.4	6999.5	6887.5	6923.1
136	13606.4	9999.8	10168.4	9927.6	9885.8	**198**	9531.2	7788.6	7887.8	7771.7	7807.3
137	19104.8	15282.5	15666.1	15224.5	15307.0	**199**	8482.9	6756.7	6852.7	6738.2	6768.5
138	15398.3	11700.4	11834.3	11630.3	11568.7	**200**	6675.2	5042.1	5250.2	5010.6	5047.9
139	12889.5	8825.6	9049.5	8701.6	8556.3	**201**	12630.8	9070.1	9307.8	8969.8	8883.7
140	11938.1	8183.5	8350.6	8087.0	7984.4	**202**	7455.4	5621.1	5851.0	5573.7	5580.9
141	14272.3	10494.1	10925.6	10390.3	10378.1	**203**	6675.2	5042.1	5250.2	5010.6	5047.9
142	10489.9	7262.1	7583.5	7163.7	7113.8	**204**	10641.8	7114.9	7579.8	6967.2	6824.9
143	13374.8	9665.1	9926.7	9561.8	9485.6	**205**	10641.8	7114.9	7579.8	6967.2	6824.9
144	11564.4	8249.7	8543.4	8159.8	8124.7	**206**	10890.4	8558.7	8702.7	8529.4	8562.7
145	14149.4	9680.5	9890.9	9545.8	9376.8	**207**	12504.8	8936.4	9314.8	8839.0	8821.2
146	14065.0	10412.6	10683.8	10325.3	10289.0	**208**	13007.1	9637.7	10050.8	9567.7	9625.7
147	12646.8	8636.5	8860.1	8512.6	8368.7	**209**	11571.8	9282.7	9429.8	9260.4	9311.3
148	10129.8	6618.6	7243.7	6470.5	6362.2	**210**	8589.6	6903.4	6999.5	6887.5	6923.1
149	8853.0	5909.1	6132.1	5809.1	5696.7	**211**	14594.5	10357.3	10668.8	10225.7	10107.3
150	9639.7	5710.8	6034.6	5563.1	5411.1	**212**	7415.1	5007.4	5177.5	4929.9	4852.0
151	8941.8	5910.3	6149.2	5803.6	5688.2	**213**	6111.2	4297.4	4449.2	4245.0	4213.0
152	10617.0	7343.7	7559.6	7242.7	7141.0	**214**	9926.5	7600.6	7974.7	7548.4	7602.0
153	12452.4	8555.3	8883.4	8430.0	8321.3	**215**	12368.3	10322.0	10485.9	10308.7	10379.4
154	12023.7	9580.0	9725.8	9549.1	9580.2	**216**	12387.1	9968.6	10183.2	9949.0	10032.6
155	11989.9	8943.8	9162.4	8883.5	8887.2	**217**	9625.1	5809.7	6498.7	5589.0	5320.9
156	13375.7	9649.8	9927.0	9549.1	9483.8	**218**	15161.3	12523.2	12862.2	12488.3	12580.0
157	8458.7	5910.7	6284.8	5835.2	5830.9	**219**	9884.3	6542.1	6922.4	6402.6	6268.4
158	10285.5	7463.7	7725.9	7393.4	7381.0	**220**	7787.1	5304.6	5404.4	5236.6	5150.0
159	10285.5	7463.7	7725.9	7393.4	7381.0	**221**	10704.7	7993.6	8170.1	7936.7	7924.3
160	9120.5	6304.8	6451.6	6225.0	6136.0	**222**	9831.5	7224.6	7427.6	7155.7	7118.8
161	9494.5	6494.0	6704.9	6401.6	6316.4	**223**	7835.6	6048.6	6162.6	6017.4	6024.6
162	9433.6	6335.1	6593.1	6231.5	6132.9	**224**	6647.1	4997.4	5126.4	4963.1	4965.0
163	11989.9	8943.8	9162.4	8883.5	8887.2	**225**	5817.8	3921.4	4165.0	3851.3	3806.0
164	11502.9	9052.6	9187.4	9023.7	9054.3	**226**	11111.9	8737.5	9026.1	8691.4	8733.2
165	11934.5	9428.0	9572.6	9396.0	9424.6	**227**	17717.0	13394.4	14244.3	13250.7	13265.0
166	9972.3	7869.6	8021.9	7841.6	7880.0	**228**	11413.0	8689.8	8921.6	8630.7	8634.1
167	11934.5	9428.0	9572.6	9396.0	9424.6	**229**	7453.1	5066.5	5326.0	4978.5	4908.4
168	11934.5	9428.0	9572.6	9396.0	9424.6	**230**	11111.9	8737.5	9026.1	8691.4	8733.2
169	11860.9	9447.2	9587.6	9413.9	9437.6	**231**	8923.8	7036.0	7208.2	7004.9	7035.8
170	11248.5	9064.1	9238.1	9038.5	9092.2	**232**	9595.5	7351.2	7653.4	7299.5	7333.8
171	11832.6	8461.7	8616.3	8381.2	8304.4	**233**	4471.6	2530.3	2751.6	2413.4	2249.0
172	12717.1	8897.3	9108.7	8793.6	8696.0	**234**	3336.6	1880.2	1915.7	1828.3	1723.2
173	13726.7	9833.9	9999.0	9728.0	9595.1	**235**	8302.8	5411.9	5808.1	5272.6	5127.9
174	13726.7	9833.9	9999.0	9728.0	9595.1	**236**	6282.5	4396.2	4623.6	4334.1	4306.7
175	6587.1	4821.1	5043.9	4773.2	4775.1	**237**	7364.5	5375.9	5569.7	5321.7	5302.4
176	6460.0	4747.5	4923.8	4705.1	4706.0	**238**	6665.8	5020.7	5147.5	4984.4	4980.1
177	7538.9	4889.6	5056.4	4791.0	4652.8	**239**	6279.3	4672.6	4803.0	4630.8	4611.3
178	10664.6	7139.3	7362.1	7025.2	6896.3	**240**	3684.0	2605.4	2814.0	2568.6	2563.0
179	9972.3	7869.6	8021.9	7841.6	7880.0	**241**	8970.5	5148.9	5706.1	4924.4	4649.7
180	10860.0	8779.4	8939.2	8757.2	8810.3	**242**	8064.0	4666.4	4925.7	4487.3	4219.7
181	11353.8	9113.0	9320.7	9084.7	9144.8	**243**	12268.9	8761.9	9148.7	8654.2	8598.8
182	11876.8	8919.3	9095.0	8859.5	8841.4	**244**	8850.0	6259.3	6678.9	6166.2	6135.8
						245	6977.7	4732.6	4941.0	4659.3	4608.2

APPENDIX A.2

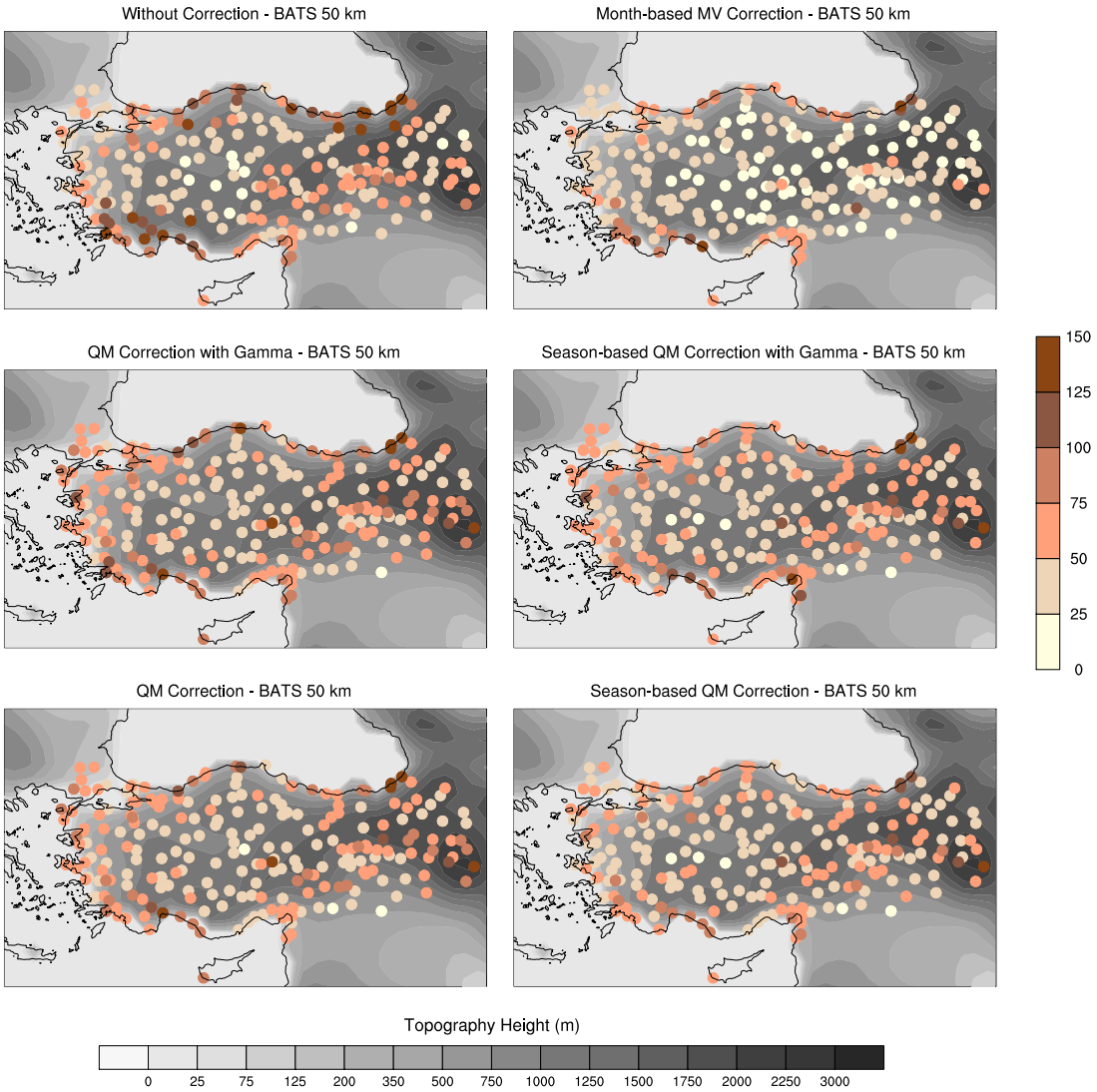

Figure B.1: BATS 50 km RMSE distributions.

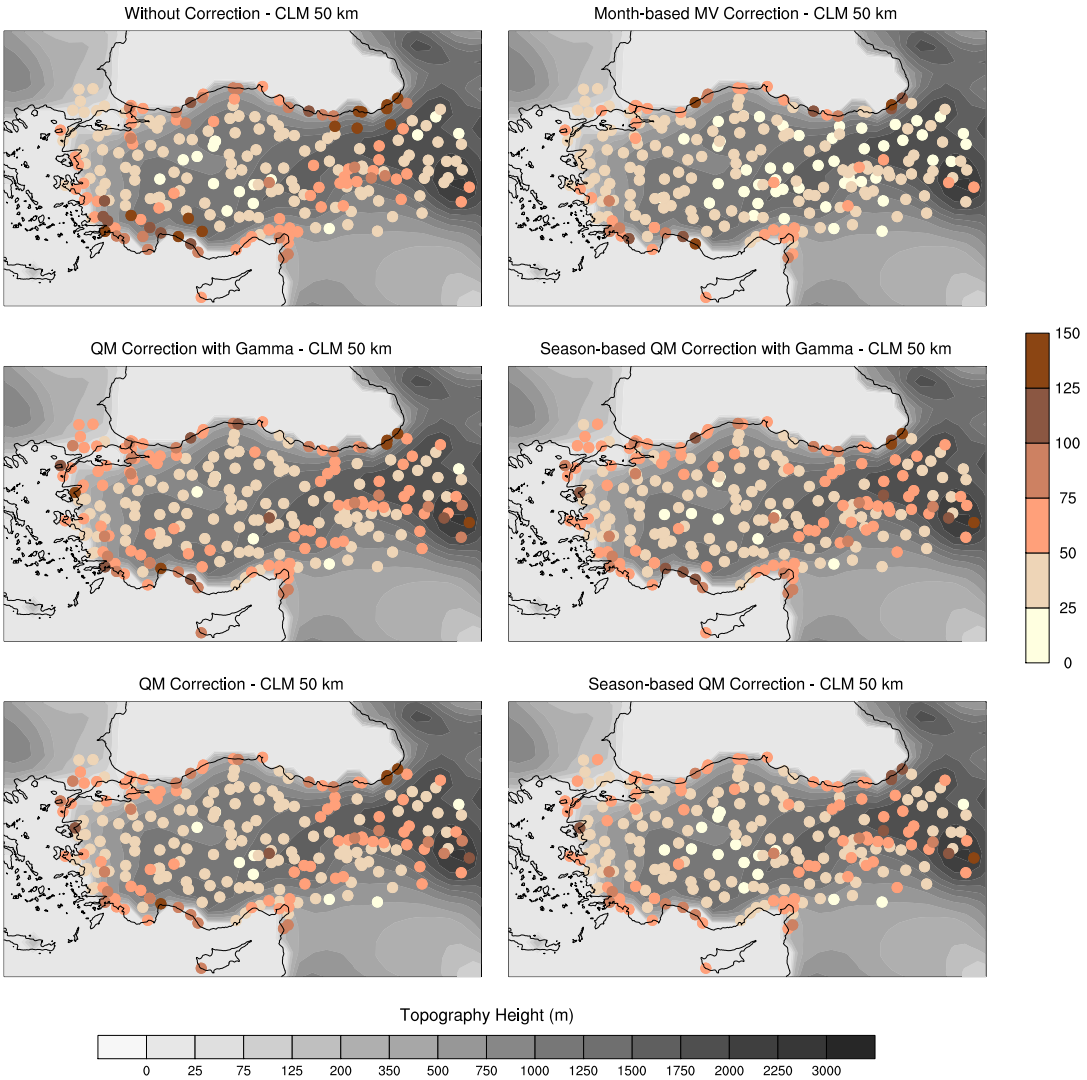

Figure B.2: CLM 50 km RMSE distributions.

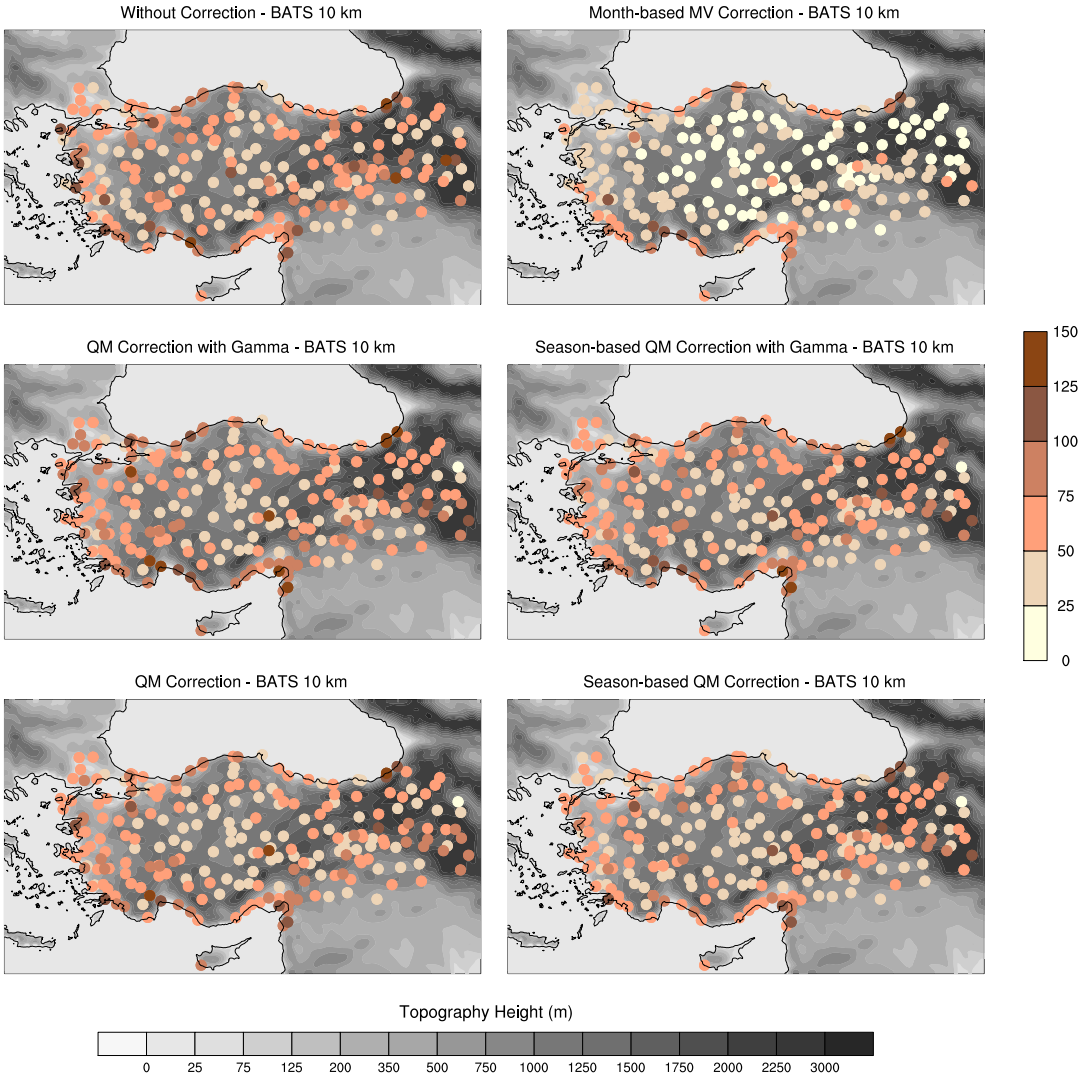

Figure B.3: BATS 10 km RMSE distributions.

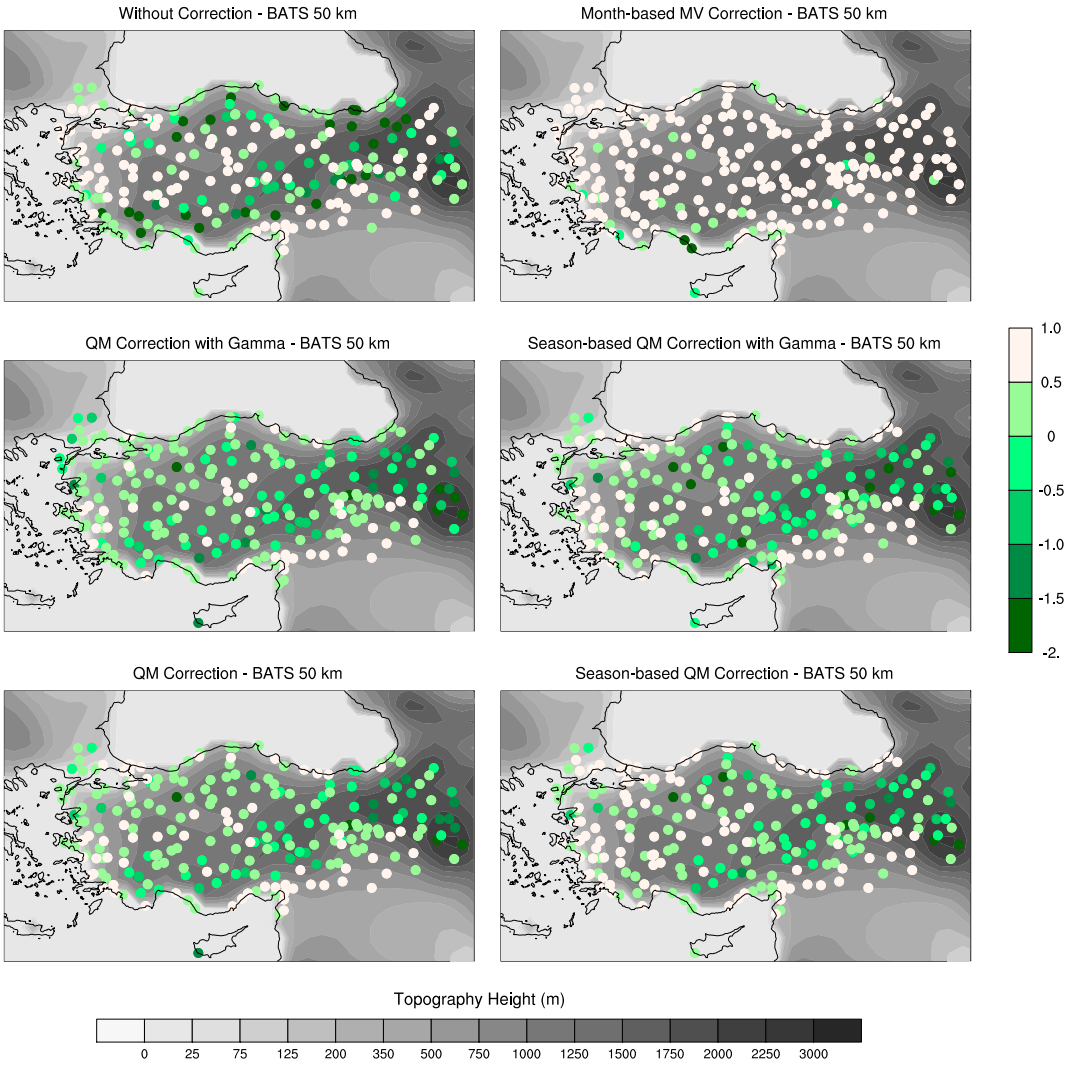

Figure B.4: BATS 50 km NSE distributions.

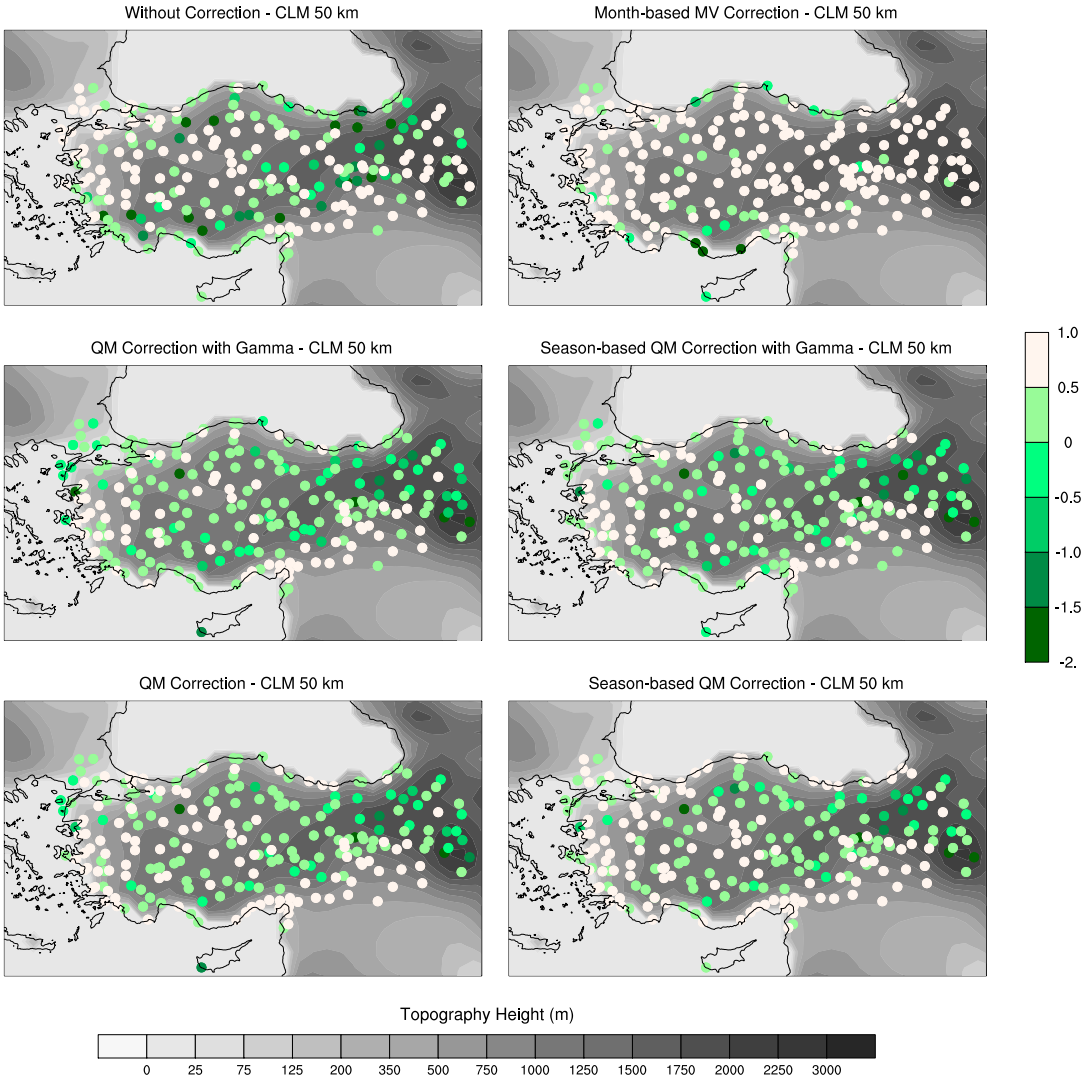

Figure B.5: CLM 50 km NSE distributions.

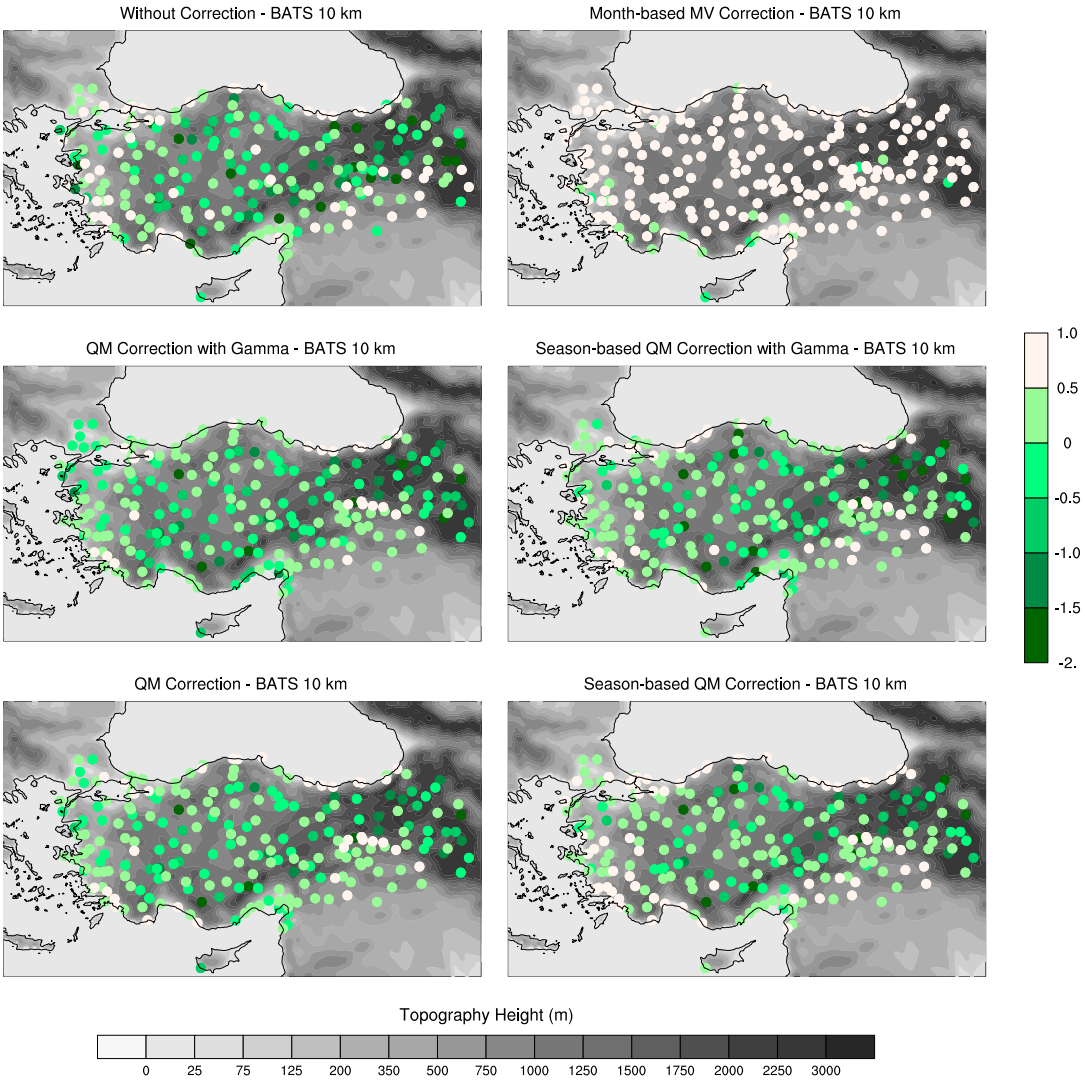

Figure B.6: BATS 10 km NSE distributions.

CURRICULUM VITAE

Name Surname: Ceren BALLI

Place and Date of Birth: Pendik, 18.01.1989

E-Mail: cerenballi@gmail.com

B.Sc.: Istanbul Technical University Meteorological Engineering

M.Sc.: Istanbul Technical University Atmospheric Science Program Meteorological Engineering
ERASMUS: Karlsruhe Institute of Technology (KIT IMK-IFU)

Projects:

- İklim değişikliğinin su kaynaklarına etkisi projesi, 201 *Ministry of Forest and Water Affairs*.
- Determination of Hazardous Gaseous and Air Pollutant Transport and Distribution in Istanbul and its neighbors using a Lagrangian Model, which is coupled with the WRF model including radar wind data assimilation, 2011-2013. *TUBITAK EVRENA Project*.
- Precipitation Augmentation Program and Research on Istanbul Clouds and Aerosols, 2007-2008. *ITU, SOAR and NCAR, funded by IBB*.

Publications and Presentations:

- Bilgen S. I., **Ballı C.**, Ünal Y. S., 2014: Assessment of Regional Climate Model (RegCM) Simulations for High and Low Resolutions over Turkey between 1971-2000: Temperature and Precipitation. *EMS2014*, Prague, Czech Republic.
- **Ballı C.**, Ünal Y. S., Vogl S. and Kunstmann H., 2014: Bias Correction of Precipitation Simulated by Regional Climate Model over Turkey. *MEDCLIVAR 2014*, Ankara, Turkey.
- Ünal Y. S., Acar M., **Ballı C.**, Tan E., Aksoy A., Karadavut C., Aktaş D., Karan H., Önol B., Tilev Ş., Kahraman A., Demir F., Beştepe F. and Menteş S., 2013: Radarlardan Elde Edilen Rüzgar Ölçümlerinin Sayısal Modellemede Kullanılarak İstanbul ve Çevresinde Tehlikeli Gaz ve Hava Kirleticilerinin Taşınım ve Dağılımlarının Lagrangian Model Kullanılarak Tahmini. *TUBITAK EVRENA Project Report - 110Y155*
- Acar M., **Ballı C.**, Tan E., Karan H., Aksoy A., Çağlar F., Önol B., Kahraman A., Tilev Ş., Demir F. and Ünal Y. S., 2013: Lagrangian Model Forecast of the

Transport and Dispersion of Toxic Gases/Particles over Istanbul. *6th Atmospheric Science Symposium*, Istanbul, Turkey.

▪ Acar M., **Ballı C.**, Tan E., Aksoy A. and Ünal Y. S., 2013: An Improvement in high-resolution wind forecasting of the WRF Model by using a 3DVAR analysis with radar data for Istanbul/Turkey. *EGU2013*, Vienna, Austria.

▪ **Ballı C.**, Acar M., Çağlar F., Tan E., Önol B., Karan H. and Ünal Y. S., 2012: The Figure of Merit in Space (FMS) and Probability Analyses of the Concentrations for Forecasted Transport of Particles using the WRF and HYSPLIT Models over Istanbul for January and July, 2009. *EGU2012*, Vienna, Austria.

▪ Acar M., **Ballı C.**, Çağlar F., Tan E., Önol B., Karan H. and Ünal Y. S., 2012: Cluster Analysis of the Trajectories for Forecasted Transport of Air Pollutants using WRF and HYSPLIT Models over Istanbul for January and July, 2009. *EGU2012*, Vienna, Austria.

▪ Çağlar F., Acar M., **Ballı C.**, Tan E. and and Ünal Y. S., 2012: Verification of 24 hours Wind Field Forecast Generated by WRF-ARW for January and July of 2009. *EGU2012*, Vienna, Austria.

Participation at Workshops:

▪ Sixth ICTP Workshop on the Theory and Use of Regional Climate Models. *The Abdus Salam International Centre for Theoretical Physics*, Trieste, Italy, May 7-18, 2012.

▪ Remote Sensing of Precipitation Using Microwave Links: Techniques and Applications *Karlsruhe Institute of Technology (KIT IMK-IFU)*, Garmisch-Partenkirchen, Germany, February 27- March 3, 2012.